NASA CR-134766

AET CORP NAS 3-18904

Acoustic Emission Characteristics Of Copper Alloys Under Low-Cycle Fatigue Conditions

by

Y. Krampfner, A. Kawamoto, K. Ono
and A. T. Green

Prepared for
National Aeronautics and Space Administration
NASA Lewis Research Center
Contract NAS3-18904
April 1975

ACOUSTIC EMISSION TECHNOLOGY CORPORATION

TECHNICAL REPORT STANDARD TITLE PAGE

1. Report No.	2. Government Accession No.	3. Recipient's Catalog No.
NASA CR-134766		
4. Title and Subtitle Acoustic Emission Characteristics of Copper Alloys Under Low-Cycle Fatigue Conditions		5. Report Date April 1975 6. Performing Organization Code
7. Author(s) Y. Krampfner, A. Kawamoto, Kanji Ono and A. Green		8. Performing Organization Report No. UCLA-ENG-7529
9. Performing Organization Name and Address University of California, Los Angeles, CA Acoustic Emission Technology Corporation, Sacramento, California		10. Work Unit No. YOR 6201 11. Contract or Grant No. NAS3-18904 13. Type of Report and Period Covered
12. Sponsoring Agency Name and Address National Aeronautics & Space Administration Washington, D.C. 20546		Contractor Report 14. Sponsoring Agency Code

15. Supplementary Notes

Technical Monitor, Rudolph A. Duscha, NASA Lewis Research Center, Cleveland, Ohio

16. Abstract

The acoustic emission (AE) characteristics of pure copper, zirconium-copper, NARloy-Z, Glid Cop Aℓ 10 and NASA 1-1 have been determined in order to aid the development of nondestructive evaluation schemes of thrust chambers via AE techniques. The AE counts rms voltages, frequency spectrum and amplitude distribution analysis were employed to evaluate the AE behavior under fatigue loading conditions. The results of AE testing were interpreted with the detailed evaluation of wave forms, crack propagation characteristics as well as scanning electron fractographs of fatigue tested samples.

In the cold worked condition, crack propagation in NARloy-Z produces AE signals that can be utilized for its detection. In other alloys, with a possible exception of NASA 1-1, AE signals are too weak to reliably detect the propagation of a crack. A sample of annealed alloys produces continuous type AE signals at the beginning of a fatigue test. However, as the sample work-hardens, the AE behavior becomes similar to that of a cold worked sample. When a sample of zirconium containing alloys is annealed repeatedly after each fatigue loading cycle, numerous surface cracks are produced during the subsequent fatigue cycle, emitting strong burst type AE signals. While frequency spectrum analysis of the AE signals does not readily identify the type of AE signals or their origins, amplitude distribution analysis exhibits responses that are characteristic of certain types of AE signals. The latter can be incorporated in nondestructive evaluation schemes of thrust chambers using AE techniques.

17. Key Words	18. Distribution Statement
Acoustic Emission Fatigue Tests Copper Alloys	Unclassified - unlimited

19. Security Classif. (of this report)	20. Security Classif. (of this page)	21. No. of Pages	22. Price
Unclassified	Unclassified		

Form DOT F 1700.7 (8-69)

NASA CR-134766
UCLA-ENG-7529

Acoustic Emission Characteristics of Copper Alloys under Low-Cycle Fatigue Conditions

by

Y. Krampfner,* A. Kawamoto,* Kanji Ono* and A. Green**

*MATERIALS DEPARTMENT
School of Engineering and Applied Science
University of California
Los Angeles, California

and

**Acoustic Emission Technology Corporation
Sacramento, California

Prepared for

NASA Lewis Research Center
NAS3-18904

April 1975

ACOUSTIC EMISSION TECHNOLOGY CORPORATION

1828A Tribute Road, Sacramento, Calif. 95815
Phone (916) 927-3861

Foreward

The work reported herein was performed for NASA Lewis Research Center under contract NAS3-18904, entitled "Acoustic Emission Characterization of Copper Alloys." The authors are grateful for the assistance of Mr. R. A. Duscha, the NASA/LeRC project manager, and wish to acknowledge contributions of Mr. N.L. Guiles for scanning electron fractography.

Mr. A. Green was responsible for the overall management as Program Manager. Experimental investigation was performed at University of California, Los Angeles under a subcontract to Acoustic Emission Technology Corporation. Dr. Kanji Ono was the Principal Investigator and directed the investigation at UCLA. Messrs. Y. Krampfner and A. Kawamoto conducted the acoustic emission research, which comprises their respective M.S. thesis research.

TABLE OF CONTENTS

SUMMARY

The acoustic emission (AE) characteristics of pure copper, zirconium-copper, NARloy-Z, Glid Cop Aℓ 10 and NASA 1-1 have been determined in order to aid the development of nondestructive evaluation schemes of thrust chambers via AE techniques. The AE counts rms voltages, frequency spectrum and amplitude distribution analysis were employed to evaluate the AE behavior under fatigue loading conditions. The results of AE testing were interpreted with the detailed evaluation of wave forms, crack propagation characteristics as well as scanning electron fractographs of fatigue tested samples.

In the cold worked condition, crack propagation in NARloy-Z produces AE signals that can be utilized for its detection. In other alloys, with a possible exception of NASA 1-1, AE signals are too weak to reliably detect the propagation of a crack. A sample of annealed alloys produces continuous type AE signals at the beginning of a fatigue test. However, as the sample work-hardens, the AE behavior becomes similar to that of a cold worked sample. When a sample of zirconium containing alloys is annealed repeatedly after each fatigue loading cycle, numerous surface cracks are produced during the subsequent fatigue cycle, emitting strong burst type AE signals. While frequency spectrum analysis of the AE signals does not readily identify the type of AE signals or their origins, amplitude distribution analysis exhibits responses that are characteristic of certain types of AE signals. The latter can be incorporated in nondestructive evaluation schemes of thrust chambers using AE techniques.

LIST OF FIGURES

LIST OF PHOTOGRAPHS

LIST OF TABLES

LIST OF SYMBOLS

B - constant

c - constant

f - percentage of the cumulative AE count with respect to total counts

ℓ - crack length (mm)

n - number of fatigue cycles

n_f - number of fatigue cycles to failure

ΔN_e - number of AE counts from elastic region

ΔN_i - number of AE counts from inelastic region

ΔNu - number of AE counts from unloading region

$\Sigma\Delta N$ - total cumulative AE counts

N - AE count rate

$N_D\ (V_t)$ - cumulative amplitude distribution function

$N_p\ (V_t)$ - number of AE events that have peak amplitude exceeding the threshold value V_t

R - ratio of maximum t minimum load

~~R_A - Rockwell A-scale hardness number~~

R_E - Rockwell E-scale hardness number

$\overline{V}_r$ - rms voltage of AE signal

V_t - threshold value (dB)

ϵ - strain

$\Sigma\epsilon$ - total strain

$\Sigma\epsilon_i$ - inelastic strain

ϵ_i - total inelastic strain

I. INTRODUCTION

Acoustic Emission (AE) is the common name given to mechanical waves propagating in a solid. These waves are generated within the solid by certain processes that take place on the microscopic or submicroscopic scale, for example, yielding, dislocation motion, martensitic transformation and crack nucleation and growth. Other processes are also known to generate AE as well. Because of its potential as a useful research tool in learning dynamic events within a material, much efforts of correlating AE observations to microscopic processes have been devoted, although our understanding is still inadequate (ref. 1-3).

The application of AE techniques to detect and locate growing defects within structures has been successfully accomplished many times over the past dozen years. Most significant accomplishments have been in the areas of inspecting rocket motor cases and nuclear reactor vessels, but numerous other uses of AE have been successful (ref. 4-10).

One of the important applications of AE is the detection of fatigue failure in its early stages. Certain successes have been reported both under laboratory conditions and large-scale structural testing conditions (ref. 11-22). It has been noted that, while even a small crack growth of the order of 25μm can be detected in small high strength steel samples, the vast majority of AE signals originates from the friction of fractured surfaces. Depending on materials, however, the level of AE signals during fatigue crack extension can be very low, especially in soft, ductile materials.

In the Space Shuttle or Space Tug Program, the capabilities of nondestructive evaluation of various systems components are of crucial importance, since successful continuation of the program requires a rigorous standard of systems reliability. One of the difficult tasks is the detection of bond failures in electroformed-regeneratively-cooled thrust chambers. Thrust chamber panels are subjected to a large thermal strain of the order of 1% during each firing. While the firing lasts only a short time (much less than one minute), the surface metal temperature may reach 500°C while the coolant of gaseous hydrogen at temperatures in the vicinity of room temperature circulates through cooling channels. Thus, fatigue failures due to repeated applicatons of thermal strain are expected.

An initial study of nondestructive tests of simulated thrust chamber panels was completed by Malone, et al. (ref. 23). They concluded that AE technique discloses nonbonds and unexpected weak bonds existing on flat test panels with electroformed copper cover plates, and that such disclosures make it possible to determine the processing variables, which has caused these weak bonds, and to correct the fabrication operation. While no correlation between AE results and bond strength could be established, the rate of AE provided a forewarning of impending failure of bonds or coverplate.

In order to utilize AE techniques more effectively in the integrity evaluation of flight hardwares, it is essential to determine the AE characteristics of candidate materials under fatigue loading conditions. This is the primary objective of this investigation. It is well known that copper and its alloys, that is, the candidate materials for thrust chamber panels, are among those materials that produce low amplitude AE signals during tensile testing at room temperature. This group includes low-carbon steels and stainless steels. AE data on candidate copper alloys, especially under fatigue loading conditions, is almost non-existent. Thus, the present study has evaluated the AE characteristics of pure copper and four copper alloys, i.e., Zr-copper, NARloy-Z, Glid-cop and NASA 1-1. The materials in a cold-worked condition have been primarily evaluated, but effects of initial annealing and repeated annealing to simulate the high temperature excursion during a firing have also been studied. Tension-tension low-cycle fatigue tests have been performed. Both conventional and advanced AE data processing methods have been utilized. The data obtained have been analyzed and discussed in order to provide characterization of the AE with respect to the materials and their performance. Certain metallurgical problems have been discovered during the course of this investigation. Other application related problems as well as possible remedies are also discussed in this report.

II. Materials and Specimen Preparation

The starting materials for this project were supplied in the cold-worked condition in sheets of 1.6mm thick. These include the following five materials:

I. OFHC (99.9+%Cu)
II. Zirconium Copper (.15%Zr-Cu)
III. NARloy-Z (3%Ag-.5%Zr-Cu)
IV. Glid Cop Aℓ 10 (0.2%Aℓ Oxide-Cu)
V. NASA 1-1 (1.1%Ag-0.11%Zr-Cu)

Through the rest of this paper, the materials will be identified by their Roman numeral designation. These cold rolled sheets were received from NASA Lewis Research Center, Cleveland, Ohio, and had been prepared from bar or plate stocks with the final rolling performed on 2.5mm thick annealed sheets. Therefore, the amount of cold work is 37% reduction in thickness. In the case of Alloy III, a piece of 3 cm wide, 30 cm long, 2.5 cm thick hot-rolled plate was also received. Strips of 2.5mm thick were machined from the piece, some of which were cold rolled to 1.6mm thickness using a two-high rolling mill at UCLA.

The specimen geometry was chosen to be of the type single edge notch (SEN), and details are given in Fig. 1. Several tensile tests without a notch were performed, where the half-size ASTM standard sheet specimen geometry was used. The strain rate of the tensile tests was 1.67×10^{-3} sec^{-1},

and the specimen thickness was also 1.6mm.

Before fatigue testing, the gage length of each specimen was polished both mechanically using fine emery paper and electrolytically using phosphoric acid (density 1.40) diluted by equal amount of water at 3V and 0.7 A/cm^2. The purpose of the polishing is to remove small surface defects and also to facilitate accurate optical monitoring of the crack growth. Approximately 0.05mm was removed by the polishing procedures.

III. Experimental Procedures

3.1 Mechanical Testing

All the mechanical testing in this study was performed using a floor model Instron with a loading capacity of 5000 kg. Strain cycling was controlled manually, since large amounts of plastic deformation made it impossible to use the extension control cycle of the testing machine. A load cell (9000 kg capacity, Model U-L, manufactured by Baldwin-Lima-Hamilton Corporation), and a Sanborn 350-1100 carrier amplifier were employed for load measurements. The load measuring system was calibrated using a proof ring (Model RR-60, 900 kg capacity, manufactured by Soiltest, Inc.). The extension of the gage length section of a sample was measured using a clip gage originally designed for fracture toughness measurements (Instron Model AR1627-1). The clip gage was attached to two wedges that were clamped immediately next to the reduced section along the center line. While the distance between the bases of the wedges was 21mm, the effective gage length is equal to the length of the reduced section, namely, 12.7mm, as the deformation was confined to the reduced section. The test set-up is shown in Photo 1.

The deformation within the gage section is non-uniform because of the notch. Any reference to strain should be considered as a nominal representation of an average strain within the gage section. The accuracy of the extension measurements was 0.01mm in the early stages of fatigue cycling. Following the extension of a crack, the wedge tips becomes non-parallel making the extension measurements much less accurate. The extension measurements after a crack has extended a half way may be in error by as much as 1mm. However, this is considered by being non-critical since the value of extension can differ as much as 5mm depending on the location where it is measured. A regulated DC power supply of 5 V was fed to the strain gage bridge circuit of the clip gage and the output was recorded directly on a chart recorder (and/or an X-Y recorder). It was calibrated using a micrometer.

The nominal strain cycling conditions were as follow:

Condition	Strain Amplitude	Strain rate
1f	1%	2×10^{-3} (sec^{-1})
2s	2%	4×10^{-4}
2f	2%	2×10^{-3}

Nominal strain rate is computed from a cross-head speed employed and the length of the reduced section. Because of elastic relaxation of testing apparatus, actual strain rates were not constant especially during crack propagation. The fatigue cycling was in a tension-tension mode with R = 0. Specimen grips had a ball and spherical seat arrangement and no alignment difficulty was encountered during unloading and reloading. Crack length was measured using a 20-power microscope with a calibrated reticule of 0.05mm step.

Basically, three types of material conditions were used in fatigue tests. These are (i) the cold rolled condition, (ii) the cold rolled and annealed condition (650°C, 10 min.) and (iii) the initially annealed condition (650°C, 10 min.) with repeated annealing after each straining cycle (538°C, 10 min.) During the repeated annealing operations, the sample was left in the grips, and the wedges for clip gage remained on the sample. An AE transducer, however, was removed and reattached. No polishing was done after the first straining cycle. Annealing was performed in a stainless steel retort, evacuated and back-filled with hydrogen to the pressure of 1.5cm of mercury. After annealing, the retort with sample(s) inside was allowed to air-cool, taking a half hour to room temperature.

3.2 Acoustic Emission Testing

The major part of AE testing has utilized commerically available equipment. The following components and apparatus were employed:

a) Model AC375 differential transducer with the resonance frequency of 371 kHz and peak sensitivity of -63 dB referred to 1V/μ bar.

b) Model 160 preamplifier with a 250-500 kHz bandpass filter plug-in, having the gain of 60.2 dB. The input noise with input shunted by 50Ω was 1.45 μV. With an AC375 transducer, it was 1.60 μV.

c) Model 201 signal processor. (These three items were supplied by Acoustic Emission Technology Corporation, Sacramento, California.) This signal processor provides up to 40 dB of amplification (continuously adjustable between 0 and 40 dB), determines threshold crossing counts with either a pre-set (manual) threshold level or an adjustable dead-band (automatic) threshold level, and produces DC analogue voltages proportional to rms-voltages of the input signal with a time constant of 5 msec. In addition, amplified AE signals and a voltage ramp can be obtained from this unit.

d) Data recording utilized two units of Soltec 2-pen recorders, Model 291. An X-Y recorder (Hewlett-Packard 7005A) was also utilized for simultaneous recording of load-extension curves.

The automatic threshold mode of the signal processor was utilized in the present tests except in the study of amplitude distribution analysis. The trigger level is adjusted automatically at a fixed voltage above the continuous background, counting only these signals exceeding that level. This method can be used most effectively when the AE signals are of the

burst-type. Its use allows the operator to set a high gain without the risk of loading the counter when the background noise fluctuates. The output counter is a 0-10 VDC analog signal directly proportional to zero to full scale of counter setting (10^3, 10^4 or 10^5 counts full scale). In the present experiment, the total gain of the system was fixed at 100 dB (10^5). The automatic threshold control was used and the trigger level was adjusted to 0.30 V (or 30 μV equivalent at the preamplifier input).

The experimental data was recorded on two two-pen chart recorders and on X-Y_1-Y_2 recorder. The load and rms voltage were plotted against time on one two-pen recorder. The other plotted, as a function of time, AE counts (the counter was reset at the end of each cycle), and clip gage displacement (CGD). The X-Y_1-Y_2 recorder recorded load and counts vs. CGD. A block diagram of the above setup is given in Fig. 2. It is important to note that the load was transmitted to the specimen by a universal joint and by ball joints of the upper and lower specimen grips, so as to apply pure tensile load on the specimen. The transducer was attached to the specimen just above the reduced gage section by means of a C-clamp (see Photo 1), and acoustically coupled by a resin designated as SC6, obtained from Acoustic Emission Technology Corporation, Sacramento, California.

Amplitude distribution and frequency spectrum analyses of AE signals were performed on recorded signals. The amplitude distribution analysis utilized the same signal processor described above, except the manual threshold mode (with 0.30 V threshold voltage) was employed as well. Because of the low intensity of AE signals, commercial wideband transducers could not be utilized in these tests. A PZT-5, compressional mode transducer element with 3 MHz fundamental frequency was used in this part of the study. The element was a 6.4mm diameter disc, gold-plated on both sides and was obtained from Valpey Fisher Corporation, Hopkinson, Minnesota. It was bonded to an aluminum casing with epoxy glue. No significant resonance of the transducer was detected over the frequency range of 30 to 2000 kHz, except for a small peak near 450 KHz. A model 160 preamplifier with 30 to 2000 kHz filter plug-in was used. In this configuration, the input noise was 3.4 μV. Two tape recorders were used in this investigation. One was Bell and Howell VR 3700A instrumentation tape recorder with three channels of AM (0 to 2 MHz) and four channels of FM (0 to 500 kHz), operated at 3.05 m/s. Load signals from the Instron were simultaneously recorded. Another was Sony AV 3650 video tape recorder with a proper modification (ref. 24). A gated amplifier synchronized with the video tape recorder was used to eliminate head-switching noise. The stop motion feature of the video tape recorder provided a short segment (approximately 1 to 10 msec) of the recorded signals at the rate of 60 Hz to frequency analysis equipment.

The power density spectrum of AE signals was determined in two steps (ref. 3,25,26). The autocorrelation function of a particular portion of AE signals was first obtained using a correlator (Progress Electronics 810A), the output of which was acquired and stored in a minicomputer (Digital Equipment Corporation, PDP 8/E with 8K core memory). Subsequently, the

stored data was converted to the power density spectrum by means of digital Fourier transform using the Cooley-Turkey algorithm [the so-called fast Fourier transform (FFT) method]. The power density spectrum was typically measured in the range up to 500 kHz with the resolution of 3.9 kHz. The upper frequency limit was 2 MHz in the present system. The averaging time, over which the measurement was made, was approximately 1 sec.

The PDP-8 minicomputer was programmed to read a discrete correlation function and convert the time domain analysis to the frequency spectrum by performing a FFT. The frequency spectrum is subsequently recorded permanently on an X-Y plotter or visually displayed on an oscilloscope. The system is also able to provide other options such as background subtraction and data print-out. The computer program offers several options prior to plotting the final data; the operator may choose to obtain the FFT of the background, the AE signal, or the difference of the two. Background consists of the inherent electrical and mechanical noise of the instrumentation; it is obtained prior to starting the experimental run. The FFT of the backgorund and data may be stored in the computer memory for future reference. When background subtraction is desired, a background factor is selected to compensate for differences in input gains of the signal and background. Only one storage space is available for the background and up to 32 sets are available for simultaneous storage of transformed data. Existing background and data information are automatically erased when new values are entered onto a particular storage page.

IV. Results

4.1 Preliminary Data

Hardness data of test materials is summarized in Table I. Rockwell A-scale was used. As-received sheets had hardness ranging from 33.8 for copper to 48.8 for Alloy IV. Annealing at 650°C, 10 min. reduced the hardness of Alloys III and IV to nearly one-half of the initial value, while the hardness of Alloy II was only slightly reduced by annealing at 538°C, 10 min. When the duration of annealing time at 538°C was increased to 2 hrs., additional annealing effects were small. Data of Alloy III plate stock is also included in Table I, indicating the as-recieved plate to be very soft. The cold rolling of the plate stock did not achieve the same degree of hardening as in the sheet material.

Tensile test data is given in Table II. Both smooth and notched sheet specimens were tested in the annealed and as-received (cold worked) conditions, respectively. Smooth tensile data in the cold worked condition was supplied by NASA Lewis Research Center, and is included in Table II. Yield strength at 0.2% offset is given and notch tensile strength is equal to the maximum load divided by the minimum initial cross-sectional area. Notch sensitivity is the ratio of notch tensile strength to tensile strength. An annealed smooth sample has a larger value of elongation than the corresponding cold worked sample, except for the Alloy V sample that failed at one of preexisting rolling cracks in the gage section. The yield

strenth was always lower in the annealed condition for a given material, but the tensile strength was higher in the annealed condition of Alloys II and IV (and possibly V). The observed values of notch sensitivity was always greater than unity, ranging from 1.04 for Alloy IV to 1.36 for Alloy V.

A good correlation exists between the hardness and yield strength of these alloys. However, no apparent relation can be established for the tensile strength data. The yield strength (Y.S.) can be expressed by

$$\text{Y.S. (in kg/mm}^2\text{)} = 1.45\ R_A - 26.5,$$

where R_A is the Rockwell A-scale hardness number.

Annealing of samples revealed unexpectedly the formation of blisters. In Alloys III and V, annealing produced blisters on the surface of sheet samples, as shown in Photo 2. The size of the blisters was about 0.5mm in diameter and their surfaces had small cracks as shown in Photo 2b. The blisters appear to originate from rolling defects in the sheet, as no blister formed when a piece cut from the plate stock of Alloy III was annealed. Sheet specimens of Alloy III cold rolled at UCLA also produced no blisters after identical annealing treatment.

Initial AE tests were performed using cold worked pure copper (Alloy I). Except during the first cycle, from which several burst signals and AE counts, less than 1000, typically several hundreds were observed, almost no AE counts were obtained during the macroscopic crack extension in the subsequent cycling. The oscilloscope observations revealed no burst signal, although the rms voltage of the signal increased from 1.6 to 1.65 μV while the crack propagation was observed. Because of the low signal level, especially the lack of AE counts corresponding to crack propagation, AE study of Alloy I was terminated.

4.2 Fatigue Test Results and Fractography

Results of fatigue tests are summarized in Table III. Test condition refers to the material condition (i, ii, or iii) and loading condition (1f, 2f or 2s), as designated previously. Cyclic notch strength refers to the maximum load during a fatigue test divided by initial minimum cross-sectional area. For the cold-worked materials, the cyclic notch strength is invariably lower than the notch tensile strength, given in Table II. The reduction is approximately 30% in Alloys II, III and V, and is approximately 15% in Alloy IV, respectively. The cyclic notch strength for a given material is nearly identical regardless of loading condition. Both initial annealing and repeated annealing procedures have reduced the cyclic notch strength significantly; e.g., by nearly 50% in Alloy III (cf. Specimen Nos. III-5, 6 and III-T2).

Total inelastic strain accumulated during a fatigue test ($\sum\epsilon_i$) in the cold worked condition is comparable to an elongation value in a notch tensile test of the same material. The total amount of strain imposed on a sample ($\sum\epsilon$) can be obtained by multiplying the strain amplitude and the

number of cycle to failure. The error introduced by this procedure is less than 10% of the total. This value is always greater than total inelastic strain, which generally is 70 to 90% of the total imposed strain. Because of the increased number of elastic loading contributions, the 1% strain amplitude condition has resulted in lower ratios of inelastic strain to imposed strain, the case of Specimen Nos. IV-3 and 4 being most extreme. It should be cautioned that the magnitude of the strain readings include crack opening contributions and not just the deformation of a sample material.

The observed values of $\sum \epsilon_i$ are similar to the observed elongation values in notched tensile test (cf. Table II). This comparison is obviously valid only for the cold worked condition, as no tensile data is available for other conditions. The values of $\sum \epsilon_i$ of 20.6, 14.4, 10.6, and 26.0(%) for Alloys II, III, IV and V, respectively, can be compared to 20.0, 13.4, 15.6 and 28.0(%) for the corresponding notch tensile elongation. Annealing of a sample increases the $\sum \epsilon_i$ value substantially. Increases of 50 to 200% can be seen in Table III. The major portion of the increases appears to result from the initial annealing effect (at 650°C) and subsequent annealing (at 538°C) contributes little toward the increase in $\sum \epsilon_i$, according to the observations in Alloy III. The most significant changes in $\sum \epsilon_i$ due to annealing were found in Alloy III prepared from plate stock, where $\sum \epsilon_i$ of 13% in the cold worked condition increases to 39 to 41% in annealed conditions.

The number of cycles to failure (n_f) was found to be small except for a few cases with 1% strain amplitude. When the strain amplitude was 2%, the average n_f values were 13.5, 8.0, 6.25 and 15.5 for cold worked Alloys II, III, IV and V, respectively. Annealing had beneficial effects, but n_f was still below 25. When the strain amplitude was 1%, larger n_f was observed except in Alloy II. In Alloy IV, n_f was 8 to 17 times larger with the lower strain amplitude.

The crack growth data is tabulated in Table IV together with AE results. When the crack length (ℓ) is plotted against the number of cycles (n) in a log-log plot, a straight line with the slope of 2 describes the ℓ-n relationship; i.e., $\ell \propto n^2$. Crack growth can also be correlated to inelastic strain, as shown in Fig. 3. A single straight line with the slope of 2.0 to 2.6 can represent the $\ell - \epsilon_i$ relationship of a given material reasonably well. However, the scatter in Alloy III is quite large and appears to be a consequence of material variability, primarily due to preexisting flaws introduced by cold rolling. Effects of different strain rates or strain amplitude are not evident. When specimens (except Alloy IV) were annealed between loading cycles, numerous fine cracks developed ahead of the crack tip and within the plastic zone, the boundaries of which are initially inclined approximately 45° to the tensile axis (see Photo 3). Subsequently, some of those fine cracks were connected during loading (see Photos 4 and 5). This behavior prevented meaningful measurements of crack propagation except in Alloy IV. In repeatedly annealed Alloy IV, ℓ is nearly proportional to ϵ_i as can be seen in Fig. 3. The region where cracks develop from repeated annealing and loading was quite extensive as Photos 5a and b indicate. Photo 5a shows the sample with the macroscopic crack at

about one-third of the sample width, while Photo 5b shows the development of carck pattern after fracture.

Macrophotographs of fracture samples are shown in Photo 6, for the cold worked (i) and repeatedly annealed (iii) conditions. Those of the annealed conditions (ii) were similar to the cold worked ones. In the cold worked condition, Alloys II and V resulted in a knife-edge type fracture surface. As shown in Photo 6a, however, fracture of Alloy II proceeded along the direction approximately 60° to the loading axis while that of Alloy V was along the direction normal to the loading axis. The plastic zone in these alloy samples was readily noticeable. Alloys III and IV produced a slanted fracture surface. The fracture surface of Alloy III was much rougher than that of Alloy IV. In the repeated annealed condition, Alloy IV again showed a slanted fracture surface as in the cold worked samples of Alloy IV. The other three alloys produced extensive surface cracking as described above, and the fracture surface was rugged.

Scanning electron micrographs of fracture surfaces are shown in Photos 7 to 10. These were obtained using a Cambridge scanning electron microscope. In the cold worked condition, Alloy II and V showed mostly pure shear fracture mixed with some dimples and tear ridges (see Photos 7a, c and d). At the tip of a knife edge in Alloy II, more dimples were observed (Photo 7b). Alloy III exhibited elongated dimples (Photo 8a) and also some areas of pure shear (Photos 8b and c). As the arrow corresponding to the crack propagation direction indicates, the elongated dimples were due to shear tearing. Fractured particles are also visible. Alloy IV produced much finer elongated dimples as Photo 8d indicates. Annealed Alloy III exhibited more irregular mixtures of elongated dimples due to tensile tearing and shear (Photos 9a and b).

In the repeatedly annealed condition, Alloy IV produced essentially the same dimple pattern as in the cold worked condition. However, three other alloys showed more complicated fracture surfaces. As noted earlier, these samples produced surface cracks. These surface cracks extended as much as 0.3mm into the sample. As Photos 10a-c show these surface cracks resulted from intergranular fracture. This region shows a very fine equiaxed dimple (a few μm diameter) as shown in Photos 10b and c. Inside the intergranular fracture region, pure shear fracture and equiaxed dimples (Photos 10d and e) were observed in Alloy III. In contrast, only pure shear fracture was found in the center section of Alloys II and V (see Photo 10f). The shear region in Alloy III was between the intergranular fracture (outside) and equiaxed dimples (center) and the shear markings were nearly normal to the direction of macroscopic crack propagation. This suggests that the shearing occurred after the fracture of the outside and center sections of the sample. In the case of Alloys II and V, the shear markings make a sharp angle as shown in Photo 10f, suggesting that the shearing controls the process of crack advancement.

4.3 AE Results

4.3.1 General Observations

In general, the AE results can be categorized into four types:

1) Low AE activities from a cold worked sample of Alloys II, IV and V (see Fig. 4)

2) Moderately active AE signals from a cold worked sample of Alloy III (see Fig. 5).

3) High AE activities in an annealed sample (see Fig. 6).

4) Very high AE activities from a repeatedly annealed sample (see Fig. 7).

These four types are illustrated by plots of load and rms voltage values (V_r) against time and the corresponding plots of displacement and AE counts against time in Figs. 4-7. These were obtained during fatigue tests. The units of load and displacement were converted to engineering stress and strain. The rms values are given as the equivalent voltages at the pre-amplifier input. These figures are photographically reduced copies of the data recorded on chart and X-Y recorders during actual testing. In all the figures the rms voltage is shifted to the right from the corresponding stress value by one small division or one quarter of a minute due to a separation between the pens of a two-pen chart recorder. The same graphical displacement to the right applies to the AE count data relative to the strain vs. time curve. Each pair of plots that appear on the same page is aligned in such a fashion that values that correspond to a given time can be comapred. The constant V_r value at 1.6 μV between signal spikes is the background level of the signal resulting from steady-state electronic noise. The AE counts are presented on the figures in two ways; the counter being reset at the end of each cycle (as in Fig. 4b) and a continous count throughout the test (as in Fig. 5b). The strain vs. time curve for each cycle contains three distinct sections. The first, designated as elastic, is the part where the strain increases linearly with time in a moderate rate, which also corresponds to the linear portion of the stress-time curve. The second, or inelastic, part starts at the point where the strain rate tend to increase and reaches a higher value. This part includes the plastic deformation and the crack propagation and is reflected in the stress-time curve as a non-linear portion. At the end of the inelastic stage the strain-time curve reaches a peak, but it does not correspond to the point of maximum stress since the crack continues to propagate even under decreasing load. The third part of the curve is the unloading. This stage starts from the peak of the strain-time curve to the minimum value.

The AE count data are summarized in Tables IV-VI. Detailed cycle-by-cycle AE data are tabulated and attached as Table VI and their summaries in Tables IV and V. An individual listing in Table VI present the

cycle-by-cycle accounts of the following information: the number of AE counts per cycle from the elastic region, ΔN_e; that from the inelastic region, ΔN_i; that from the unloading region, ΔN_u; the total number of AE counts during each cycle, ΔN; the cumulative AE counts, $\Sigma \Delta N$; percentage of the cumulative AE count with respect to the total counts, f; the cumulative inelastic strain, $\Sigma \epsilon_i$; the length of a crack, ℓ. Total counts and their distribution among the three regions as well as the corresponding quantities for all the cycles less those of the first cycle are also given. The values in parenthesis are rounded percentage figures of these quantitites. The values designated as elastic, inelastic, and unloading were determined by the change in slope of the strain vs. time curves.

The most common behavior of the cold worked specimens tested (except Alloy III) was the low level of the AE signals. This was reflected in low levels of rms voltage output and small numbers of counts per cycle as can be seen in Fig. 4a and b. The AE count rates started to increase as the yielding process of the first cycle began. In this cycle the crack initiation and the very early stages of crack propagation occurred and are reflected in the stress-time plot in the form of the maximum stress. During all of the subsequent cycles, less than 25% of the total counts were typically observed. Beyond the first cycle, most of the AE counts were observed. The output was essentially at the same level as the continuous background, but contained a limited number of burst type emissions, especially during the first cycle. These observations were not unexpected from the ductility of the materials tested, as it is well known that AE signal levels are low for ductile materials and that ductile fracture produces low amplitude AE signals. Nevertheless, the extremity of the low level AE signals was surprising. It is also expected that extraneous noise from grips and the loading train are most numerous during the first cycle. The subsequent cycles showed only small number of counts (typically below 100 counts per cycle). Occasionally a few bursts of emissions from the peak stress range of a certain cycle resulted in an increase of the number of counts for that particular cycle, thus raising the total for the test.

The second type of behavior was observed in cold worked Alloy III samples. Most counts were observed also during the first cycle as shown in Fig. 5b. This type did have an observable change in rms voltages at each cycle although the increase was small. The signal accompanied the inelastic portion of the stress-strain curve and produced a small number of counts per cycle. At the beginning of the first loading cycle, spikes in the $\bar{V}_r$ vs. time curve appeared, but the remainder was essentially the continuous type signals judging from Fig. 5a. More detailed observations on the nature of AE signals will be described later.

The specimens tested in the annealed condition differed from the cold worked ones in the early stages of deformation, before reaching the maximum load, as shown in Fig. 6a. The same figure also shows the three cycles at the maximum stress region and the four cycles just preceding the fracture where the stress-time curve behaved similarly as that of the cold worked sample. The early cycles produced a significant increase in the

rms voltages of the signals. The oscilloscope observations revealed most of the signals to be of the continuous type. The shape of the $\bar{V}_r$ vs. time curve was very similar to that resulting from the yielding portion of a notch tensile test of the same material. The total AE counts were very similar to those observed on a cold worked specimen, but the effect of the first cycle was less pronounced.

The signals from the repeatedly annealed specimens were completely different from all those discussed above. Figure 7 shows typical AE behavior of this condition. The first cycle was similar to that obtained from an annealed specimen, and showed a peak in the V_r vs. time curve just before yielding. The AE behavior after additional annealing showed an increase in AE activity. The total number of counts was high. Oscilloscope observations and the rms voltage showed very strong burst-type activities beginning at the early part of the loading cycle. The majority of the signals was of the burst type, but the continuous type signal was also present during the inelastic portion of the stress-time curve as evidenced by the raised level of $\bar{V}_r$.

4.3.2 Alloy II

A total of six specimens were tested in the cold worked condition. The total number of AE counts for this condition was in the range of 1.5×10^3 to 18×10^3 with the exception of Specimen II-7 that produced a total of 1.4×10^5 counts (see Table IV). During the first cycle, most of the AE counts, more specifically between 77 and 95% of the total counts for the entire test, were generated. While specimen-to-specimen variations were large, approximately one-half of the AE counts resulted from the elastic part and the other half from the inelastic part during the first cycle. A small fraction of the AE counts was generated in the unloading position. When the counts of the first cycle were subtracted from the total, the number of counts was in the range of 200-4000 AE counts, and the distribution was the following: 50, 25, 25% from the elastic, inelastic and unloading part, respectively. The number of AE counts from the inelastic part, during which the crack propagation occurred, was extremely low beyond the first five cycles. Observed AE counts for this part, ΔN_i, were typically below 10 counts, even when the crack was propagating at steps of 0.1mm to as much as 5mm per cycle. The effect of strain rate and strain amplitude on the AE count results was within the scatter and could not be discerned. The rms voltage of the AE signal was almost always at the background level, except for the first loading cycle. During the first cycle, spikes in the $\bar{V}_r$ vs. time curves were noticed, indicating the presence of burst-type emissions. These spikes appear to be due to extraneous signals, since most of these were generated at low stress levels in the elastic part. It can, therefore, be concluded that Alloy II produces few AE counts originating from the propagation of a fatigue crack. Some of the AE counts during the first cycle may originate from plastic deformation, but most of them apparently come from the grips. Effects of the gripping noise, however, become insignificant after the first cycle.

In the case of Specimen II-7 that generated an exceptionally large number of counts, a large number of spikes were observed on the $\bar{V}_r$ vs. time curve in most of the loading cycles. Table VI also shows that the high number of counts for this specimen were generated from the elastic and unloading parts, but ΔN_i was quite low. Thus, almost all of the observed AE counts for Specimen II-7 can be attributed to a large amount of noise generated from a faulty specimen gripping.

4.3.3 Alloy III; Cold Worked

Ten specimens were tested in the cold worked condition. Two of them (III-N2 and III-N3) were prepared from a plate stock as noted earlier while the rest were machined from the as-received sheets. The AE test results from the two types of materials were within the observed scatter. The total number of counts for this condition ranged between 2.3 x 10^3 and 34 x 10^3. The average distribution of these counts was: 40% for the elastic part and 50% for the inelastic part. After subtracting the AE count of the first cycle, the total was 700-7200 counts with 20% of the AE counts generated from the elastic part and 75% from the inelastic part. The elastic part produced a high number of counts for the first four cycles. The inelastic part generated moderately high AE counts throughout the test. While the number of AE counts from the inelastic part, N_i, was slowly decreasing toward the end of a fatigue test and a few cycles deviated from the general pattern, the number of AE counts was typically in the hundreds (see Table VI). The AE count information from this alloy serves as a definite indication of the crack propagation process. The rms voltage of the AE signal was mainly of the burst type during the first cycle. This changed during the rest of the test; that is, a small increase of approximately 0.05 μV above the background level was observed during the inelastic part of each loading cycle. This signal was mainly of the continous type as observed on the oscilloscope, but even when the $\bar{V}_r$ vs. time curve did not display any spikes the signal did contain many burst-type emissions.

4.3.4 Alloy III; Annealed

a. Standard Size Specimens

A total of three specimens was tested in an annealed condition. The number of AE counts ranged from 2.5 x 10^3 to 6.3 x 10^3. Between 94% and 98% of the counts were generated in the inelastic part, thus giving a good correlation between the observed AE counts and the crack propagation and plastic deformation. Only 4% of the counts were originated in the elastic portion of the cycle. The AE counts during the first cycle made only a small contribution to the total, as seen in Table V. The rms voltage of the AE signal was high for the first three or four cycles reaching values of about 1 μV above the background level. Beyond those early cycles the $\bar{V}_r$ vs. time curve was similar to those of the cold worked specimens of this alloy. As Fig. 5 shows, $\bar{V}_r$ increased approximately 0.05 μV (to 1.65 μV) when the work hardening occurred following the elastic part, i.e., before the appearance of a crack, as well as when the crack propagation occurred

in the inelastic part during those cycles following the highest stress. The surface cracks that had become visible during the initial annealing treatment opened up during the first cycle, but did not grow. No corresponding spike on the $\bar{V}_r$ curve was observed and no unusual increase in the number of AE counts resulted from the opening of these surface cracks. When these cracks were in the path of a propagating fatigue crack, the propagation of fatigue crack occurred by joining some of the surface cracks. The surface cracks in other parts of the sample changed little throughout the fatigue test.

b. <u>Thick Specimens in the As-Received Conditions</u>

Two specimens were tested in this condition; i.e., III-S1 and III-S2. These specimens were machined from the soft, as-received plate to the same geometry as the regular specimens, but their thickness was 2.5mm as compared to the standard 1.6mm. Both specimens had generated a large number of AE counts, 2.3×10^5 and 2.9×10^5, which is almost two orders of magnitude above the number of counts obtained from the annealed specimens described in the preceding section. The inelastic part of the cycle was the major source of the AE counts with values of 78% and 89% with a minor contribution in the elastic part. The contribution of the first cycle was small. Most of these increased AE counts were generated from strong burst signals observed during the development of a plastic zone ahead of the crack starter notch; that is, before the highest stress was reached and before a macroscopic crack started to propagate.

The $\bar{V}_r$ vs. time curve of these specimens was quite different from the one obtained from the other annealed specimens. The large increase in the continuous emissions level for the first four cycles did not occur. Instead, the continuous level increased from the background level by 0.05 μV to about 0.2 μV. This continuous type of emission was generated during the inelastic part of the cycle for both specimens. In the case of III-S1, these were accompanied by the presence of burst spikes both during the elastic and inelastic parts of the fourth through the fourteenth cycles. The highest stress was reached at the fourteenth cycle and macroscopic crack growth also was initiated in this loading cycle. The occurrence of the spikes was predominantly from the inelastic part as indicated also by the number of observed AE counts as shown in Table VI. Specimen III-S2 was somewhat different as seen in Fig. 8. The increase in the continous type rms voltage level was at most 0.05μV. The majority of the spikes, however, were observed from the inelastic portions of the seventh, eighth, and ninth cycles. This was reflected also in the AE counts presented in Table VI. In both cases, the middle part of the fatigue test produced most of the total AE counts, which increased approximately by an order of magnitude in comparison to other annealed samples as shown in the listings for Specimens III-S1 and III-S2 in Tables VI. When the specimen reached its highest stress for the fatigue test and a crack started to propagate, the AE characteristics of the specimen were essentially the same as those of the cold worked specimens of this alloy. The number of AE counts, however, was slightly larger than those in the cold worked specimens. These specimens showed no evidence of any surface cracks when a large number of AE counts

were observed accompanied by numerous spikes in the $\bar{V}_r$ vs. time curve. However, the presence of an extensive plastic zone ahead of the notch was clearly recognized.

4.3.5 Alloy IV

A total of seven specimens was tested in the cold worked condition. The total number of AE counts was between 1.5 x 10^3 and 27 x 10^3 with the following distribution: 60% generated during the elastic part and more than 30% during the inelastic part, on the average. Without including the first cycle the AE counts ranged from 150 to 9000 out of which 30% resulted from the elastic part and 55% from the inelastic part, on the average, as indicated in Table IV. There was a large scatter of the AE count data among various specimens. The number of counts usually declined drastically after the initial few cycles. It is significant that the number of the counts per cycle generated during the inelastic part is low. Most of the ΔN_i were generated in a few large jumps, for which corresponding large spikes in the $\bar{V}_r$ vs. time curve were observed. For instance, large ΔN_i counts and the corresponding spike were observed during the following cycles; the eighth, thirtieth and thirty-fifth cycles of Specimen IV-3, the eighth and ninth cycles of Specimen IV-4, and the fourth cycle of Specimen IV-8. These are likely to be of the extraneous origin, rather than valid AE signals. During many cycles when the crack was propagating 0.5 to 1.5mm per cycle, no AE count was observed. The rms voltage was typically the same as Alloy II; that is, no increase over the background level except for spikes in the V_r vs. time curve during the first loading cycle and occasionally observed spikes. Thus, much of the observed AE indications from Alloy IV samples appear to have little correlation to fatigue crack propagation, as in the case of Alloy II.

4.3.6 Alloy V

The eight specimens tested in the cold worked condition had the total AE counts in the range of 3.9 x 10^3 to 32.6 x 10^3. One specimen (V-2) produced only 878 counts, which appear to be due to an ineffective bonding between the transducer and the specimen. Excluding the data of Specimen V-2, the above counts were distributed, on the average, as follows: 43% of the AE counts were generated during the elastic part and 55% during the inelastic part. After subtracting the first cycle, the total AE counts were reduced to 472 to 4200, with 30% of the total resulting from the elastic part and 60% from the inelastic part, as shown in Table IV. The general features of the AE counts and rms voltages are basically similar to those observed in Alloys II and IV. In the case of Alloy V, however, certain samples (e.g., V-8, 9 and 10) generated reasonably high levels of ΔN_i (up to several hundreds counts) corresponding to fatigue crack propagation. Most of these AE counts were observed without accompanying large spikes in the $\bar{V}_r$ vs. time curve. Therefore, some of the observed AE counts appear to be produced from an advancing fatigue crack.

4.3.7 Repeatedly Annealed Condition

a. Alloys II, III and V

Two specimens of Alloy II and one specimen each of Alloys III and V were tested in this condition, that is, initial annealing at 650°C plus repeated annealing at 538°C after each fatigue cycle.

The total number of AE counts was quite high and was in the range of 2.6×10^5 to 9.2×10^5, as shown in Table V. The distribution of the counts was the following: the elastic part of the fatigue cycle produced 75% of the total, and the inelastic contribution was 25%. This distribution changed little after the first cycle, which produced only a small percentage (3% to 18%) of the total AE counts in contrast to the cold worked sample results. During the first cycle, the V_r vs. time curve showed a smooth increase at the yielding due to the continuous type emissions. The increase over the background level was from 0.1 μV in the case of Alloy V and up to 0.5 μV in the case of Alloy III. A small number of spikes were superimposed, as shown in Fig. 7a. In the subsequent loading cycles,the contribution from continuous type emissions was reduced to less than 0.08 μV in Alloy III and even lower in other alloys. In contrast, the magnitude of the burst spikes became quite large, i.e., over several μV above the background level. The magnitude of the spikes was reduced beyond several cycles to the level of bursts often seen at the first cycle of the cold worked speimens, and with the exception of Alloy III, the contribution from continuous type emissions was absent on the V_r vs. time curve. The number of observed AE counts per cycle increased for the initial several cycles as shown in Fig. 7b, but beyond the middle of the test it started to decline gradually as indicated in Fig. 7c. The small spikes seen in Fig. 7a both in the early portion of elastic part and the unloading part can be attributed to extraneous noise from the loading system present in each cycle. These are due to the removal and remounting of the specimen grips for annealing between each fatigue cycle, although the specimen itself was not removed from the grips. The large spikes, although originating from the elastic state are believed to be intrinsic AE signals and are likely to be a product of the intergranular cracking (see Section 4.2). Those spikes may also be due to the fracture of oxide particles as the surface cracks began to open. The oxide particles (or films) can be formed at the tip of the cracks during the heat treatments.

Effect of the heat treatments on the mechanical properties is indicated in Fig. 7c. The recovery of the flow stress and low strain hardening rates can be seen.

b. Alloy IV

One specimen, IV-T1, of this alloy was tested in the repeatedly annealed condition. Judging from the total number of AE counts of 5.4×10^5, this alloy was within the range of the rest of the alloys for this condition. However, its behavior was quite different. Over 50% of the total AE counts were generated during the first cycle. The distribution of the AE counts was the following: 61% resulting from the elastic part and 35% from

the inelastic part. This distribution changed very little after the first cycle. 65% of the AE counts were generated in the elastic part and 31% in the inelastic part, as shown in Table V. The first cycle produced most of the AE counts, after which the number of AE counts per cycle tended to decrease although some cycles deviated from this pattern. The rms voltage of the AE signal was mainly of the burst type with most spikes being in the elastic part. The number and magnitude of these spikes was declining as the cycling continued. The amount of continuous emissions on the $\bar{V}_r$ vs. time curve was small, less than 0.05 μV and was present during the first three cycles only. This alloy sample was annealed similarly to the other alloys, but showed only a partial softening. This was also reflected in the stress-strain curve, exhibiting only a partial recovery of the yield strength. These results suggest that the observed AE activities for Specimen IV-T1 consist mostly of extraneous origins. In particular, the large number of bursts in the first cycle appear to be suspicious, because primarily plastic deformation occurred during this loading cycle. As no surface crack appeared and fatigue crack propagation was minimal, only continuous type emissions should have been observed in the first cycle. The fractographic observation also revealed no significant change from those of the cold worked condition of this alloy. Thus, further efforts to clarify annealing effects on AE characteristics of Alloy IV will be required.

V. DISCUSSIONS

5.1 The Nature of AE Signals

In order to assess the significance of AE test results, recorded AE signals from several Alloy III samples were evaluated in detail by the observation of wave forms and frequency spectrum analysis. A video tape recorder was primarily used for this study. The following specimens were employed: III-9, III-N2, III-N3, III-T1, III-NT2, III-S2 and a couple of smooth tensile specimens of this alloy.

Observed wave forms of burst type AE signals were quite varied, but could be broadly classified into seven types. In Figs. 9 to 16, typical examples of the wave forms are shown together with the corresponding frequency spectra.

A -type: a clipped, high amplitude burst with a short rise time and a decay time of approximately 1 msec (Fig. 9).

B -type: a large peak amplitude burst similar to A-type, but no clipping (Figs. 10 and 11).

C -type: a moderately strong peak with a rise time of approximately 100 μsec, followed by a series of smaller peaks over 0.5 to 1 msec. No exponential decay pattern (Fig. 12).

D -type: a short duration (0.5 msec), low to medium amplitude burst, which is intermediate between B- and C-types (Fig. 13).

E -type: a short burst signal lasting less than 100 μsec (Fig. 9).

E'-type: an E-type burst, but its amplitude is low and is impossible to clearly distinguish from the continuous type signal or the background noise (Fig. 14).

F -type: a group of numerous low amplitude bursts occurring over 2 to 3 msec (Fig. 15).

G -type: a slow rising and decaying burst lasting 1 to 2 msec with several peaks and crests (Fig. 16).

Distinction between different type signals was often not clear; especially among B-, C- and D-types. A-type signals were presumably of the same origin as B-type bursts, except for the peak amplitude. While it was not possible to positively identify the source of a particular type burst, the most likely mechanism of AE generation can be deduced from a specific test condition. F- and G-types can be attributed to extraneous noise sources; the former was observed coinciding with the switching of tensile testing machine. Consequently, an electrical spark can be suspected, although the regular AE transducer (AC 375) was much less sensitive to such an interface because of differential circuit employed. The latter appears to be a mechanical noise

because this type was observed, albeit infrequently and irregularly, during the yielding of annealed samples where mostly continuous type signals were present. The slow rise time also suggests a long travel time of the burst signal from the source to a transducer, possibily from the ball joint of a grip. Burst signals of A-type were associated with the slipping in a grip during one of the tests, in which the particular sample had failed within the grip. Such signals were also found at the lower stress levels of the first fatigue cycle, again suggesting the grip area to be the likeliest noise source.

In order to gain better understanding of the AE sources, all the burst signals found during the tests of Specimen III-N2 and III-NT2 were evaluated visually, and classified. The results are shown in Figs. 17 and 18, respectively. In the cold worked condition, the first cycle was most active from the observation of $\bar{V}_r$ curve (see Fig. 5a). Actual observation of recorded signals was consistent with this expectation. As Fig. 17 indicates, 11 bursts with more than one-half to be A- and B-types were observed in the stress range of up to 20 kg/mm^2. The higher stress elastic range (21 to 35 kg/mm^2) showed the highest burst activities. Most of the burst signals were D- and E-types. This range, however, showed only a few spikes in the $\bar{V}_r$ vs. time plot (Fig. 5a). As strain increased rapidly, and the crack started to propagate at a higher stress range (36-38 kg/mm), a smooth increase in $\bar{V}_r$ was noted, but the number of burst signals was reduced significantly. During the second cycle, only two bursts were observed, but the number of E-type burst signals increased to 5~6 in the third and fourth cycles. Both E- and E'-type bursts became still higher in the subsequent cycles. Results from Specimen III-NT2 were different, as one may expect from the $\bar{V}_r$ vs. time curve for this condition (Fig. 6a). Although the observed V_r vs. time curve exhibited little evidence of burst signals, a moderate number of burst signals was noticed as can be seen in Fig. 18. Again, A- and B-types were found at an earlier stage, while E-type was dominant in the third through fifth cycles. The burst activities were low between the seventh and fourteenth cycles, but E-type became quite active once crack propagation started to occur at the fourteenth cycle. In this portion, smaller amplitude burst signals of E'-type were also quite active. However, the number of these signals was impossible to determine and was not counted.

Since E- and E'-types have been observed during both plastic deformation and crack propagation, these signals are concluded to be intrinsic AE signals. Since dislocation glide and void coalescence cannot be expected to produce such a burst signal, it is likely that the cracking of a second-phase particle, say, zirconium oxide, is the source of the observed AE burst. Fractographic observations on Alloy III also lend support to this interpretation.

Another observation provides a strong confirmation of the AE generation mechanism via particle cracking. When Specimen III-S2 was deformed, strong burst signals of B-type were detected without any sign of crack initiation. Since only plastic deformation occurred, the source of the burst signals again must be sought from the cracking of second-phase particles. As this

specimen material was the softest among the four alloys tested, it is expected that the second phase particles were quite coarse, explaining the magnitude of the burst signals. It is not clear, however, why the exponential decay pattern arises for B- (or A-) type, but not for E-type, even when the peak amplitudes were comparable.

At present, C- and D-type burst signals cannot be correlated to specific mechanisms, although these also appear to be intrinsic AE signals. In the case of C-type burst, more than one physical process may result in the observed wave form. Particle cracking followed either by shearing or by normal rupture via equiaxed dimple formation can be possible AE generation mechanisms for the C-type signal.

During careful examination of recorded AE signals, it was noted that some continuous type signals differ from usual random noise. The wave form is not a suitable means to characterize such a quasi-continuous signal. An example is shown in Fig. 19. While the wave form is little different from white noise, the accompanying frequency spectrum clearly shows the presence of resonances at 40 and 100 kHz. The physical meaning of these quasi-continuous AE signals is not known at present.

5.2 Frequency Spectrum Analysis

Because of low AE signal levels in all the tests, the frequency spectrum analysis method used in our previous studies (ref. 3, 25, 26) produced no detectable change in the frequency spectrum compared to the spectrum of the background, which is shown in Fig. 20a. Note that the transducer resonance at 470 kHz is excited by mechanical noise in the specimen or by resonating the preamplifier imput circuit. Subsequently, the method was modified, in which a short segment of the AE signal was fed repeatedly to the correlation analyzer through a gated amplifier, effectively enhancing the desired signal. Results of frequency spectrum analyses are shown with the corresponding wave forms in Figs. 9 through 16 and in Fig. 19.

Generally, low frequency resonances below 100 kHz were present. A weak and broad transducer resonance exists at 440-500 kHz, with the peak frequency of approximately 470 kHz. The transducer resonance peak was not always detected. Except for these resonances, observed frequency spectra exhibited nearly flat response. The strongest resonance peak was observed most often at 38-40 kHz. Peaks were also found at 20-25 kHz, 57-60 kHz, 78-82 kHz, 90-100 kHz as well as at 110-120 kHz. The wave form and frequency spectrum of a burst signal in Fig. 11 were obtained by recording the signal in an instrumentation tape recorder, reproducing it at one-quarter of the original tape speed and re-recording on a video tape recorder. Thus, the frequency range of 0-2 MHz was obtained. The strongest peak in this case was the transducer resonance peak at 470 kHz. A group of peaks at the 700-1000 kHz frequency range was also detected.

These low frequency resonance peaks appear to be produced by specimen resonances. While no theoretical analysis of the waves existing in the specimen is available, resonance frequencies can be estimated on the basis of

probable standing wave modes for the extensional and Lamb waves (ref. 26, 27). Using the data of copper,the extensional wave velocity is 3.71×10^5 cm/sec and the shear wave velocity is 2.26×10^5 cm/sec, respectively. The principal specimen dimensions are: 9.1 cm between grips, 1.9cm width, 1.3 cm gauge section width and length and 0.16 cm thickness. Obviously, the thickness resonance occurs at frequencies close to 1 MHz and cannot produce the observed peaks. One of the plausible origins of the resonances is the extensional wave resonances along the specimen length, which occur at $(3.71 \times 10^5)/(2 \times 9.1) = 20.3$ kHz and at its harmonics. These can be excited by a sudden extension of a specimen via rupture and particle cracking. Thus, these appear to be responsible for the strong peak near 40 kHz as well as the peaks at 20, 60, 80 and 100 kHz. Because of a high-pass filter cutoff frequency of 30 kHz, the peak amplitude at 20 kHz is expected to be lower. When the strongest peak occurs near 80 or 100 kHz, however, the above explanation becomes untenable, This is due to the fact that lower harmonics are expected to produce larger displacements, resulting in higher transducer output. When a strong peak is found near 100 kHz, this may be related to the resonance of extensional waves at the specimen width or the gauge section length, which is expected at 97 kHz for the resonating length of 1.9 cm. A similar resonance may also exist at 146 kHz due to the gauge section width of 1.3 cm. Since the transducer used in this study detects the surface displacement normal to the broad face of the sample, it is not clear whether these resonances can be detected efficiently with the present configuration. However, other probable resonance modes are less attractive. For example, shear wave resonances have the fundamental frequencies of 89, 59 and 12.4 kHz corresponding to the resonating length of 1.3, 1.9 and 9.1 cm, respectively. It is more difficult to reconcile the observed results with these predictions.

In order to evaluate the mode of transducer excitation and the nature of AE signals, the frequency spectra were determined by exciting a specimen mounted in grips with a highly damped compression mode transducer for the ultrasonic pulse-echo flaw detection (Branson Type Z101C 5.0 MHz, 1.3 cm). This was excited by amplified random noise at $5V_{rms}$, band-limited to 0.02-5 MHz. Frequency spectrum shown in Fig. 20b was obtained by coupling the 5 MHz transducer on the specimen surface at the center of gauge section. This spectrum shows several strong peaks in the 150-300 kHz can also be recognized. The peaks at 100, 150 and 300 kHz are likely to be related to the width resonances discussed above. The power density in the low frequency range below 100 kHz was low, indicating that the observed AE signals from fatigue tests were not excited by the displacement normal to the sample surface. When the specimen was excited from one end along the specimen length direction, keeping the distance between the grips at 9.1 cm, the resultant frequency spectrum had stronger low frequency peaks as shown in Fig. 20c. The peaks at 100 kHz were the strongest, but peaks at 40, 60 and 82 kHz were also present. Numerous peaks were also observed at higher frequencies, especially between 180 and 340 kHz, and at 420, 465 and 480 kHz. The presence of the low frequency peaks similar to those observed in the fatigue tests suggests that the lengthwise propagation of extensional wave is indeed responsible for the resonance characteristics detected. In still another series of tests, random shear waves travelling along the specimen length direction inclined 45° to the

specimen surface were generated. For this purpose, an ultrasonic transducer with a built-in plastic wedge (Automation Industries SMZ 2.25 MHz) was used. This transducer was placed at 6.5 cm from the regular position of the wide-band AE transducer. In addition to strong power density in the 200-310 kHz range, a strong peak at 80 kHz as well as peaks at 100 and 125 kHz were found. Thus, the strong peak at 82 kHz found in Fig. 12 can be related to shear waves generated during crack propagation.

These results with random wave excitation further support our contention that the significant variations in the observed frequency spectra of AE signals are primarily related to sample resonances. It also demonstrates that the mode of AE waves is an important parameter in total characterization of AE signals.

5.3 Amplitude Distribution Analysis

The AE signals recorded during testing of several Alloy III samples were repeatedly processed through a signal processor, each time with a different threshold voltage setting. Both automatic and manual modes of Model 201 Signal Processor were utilized. This analysis technique provides the cumulative amplitude distribution function $N_D(V_t)$, defined as the number of counts measured with a threshold value V_t, for a particular segment of AE testing. N_D can also be expressed in terms of count rate, when the duration of the analyzed segment is normalized. N_D is the product of peak amplitude distribution function $N_p(V_t)$, which is the number of AE events that have the peak amplitude exceeding V_t and the number of counts per AE event, n_e; i.e., $N_D = N_p \cdot n_e$ (ref. 3, 28). Since the number of AE events in any of the present tests has been small, as discussed previously, no statistically meaningful analysis of N_p is possible from our determination of N_D. However, the characteristic mixtures of continuous and burst type AE signals have been reflected in the observed N_D - V_t relationships, which may possibly be utilized in future AE applications for nondestructive testing.

Typical results of the present amplitude distribution analysis are shown in Figs. 21 and 22. In Fig. 21, the average AE count rates during the initial yielding portion of an unnotched tensile specimen of Alloy III are plotted against relative threshold voltage. This plot is fully logarithmic and the straight line portions represent the following power relation: $\dot{N} = B\ V_t^{\ c}$, where B and c are constants. Note that c is proportional to the slope and that V_t is given in dB scale, so that 20 dB corresponds to a factor of 10 change in V_t. Four different test conditions were utilized, combining two types of transducers (wideband and AC 375) and automatic and manual threshold modes. All the four curves show a straight line portion with c of 5.5 to 15 and a deviation at greater V_t values to a lower value of c (approaching 1.5). With the use of a more sensitive resonant sensor (AC 375), identical AE counts were observed with V_t setting of 11 to 12 dB higher. The c value was affected little by the type of transducer. The automatic threshold mode produced the identical AE counts in the signal processor at V_t set 5 to 8 dB lower in comparison to the manual mode, reflecting the background subtraction in the auotmatic mode. The c values for the straight portion

with the automatic mode was less than one-half of those with the manual mode. This again is a consequence of the background subtraction that suppresses the AE counts when the signal level approaches that of the background level. Thus, the automatic threshold is not suited for the purpose of amplitude distribution analysis of AE signals. The automatic mode also tends to obscure the transition in c values.

The observation of high c values in this case results from the continuous type AE signals generated during the yielding of the unnotched tensile sample. Oscilloscope observations support this conclusion; furthermore, this is also similar to previous findings by others. Hamstad and Mukherjee (ref. 29) reported that continuous AE signals during tensile testing of 7075-T6 Aℓ alloy produced AE count rates very sensitive to V_t setting. A 2 dB change in V_t resulted in a 10 times change in AE count rates. This is equivalent to c = 10. Jax and Eisenblätter (ref. 30) reported an exponential dependence of AE count rates on V_t in tensile tests of several alloys. Although the type of dependency was different, observed AE count rates were sensitive to the V_t setting.

Only a few burst type signals were observed on an oscilloscope. These burst signals, however, appear to produce the deviation from a straight line in Fig. 21 at higher V_t values.

Figure 22 shows effects of V_t on AE count rates during fatigue testing of Specimens III-N3 and III-NT2. The average count rate for a given fatigue cycle is plotted aginst V_t. In the annealed sample (NT2), the c values were quite large (13$\sim$20) for the initial stage of the fatigue test (n=1,3), where the increase in V_r was significant (see Fig. 6a) and mostly continuous type signals were observed. The deviation to lower c values was noted in the case of a wideband transducer, suggesting the presence of a few burst signals. Only the straight line portion was revealed in the test with an AC 375 transducer. This is probably due to a narrow range of V_t examined in the test. When the AE signals from the final stage of the fatigue test were analyzed, much smaller slopes of the $\dot{N}$ - V_t curves were found, corresponding to c = 2.7$\sim$4 with an AC 375 transducer. The results with the wideband transducer was similar to those of the initial stage, but the transition in the c values was more distinct. Considerable crack propagation occurred during these cycles of n = 15 and 16, any many burst signals of E-type (and E'-type) were observed. Similarly, the results from Specimen III-N3 indicate c of 2.2 for the first cycle and 3 to 6 for the second through the sixth cycles, as shown by the dotted lines in Fig. 22. (These and other c values are summarized in Table VII.) This specimen was in the cold worked condition and crack propagation started from the first cycle. Thus, the c values in the range of 2 to 6 can be attributed to burst-type AE signals, in particular, E- and E'-types and correlated to crack propagation in Alloy III.

During the seventh and eighth cycles of the fatigue test of Specimen III-S2, numerous strong burst signals (B-type) were observed as noted earlier. These large burst signals resulted in the c values of 1 to 1.8 (see Table VII). Consequently, the c values less than 2 can be

correlated to these strong signals with characteristic exponential decay pattern (see Fig. 10). Since mechanical noise also appears to contribute such a signal wave form as well as A- and C-types, the observation of low c values in other instances, such as in the smooth tensile specimen ($c = 1.5$), and in the first cycle of III-N2 and III-N3, can be attributed to the simultaneous detection of these large burst signals.

Low c values due to burst AE signals have been reported previously. Pollack (ref. 31) reported the range of 0.4 to 2 for the peak amplitude distribution, while Brindley et al. (ref.28) measured the value of 1.6 for AE signals due to the plastic zone growth in a low carbon steel fracture toughness sample. The latter authors also showed that c is expected to be 1.5 when n_e has a logarithmic dependence on V_t as Harris et al. originally suggested (ref. 32); i.e., when the burst signals are of B-type. This further suggests that the main V_t dependence arises through n_e rather than N_p. This accounts for the findings in Specimen III-S2.

Intermediate c values (3~7) may be, at least in part, due to mixing of the continuous type and burst type signals. However, these observations are closely related to the predominance of E- and E'-type AE signals, indicating that N_p plays a major part in determining amplitude dependence. This type of burst signals is short (less than 0.3 msec) and has a steep rise and decay pattern. While no specific experimental analysis was performed, it is expected to produce n_e that is less sensitive to V_t. Consequently, much of the observed V_t dependence must be borne by N_p. These observations are consistent with the expected AE generation mechanism for this kind of AE signals; namely, crack propagation via the second phase particle cracking and subsequent normal rupture of equiaxed dimples. No previous report of this AE behavior has been uncovered, but this finding is clearly beneficial for practical uses of AE methods. For example, usual AE source location schemes cannot identify the wave form of an AE signal. However, the amplitude distribution analysis that can be incorporated in the source location program can provide the information, which can subsequently be correlated to a specific AE generation mechanism.

5.4 Sources of AE Signals

The detailed evaluation of AE signals from Alloy III presented in the preceding sections shows that several distinct types of AE signals are generated during cyclic loading of notched specimens. These include: a) extraneous noise from electronic and mechanical sources, b) continuous type signals from the yielding and plastic flow, c) burst signals from crack propagation, and d) the closure of a crack. The extraneous noises were produced at the grips, the loading train and electrical switching and resulted in A-, B-, F- and G-type burst signals. In the cold worked condition of Alloys II, IV and V, these noises dominated the AE signals observed, especially during the first loading cycle. Since the maximum load during subsequent loading cycles was lower than that reached in the first cycle, these noise sources no longer affected significantly the AE characteristics of the succeeding cycles. In these materials, except Alloy V crack propagation

produced negligible AE responses. This behavior can be traced to their fracture modes. In Alloys II and V, the predominant mode of fracture was shearing with occasional particle cracking. Since the shearing is merely the advanced stage of plastic deformation, the lack of AE is expected. In Alloy IV, very fine dimples were found on the fracture surfaces. No visible particle can be identified. Again, low AE activities are expected. In Alloy V, however, some fractured particles were found in the SEM observations suggesting that these provided AE signal sources.

As previously described in detail, the first cycle of the fatigue test of a cold worked Alloy III sample produced numerous bursts of extraneous origin. However, E-type signals were also present as plastic deformation became extensive. These appear to arise from the cracking of second phase particles within the plastic zone ahead of the notch. The continuous signals observed throughout the inelastic parts of the fatigue test can be expected from the plastic deformation. Numerous E- and E'-type burst signals, which were detected as a crack started to propagate, can be reasonably attributed to the fracture of second phase particles on the fracture surface, that leads to dimple rupture. Since the observed high power density of C-type signals at 80 kHz coincides with the strong peak due to shear eave excitation, shearing on the fracture surface, which was inclined approximately 45° to the specimen surface, can be a source of the C-type signals. The shearing can possibly account for the trailing portion of a C-type burst, while the initial high burst is triggered by a cracking particle as in the case of E-type emission.

The main change in the AE behavior of annealed samples is the high levels of continuous type AE signals at the early stages of fatigue tests. Again, this is due to the development of a plastic zone. Burst signals that appear to be extraneous noise were observed in the first two cycles. E-type burst signals presumed to be produced by particle cracking became more numerous beyond the third cycle. Crack propagation in the annealed Alloy III samples produced AE signals similar to those found in the cold worked samples. It is also significant to note that different annealing conditions produce vastly different AE characteristics. The heat treatment of the Alloy III plate stock is not known, but, because of its low yield strength and hardness values, this material must have received high temperature annealing treatment (well above 650°C). In this condition, therefore, it is natural to expect coarser zirconium oxide particles, of which cracking during plastic deformation is apparently the origin of strong B-type burst signals. A transmission electron microscopic study may provide a direct evidence of this process. SEM fractographs have revealed no direct indication for this source, which has probably taken place internally.

In most of the cases discussed above, AE from crack closure was insignificant. This is in a marked contrast to the findings during high cycle fatigue tests, in which the friction of the fracture surfaces is the principal source of AE signals (ref. 16b, 21b). This difference is due to the high strain amplitude employed in the present study. Since extensive plastic deformation produced a large crack tip opening displacement, unloading was expected to allow only a small fracture area to close.

Repeated annealing between fatigue cycles produced numerous burst type signals in Alloys II, III and V. Similar burst signals in Alloy IV samples of this condition appear to be extraneous as described previously. It is important to note that the number of burst signals during the first cycle was comparable to other conditions. The burst signals in the repeatedly annealed conditions were much more numerous and stronger than those arising from the extraneous noise from grips or loading mechanisms. Besides, the extraneous noise cannot be expected to become more numerous during the second cycle, when the applied load is less than that reached during the first cycle. The burst signals after repeated annealing were primarily generated in the elastic part, in particular, the upper half portion. This coincided with the initiation of surface cracks within the plastic zone that had been produced by the first loading. As the SEM fratographs demonstrated earlier (Photo 10), these surface cracks were intergranular cracks. It is, thus, reasonable to conclude that the burst signals were produced by the intergranular cracking, since a sudden normal rupture at grain boundaries is expected to produce an AE burst. Since very fine dimples were found at the fractured grain boundaries (Photo 10c), the fracture was likely to have occurred in the grain immediately adjacent to the grain boundaries. This change in the fracture mode can be a consequence of strain induced precipitation, which strengthened the grains relative to the grain boundaries. Other AE sources discussed in other conditions of Alloy III samples are expected to operate in this condition as well, but their contributions to the total AE characteristics are negligibly small.

5.5 Metallurgical Problems

As revealed by repeated annealing experiments, zirconium containing copper alloys, Alloys II, III and V, are susceptible to embrittlement at grain boundaries following plastic deformation and subsequent annealing. Since the hardness of the repeatedly annealed samples sometimes was higher than the initial condition (Table I), the precipitation of zirconium rich phase at dislocations can be expected. Microstructural studies of these alloys are limited (ref. 33), so that the nature of the observed grain boundary embrittlement cannot be established. Weakening at precipitate free zones near grain boundaries (ref. 34) can be a possible cause.

Another potential problem in these zirconium containing alloys is the formation of blisters. Although no systematic attempt has been made in the present study for its cause, the presence of rolling defects and hydrogen absorption during annealing appear to be required conditions for the blistering. Thus, proposed uses of these alloys must evaluate the fabrication processes and operation conditions carefully to avoid possible damages due to the blister formation.

In Alloy III, the present study has uncovered a high degree of material variability, including the difference in the yield strength, susceptibility to cracking via rolling and crack propagation characteristics. Two starting materials of Alloy III produced quite different annealing responses. When cold rolled sheets were annealed at 650°C for 10 min., the specimen produced

from the sheet stock (received in 37% cold rolled condition) had the notch yield strength of 18.4 kg/mm². On the other hand, the annealed specimen prepared from the plate stock and given a 37% cold rolling had the corresponding quantity of 10.3 kg/mm². The latter was similar to the notch yield strength of the as-received plate. Possible sources of such strength variations may be the state of zirconium additions within the microstructures. Since this element can strengthen the matrix via precipitation and can combine with interstitial impurity atoms such as oxygen and hydrogen, it is understandable that prior thermal-mechanical history has a strong influence on the mechanical properties. The tendency of cracking during cold rolling may be traced to rolling practices, but the presence of second phase particles can also be crucial. The large variation in crack propagation rates observed in this study appears to be a consequence of rolling defects. Practical effects of such a variation are detrimental; thus, the rolling defects must be completely eliminated either by changes in rolling practices or by effective nondestructive evaluation procedures. It appears that microstructural studies of Alloy III are essential in order to clarify the origins of these degrading effects and to avoid any future problems arising from these effects.

5.6 Recommendations

1. The observed AE characteristics of cold worked Alloy III and possibly Alloy V, appear to provide the basis of developing nondestructive testing methods via AE techniques. The signal levels from crack propagation are only moderate, so that transducer spacings and detection threshold levels must be adjusted to obtain the highest sensitivity feasible. Developmental studies of establishing an AE source location scheme will be required. In the case of repeatedly annealed materials that emit numerous strong burst signals, the presently available equipment for the AE source location can be utilized without much difficulty. Annealed materials produce continuous-type AE signals during initial plastic deformation. While reasonable intensities of AE signals are produced, it is expected that AE signals may be generated from numerous non-critical sources of a structure under test. The determination of the region where crack propagation occurs may become impossible, when plastic deformation is expected over a large area of the structure. Again, a feasibility study should be undertaken for this initial material condition.

2. While zirconium containing copper alloys have been used in many applications, few detailed metallurgical studies have been performed. Since the proposed use of these materials, among which Alloy III appears to be favored, imposes severe thermal and mechanical environments, further understanding of physical metallurgy of these materials is essential. Specifically, the strength levels of Alloy III are sensitive to prior thermal and mechanical history and the microstructural optimization should improve its performance without much added cost. Another critical effect discovered in this investigation is the development of intergranular cracking via combined influence of plastic deformation and annealing. While numerous AE signals are emitted by such a cracking, fatigue resistance is no doubt

decreased. Fatigue tests with temperature cycling should be undertaken in order to evaluate possible degradation of crack propagation characteristics. At the same time, transmission electron microscopic studies of the behavior of zirconium-containing phases in these alloys are essential for the clarification of potentially serious material problems. The role of the second phase particles in the generation of AE signals also requires further investigation.

3. While this study has not touched upon the AE characteristics of bonding layers and electroformed materials, these should be examined together with their fatigue behavior. The attenuation of ultrasonic waves in these and sheet materials should also be clarified.

VI. SUMMARY OF RESULTS AND CONCLUSIONS

6.1 Summary of Results

This study has determined the AE characteristics of five copper base alloys under low-cycle fatigue conditions. The alloys tested were the following: pure copper, zirconium-copper, NARloy-Z, Glid Cop Aℓ 10, and NASA 1-1. Pure copper was eliminated after the preliminary stage, which showed that only a low number of AE counts was produced during the test. The specimen geometry was of the SEN type, and three different loading conditions with the strain amplitude of 1 to 2%, were used. All alloys were tested in the cold worked and repeatedly annealed conditions. Alloy III (NARloy-Z) was also tested in the annealed condition. The AE signal was detected by a resonance type transducer. The rms voltage of the signal and the AE counts were determined.

The AE results of various alloys tested in the cold worked condition can be generally divided into two groups, the first including Alloys II, IV and V, and the second Alloy III. The former did not produce much AE activities. The rms voltage of the AE signal was evident only during the first cycle, and beyond this cycle the rms values were at the background level, except for occasional spikes resulting mainly from extraneous noise. The total number of the AE counts was in the range of 10^3 to 10^4 with most counts generally originating from the elastic part of the first cycle and very few counts resulting from the inelastic part that corresponds to the crack propagation. In the case of Alloy V, however, some indications of crack propagation were detected by AE counts.

In the case of the cold worked Alloy III, the rms voltage of the AE signal was mainly of the burst type during the first cycle and the subsequent cycles had showed a small increase above background due to the continuous type AE counts during the inelastic stage of each cycle. The number of the AE counts was high during the first cycle as in the other alloys, but beyond the first cycle, most AE counts resulted from the inelastic part, thus providing a very clear indication of the crack propagation process. In all these tests, the overall AE counts and rms voltages were not significantly affected by changes in the strain rates and strain amplitudes.

Alloy III was also tested in the annealed condition. This testing involved two types of specimens, i.e., standard size specimens annealed from the as-received cold worked condition and 40% thicker specimens machined from the plate stock in the soft as-received condition. In the case of the standard sized specimens the total number of AE counts was of the order of 10^3, over 90% of which originated during the inelastic part. This distribution remained essentially unchanged throughout the test. The rms voltage of the AE signal show a large amount of continuous type emissions during the first four cycles. When the specimen reached the highest stress of the test and a crack started to propagate, the general appearance of the AE results was very similar to those obtained in the cold worked condition for this alloy. The thick specimens had generated a much larger number of

AE counts of the order of 10^5, most of which were strong burst type signals generated during the development of a plastic zone. Both types have demonstrated a good indication of the plastic deformation process as well as crack propagation process in terms of the measured AE variables.

When tested in the repeatedly annealed condition, the specimen was initially annealed at 650°C for 10 min. in an H_2 atmosphere and then re-annealed at 538°C between each fatigue cycle. All alloys tested except Alloy IV showed similar results; i.e., very large number of AE counts throughout the test. Many strong burst type AE signals were observed along with a large number of surface cracks that have been identified as intergranular cracks. Most AE counts (80% of the total) originated at the elastic part with no significant contribution from the first cycle.

Recorded AE signals from several Alloy III samples were analyzed in detail by the observation of wave forms, frequency spectrum, and amplitude distribution analysis. Observed wave forms were classified into seven types of burst emissions, quasi-continuous and continuous types. The continuous type was basically produced by plastic deformation, during which E'type bursts were also observed. These bursts were correlated to the cracking of second phase particles. Several types of burst signals were produced by extraneous noise. Large burst signals from thick annealed samples were interpreted to be due to the cracking of second phase particles. E- and E'-types were also found at later stages of a fatigue test and were correlated to crack propagation, in which the fracture of second phase particles and subsequent dimple rupture occurred and generated these AE signals.

Frequency spectrum analysis of a short segment of AE signals was performed using a video type recorder and correlation analysis equipment. Results basically showed various sample resonances. No significant variation due to different AE signals was detected, although comparisons with the results of random wave excitation provided certain clues for the origins of observed signals and their spectrum.

Amplitude distribution analysis indicated that dependencies of AE count rate on the threshold voltage can be classified into three types: low, intermediate and high. The low dependencies were associated with burst signals having a typical exponential decay pattern, while the high dependencies were associated with continuous type signals. The intermediate dependencies were observed with AE signals having E- and E'-types generated during crack propagation. The amplitude distribution analysis, thus, can be utilized in the discrimination of different AE sources.

6.2 Conclusions

1. The AE characteristics of five copper alloys being considered for a possible use in thrust chamber walls have been evaluated under low-cycle fatigue conditions. In the cold worked condition, crack propagation in NARloy-Z produces AE signals that can be utilized for its detection.

In other alloys, with a possible exception of NASA 1-1, AE signals are too weak to reliably detect the propagation of a crack.

2. A sample of annealed alloys produces continuous type AE signals at the beginning of a fatigue test. However, as the sample work-hardens, the AE behavior becomes similar to that of a cold worked sample.

3. When a sample of zirconium containing alloys is annealed repeatedly after each fatigue loading cycle, numerous surface cracks are produced during the subsequent fatigue cycle, emitting strong burst type AE signals.

4. While frequency spectrum analysis of the AE signals does not readily identify the type of AE signals or their origins, amplitude distribution analysis exhibits responses that are characteristic of certain types of AE signals. The latter can be incorporated in nondestructive evaluation schemes of thrust chambers using AE techniques.

REFERENCES

1. Acoustic Emission, ASTM Special Technical Publication 505, Philadelphia, Pennsylvania (1972).

2. Tetelman, A.S., "Acoustic Emission and Fracture Mechanics Testing of Metals and Composites," UCLA-ENG-7249, July 1972.

3. Ono, K. Proc. of the Second Acoustic Emission Symposium, Tokyo, Japan, September, 1974, JIPA (1974) p. 4-1.

4. Green, A.T., C.S. Lockman, and R. K. Steele, Society of Plastics Engineers Annual Conf., January 1964; Modern Plastics, 41 (1964) 137.

5. Dunegan, H.L. and D. O. Harris, Ultrasonics, 7 (1969) 160.

6. "In-Service Inspection Program for Nuclear Reactor Vessels," EEI Project RP79 Final Tech. Rep., May 1973.

7. Morais, C. and Green, A., Proc. of the Second International Conf. on Structure and Mechanics and Reactor Tech., Berlin, September 1973, Vol. 6, part A, Inst. Assoc. Structural Mech., Paper G6/3.

8. Ono, K., Significance of Defects in Welded Structures, T. Kanazawa and A.S. Kobayashi, University of Tokyo Press, Tokyo, 1974, p. 48.

9. Monitoring Structural Integrity by Acoustic Emission, Proc. of the Symposium at Bal Harbour, Florida, January 1974, ASTM STP-571, Philadelphia, Pennsylvania (1975).

10. Rettig, T.W. and M. J. Felson, Corrosion 74, Proc. International Corrosion Forum, March 1974, Paper No. 65.

11. Hutton, P. H. and R. N. Ord., Research Techniques in Nondestructive Testing, Vol. I, Academic Press, New York, 1972, p. 1.

12. Nakamura, Y., Mat. Eva. 29 (1971) 8.

13. Moore, J.F., S. Tsang and G. Martin, AFML-TR-71-185, September 1971.

14. Dunegan, H.L., D. O. Harris and A.S. Tetelman, Mat. Eva. 28 (1970) 221.

15. Egle, D. M., J. R. Mitchell, K. H. Bergey and F.J. Apple, Proc. 27th Annual Conf. of the Instrument Society of America, 1972, p. 638-701.

16 a) Bailey, C.D. and W. M. Pless, Proc. 9th Symposium on NDE, San Antonio, Texas, April 1973, Southwest Res. Inst., 1973, p. 224.

b) Vary, A. and S. J. Klima, ibid, p. 258.

17. Nakasa, H., IAEA Symposium on Nuclear Power Plant Control and Inst. Prague, Czech., January 1973.

18. a) Hartbower, C.E., C.F. Morais, W. F. Reuter and P.P. Crimmins, Engr. Fracture Mech. 5 (1973) 765.

b) Hartbower, C.E., W.W. Gerberich and P.P. Crimmins, NASA CR-66303, Aerojet General Corporation, June 1966.

19. Iida, K., M. Onoe, Y. Takahashi, H. Yamada and C. Lee, Proc. of the Second Acoustic Emission Symposium, Tokyo, Japan, September 1974, JIPA (1974) p. 6-15.

20. Morton, T.M., R.M. Harrington and J.G. Bjeletich, Engr. Fracture Mech. 5 (1973) 691.

21 a) Eisenblätter, J., W. Heide, P. Jax, H. Jöst and R.V. Klot, Conf. Publ. 8 Instn. Mech. Engrs., London (1974) p. 168.

b) Eisenblätter, J. P. Jax and H.J. Schwalbe, Proc. of the Second Acoustic Emission Symposium, Tokyo, Japan, September 1974, JIPA (1974) p. 7-1.

~~22. Singh, J.J., W.T. Davis and J.H. Crews, Jr., NASA TN D-7695,~~ Langley Res. Center, October 1974.

23. a) Malone, G.A., L. Vecchies and R. Wood, NASA CR-134657, Bell Aerospace Company, June 1975.

b) Malone, G.A., R. Stauffis and R. Wood, NASA CR-120980, Bell Aerospace Company, July 1972.

c) Malone, G.A. and R.A. Duscha, "Nondestructive Evaluation of Electroformed Outer Shells for Regeneratively Cooled Thrust Chambers," Plating Magazine (to be published).

24. Reis, J.J., Research/Development, February 1972, p. 24.

25. Ono, K., R. Stern and M. Long, Jr., Ref. 1, p. 152.

26. a) Ono, K. and H. Ucisik, UCLA-ENG-7514, February 1975.

b) Man Kwan, M., M.S. thesis, University of California, Los Angeles, March 1975.

27. Egle, D.M. and A.E. Brown, UCRL-75684, June 1974.

28. Brindley, B.J., J. Holt and I.G. Palmer, Non-Destructive Testing 6(1973) 299.

29. Hamstad, M.A. and A.K. Mukherjee, Exp. Mech. 14 (1974) 33.

30. Jax, P. and J. Eisenblätter, Battelle Info. 15 (1972) 2.

31. Pollack, A., Non-Destructive Testing 6 (1973) 264.

32. Harris, D.O., A.S. Tetelman and F.A. Darwish, Ref. 1, p. 238.

33. Sohl, C.E., A. Kidron and R.J. DeAngelis, Electron Microscopy and Structure of Crystals, edited by G. Thomas, University of California Press, Berkeley, 1972, p. 494.

34. Nicholson, R.B., Strengthening Methods in Crystals, edited by A. Kelly and R.B. Nicholson, Elsevier, Amsterdam, 1971, p. 535.

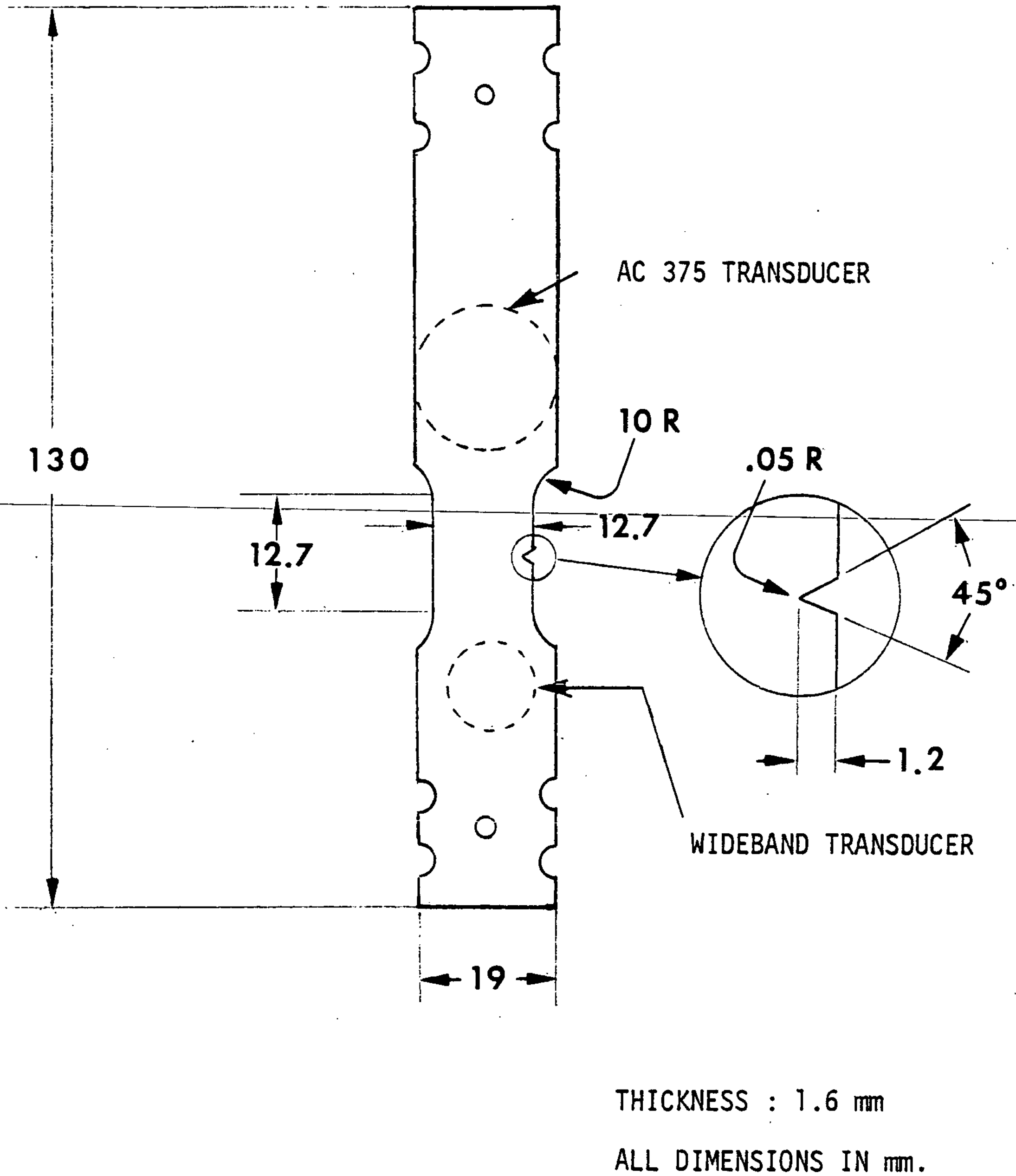

Figure 1 Test sample geometry

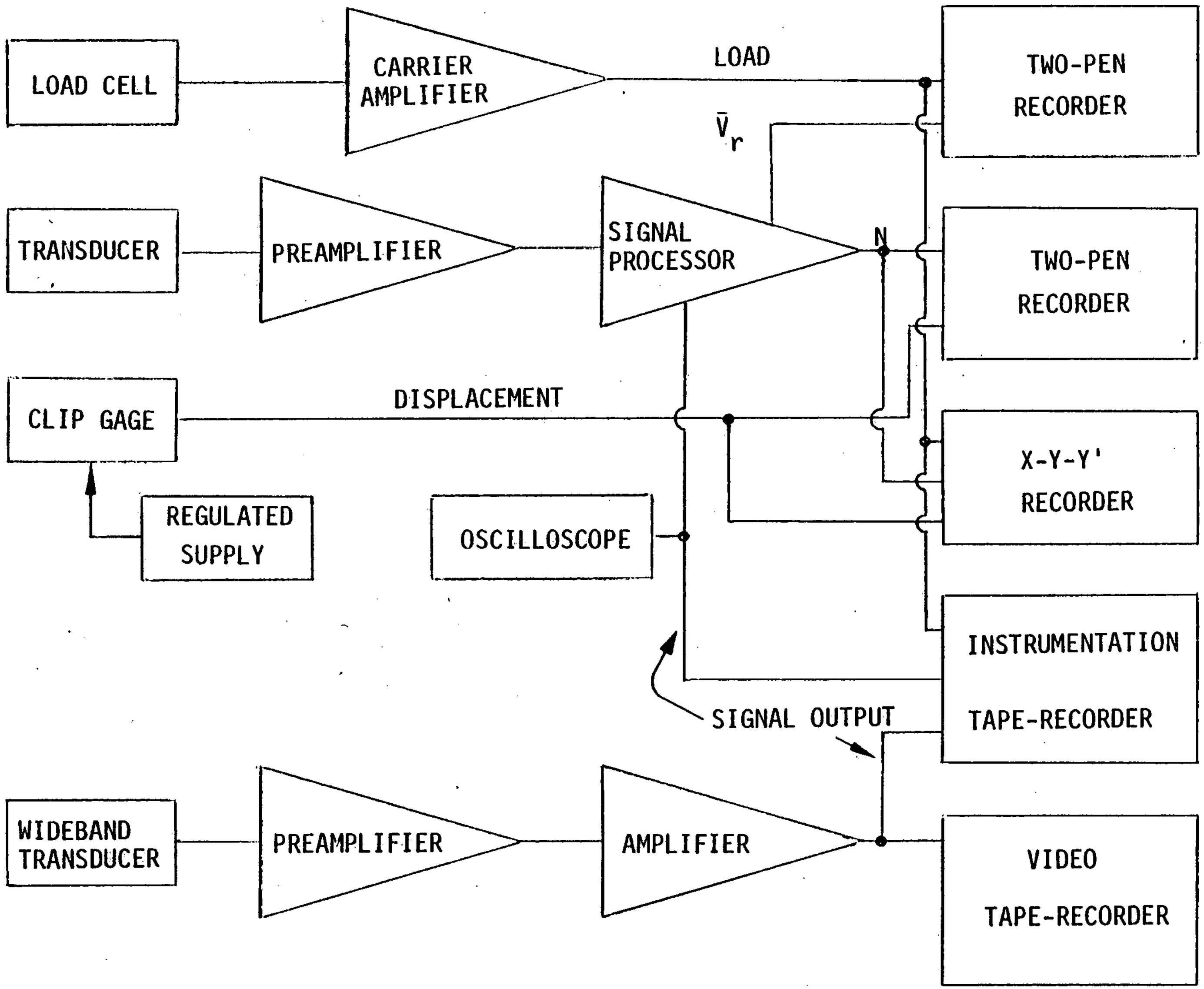

Figure 2 Block Diagram of Test Equipment

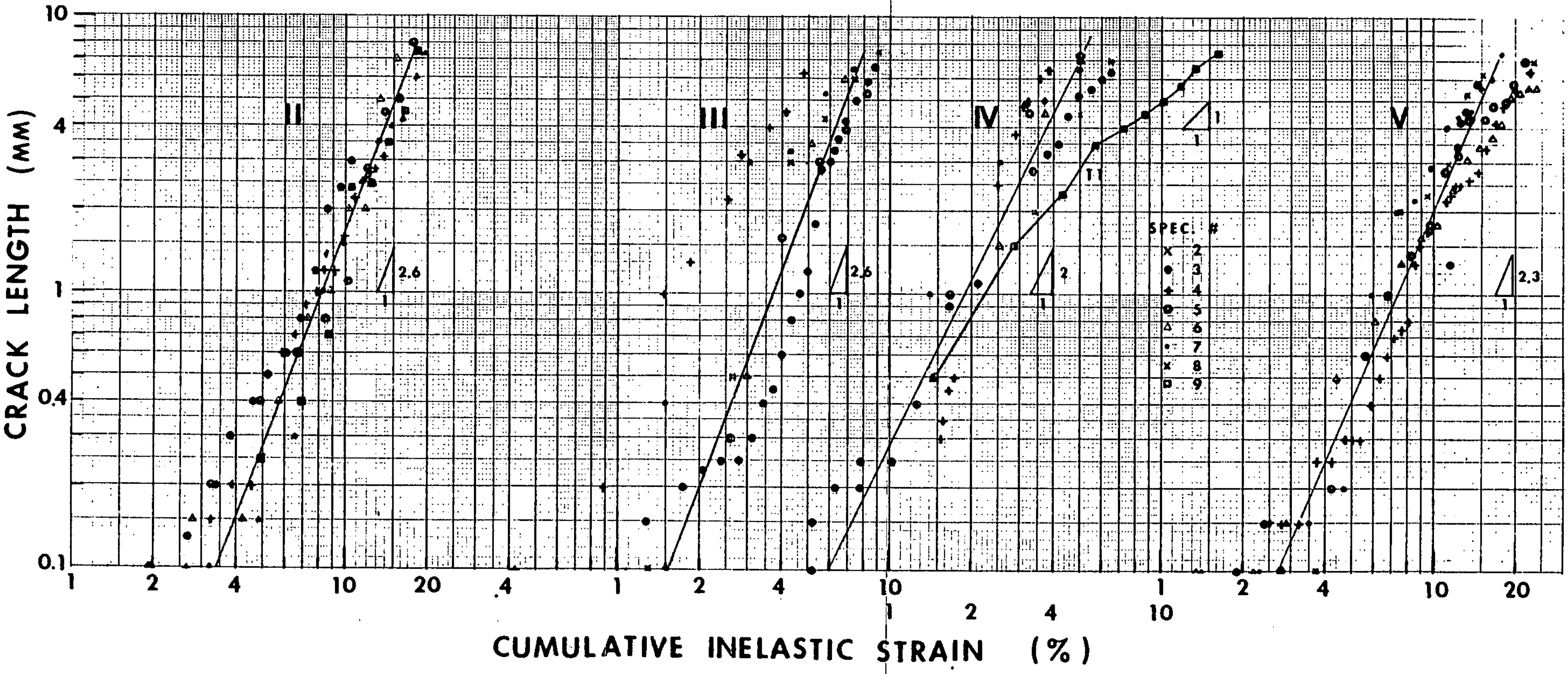

Fig. 3 Crack growth as a function of inelastic strain

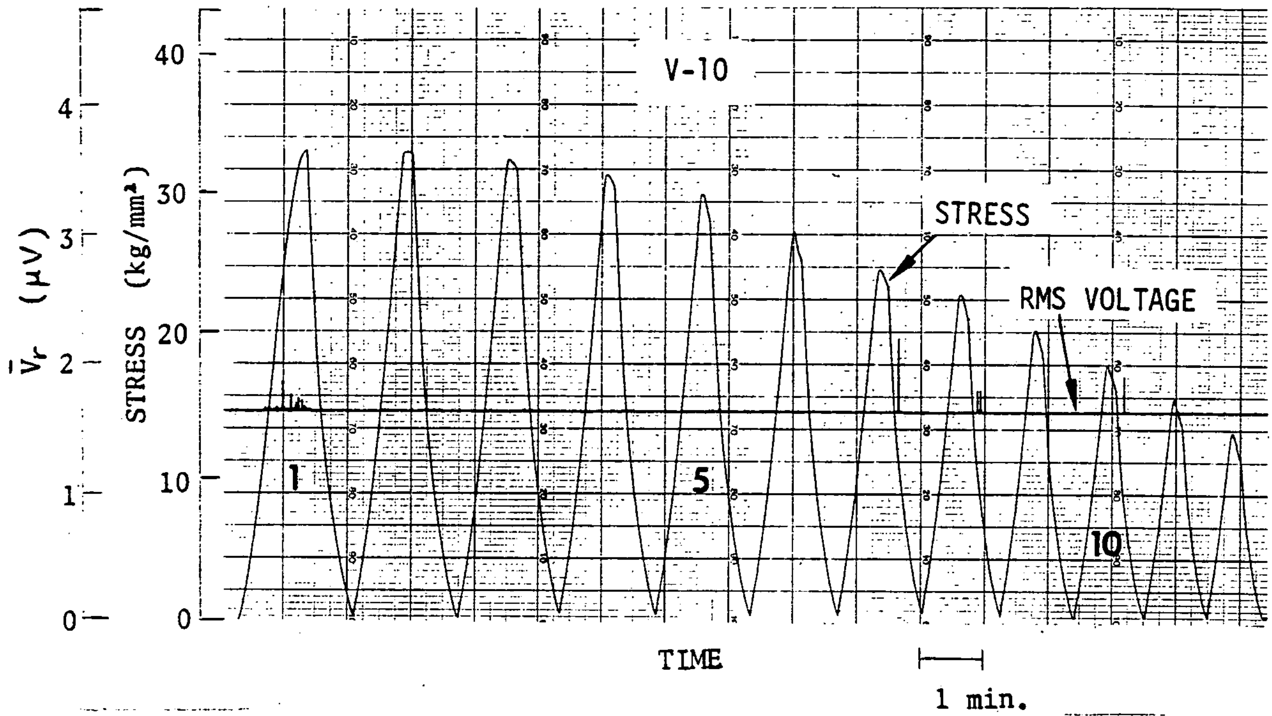

Fig. 4 AE test data of Specimen No. V-10 (cold worked, 2% strain amplitude). a) Stress and rms voltages vs. time

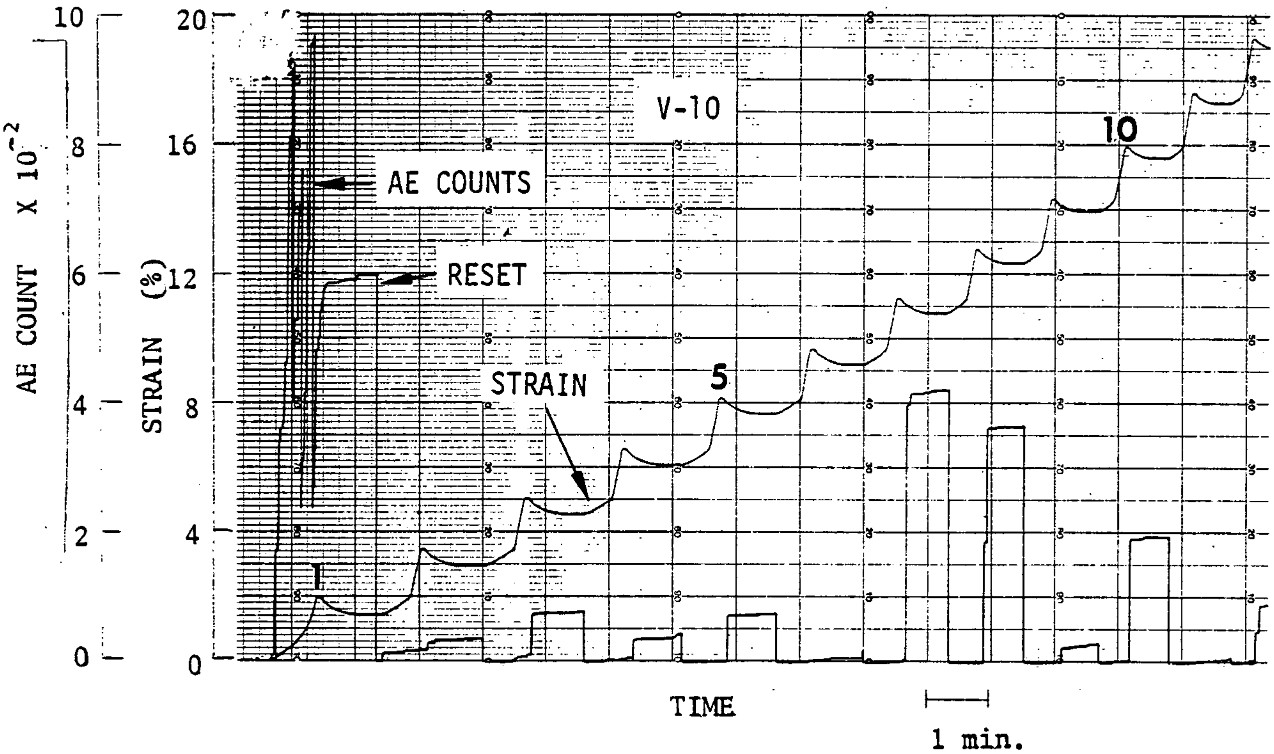

Fig. 4(b) Strain and AE counts vs. time

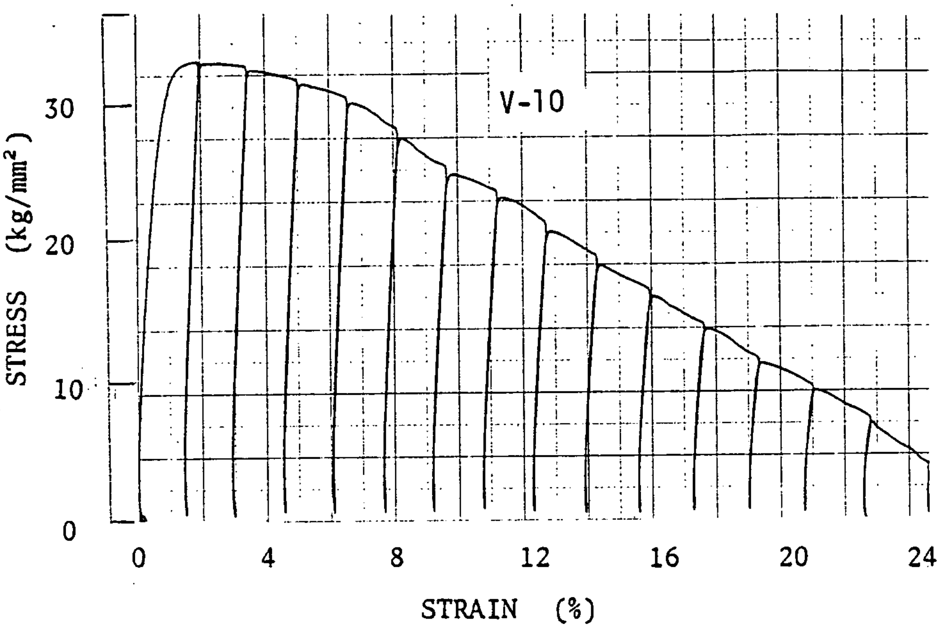

Fig. 4(c) Stress vs. strain

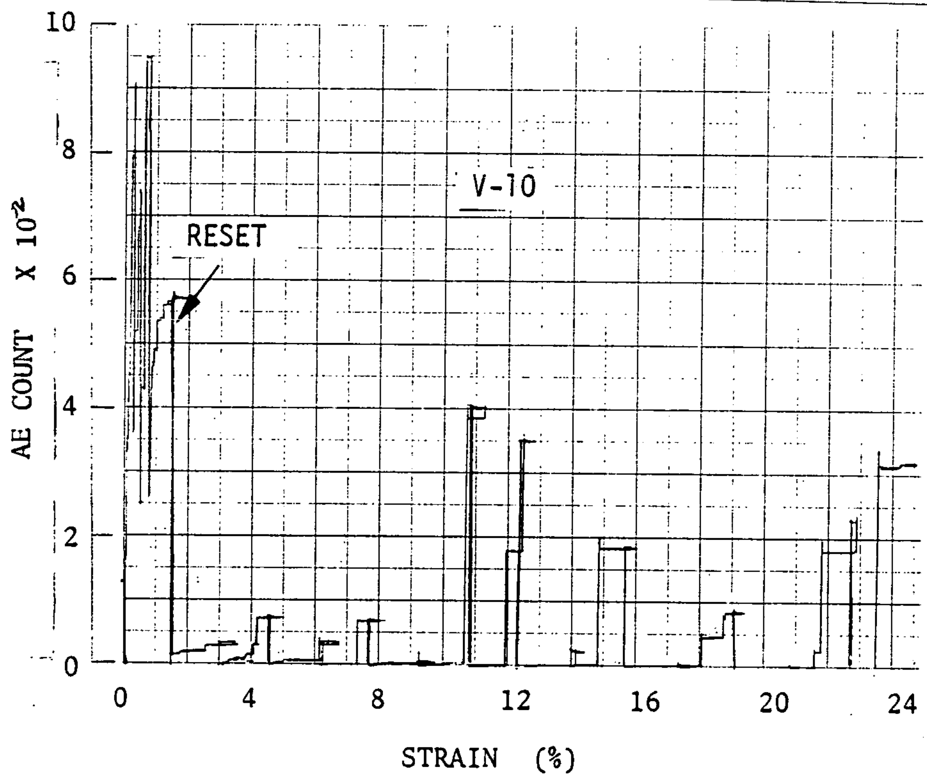

Fig. 4(d) AE counts vs. strain

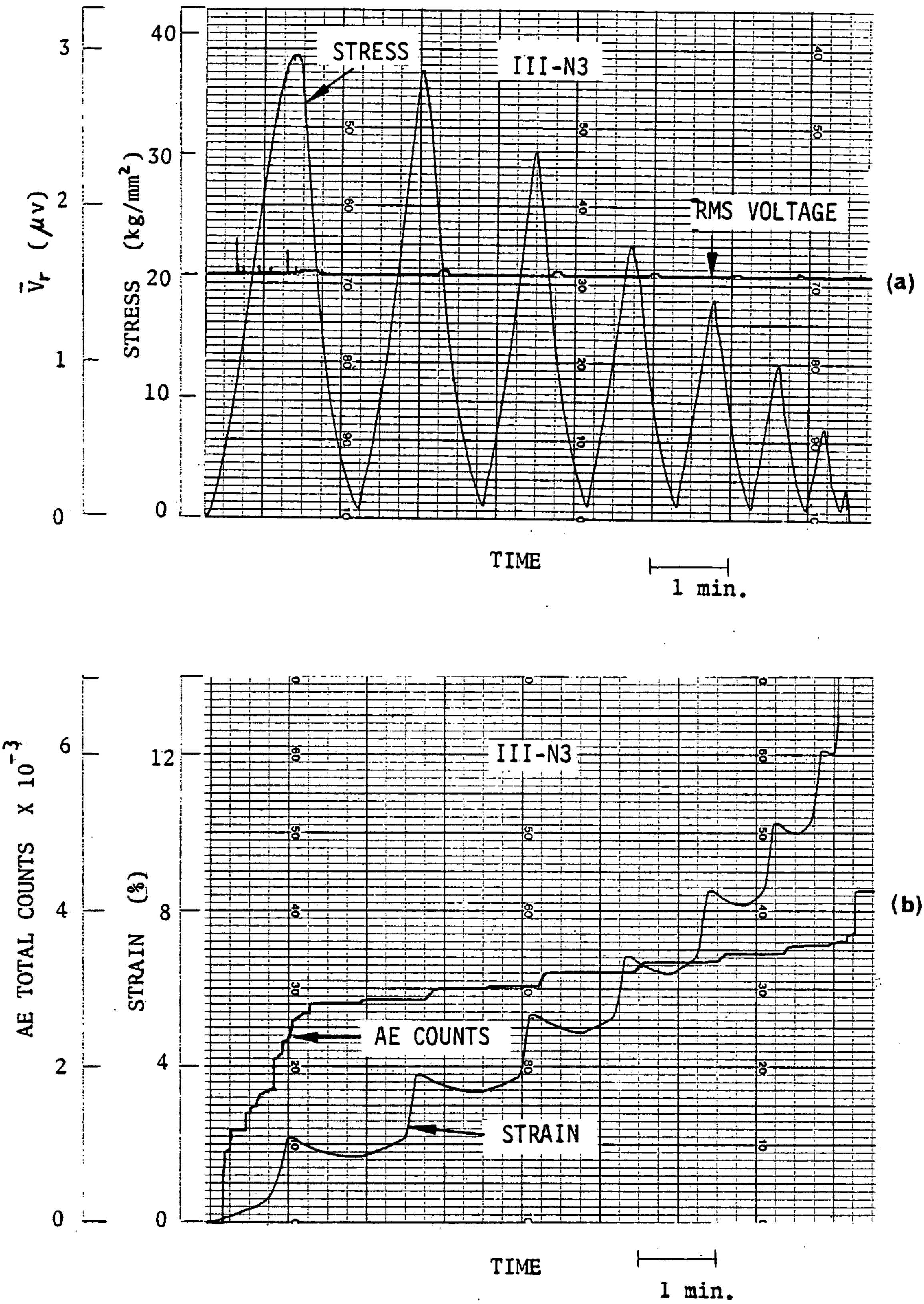

Fig. 5 AE test data of Specimen No. III-N3 (cold worked; 2% strain amplitude) a) Stress and rms voltages vs. time; b) Strain and AE counts vs. time.

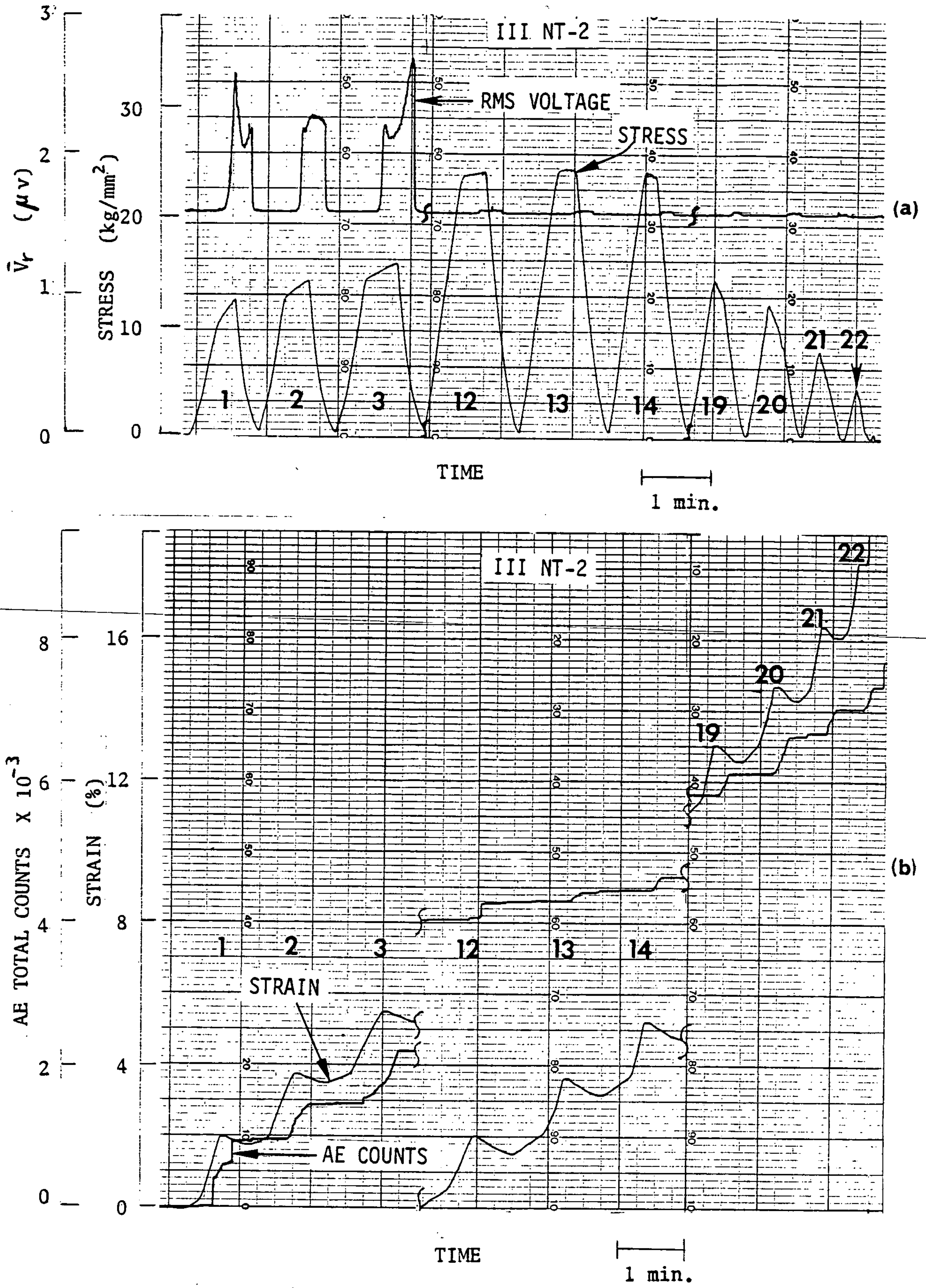

Fig. 6 Selected portions (n=1 ~ 3, 12 ~ 14, 19 ~ 22) of AE test data of Specimen No. III-NT2 (annealed, 2% strain amplitude). a) Stress and rms voltages vs. time; b) Strain and AE counts vs. time.

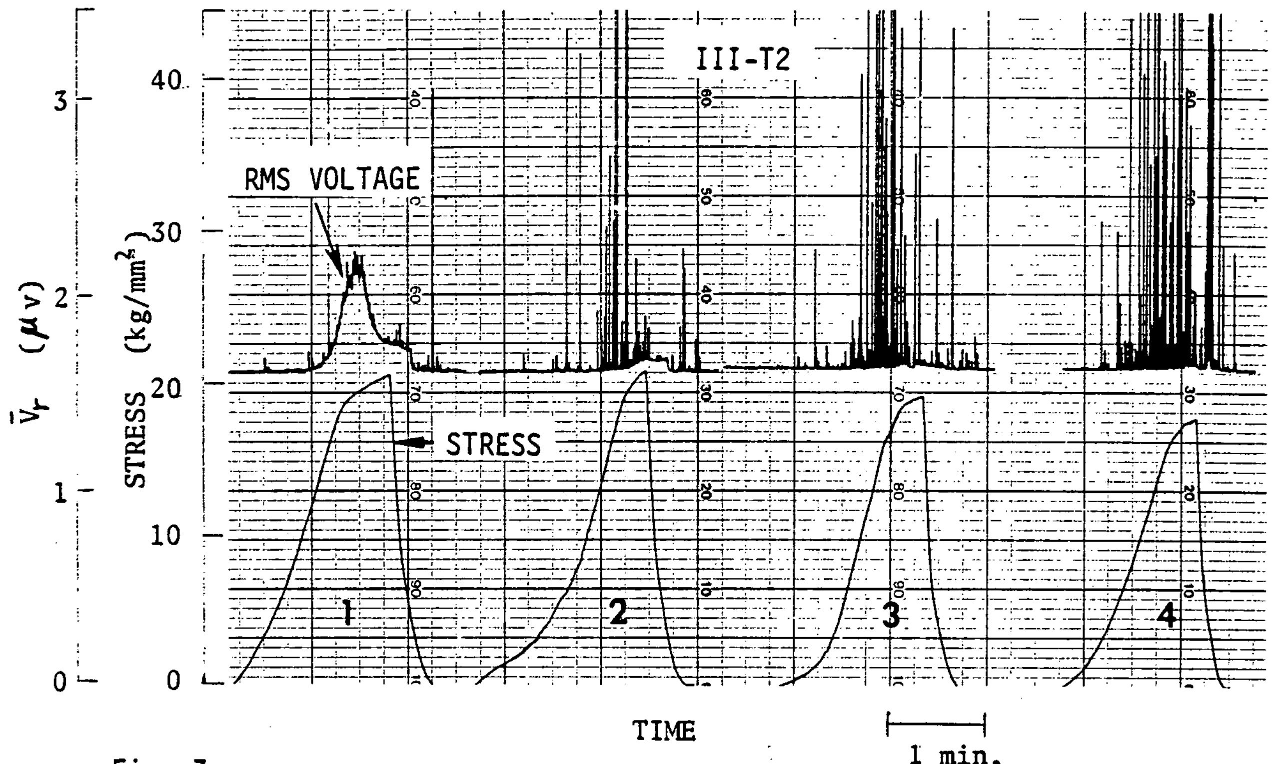

Fig. 7 AE test data during the initial four loading cycles of Specimen No. III-T2 (repeatedly annealed, 2% strain amplitude). a) Stress and rms voltages vs. time

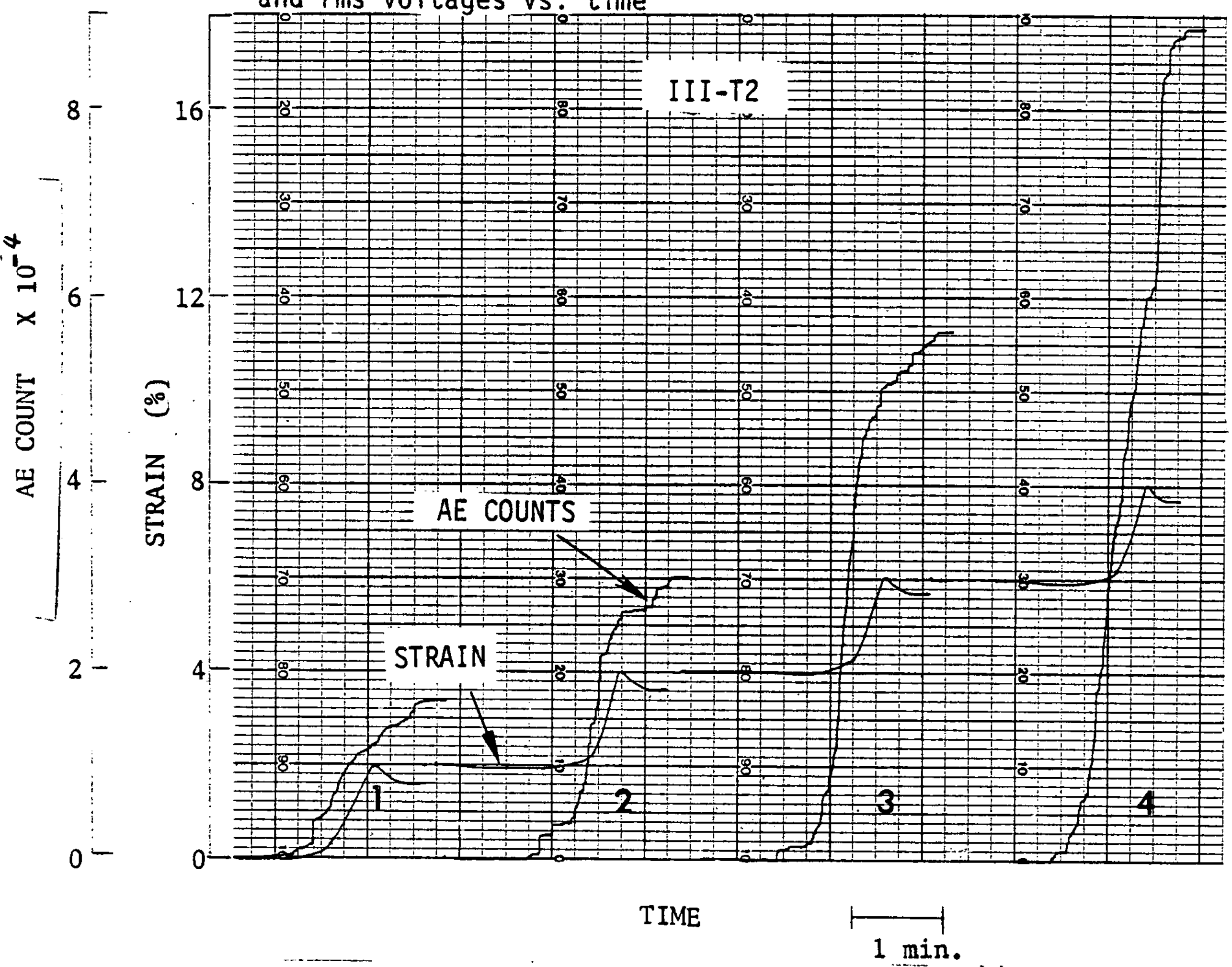

Fig. 7(b) Strain and AE counts vs. time

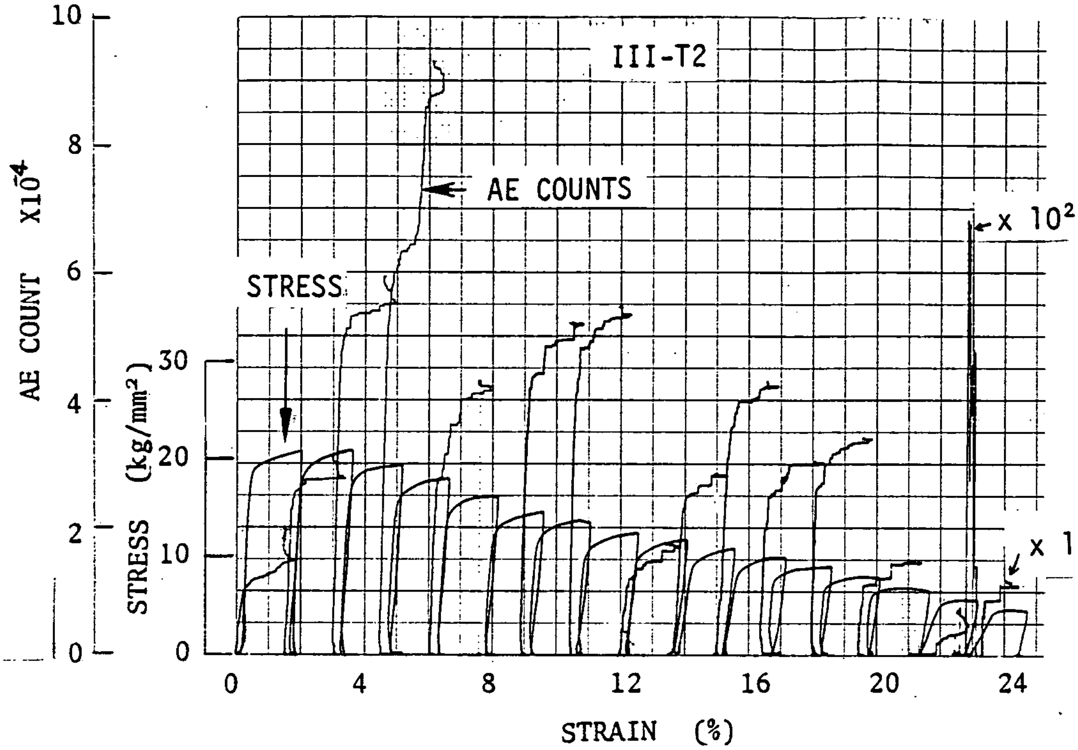

Fig. 7(c) Stress and AE counts vs. strain

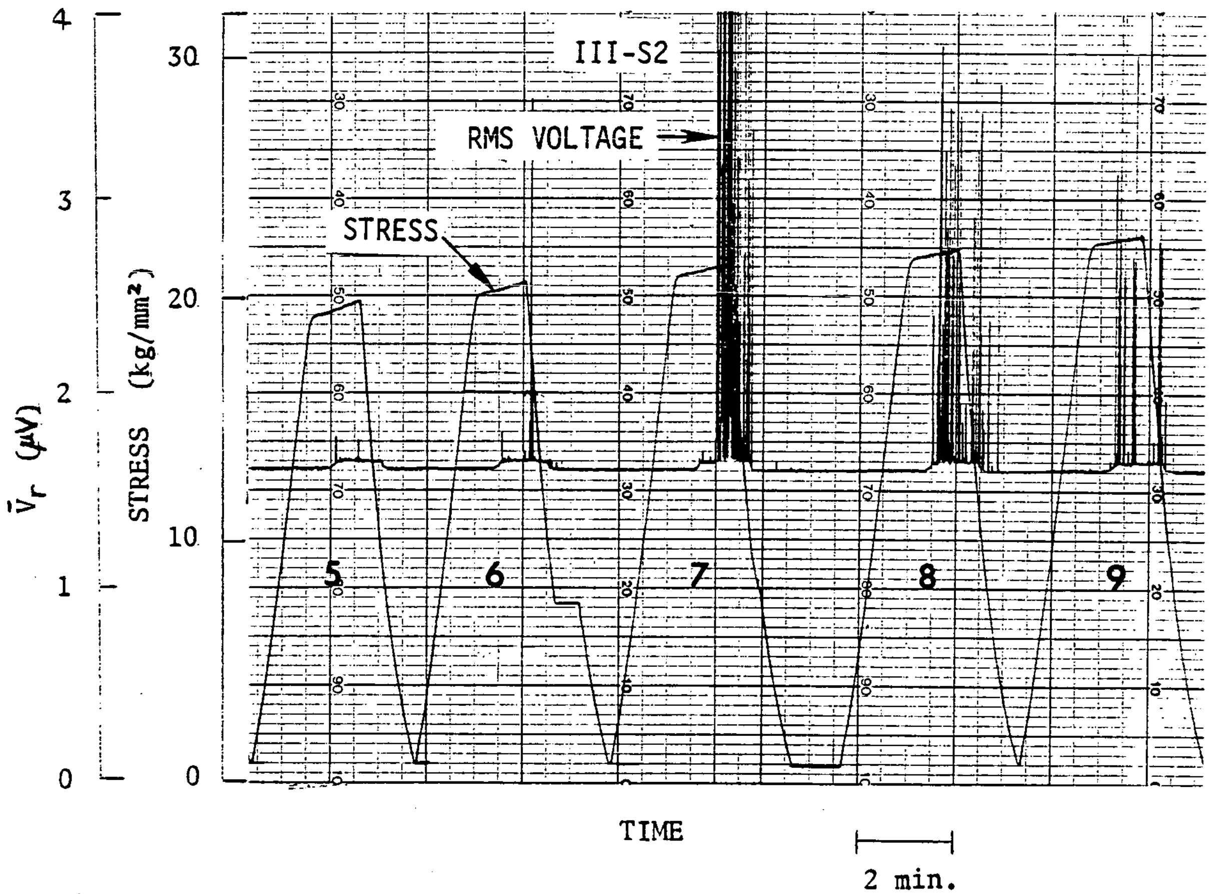

Fig. 8 AE test data during the 5th to 9th cycles of Specimen No. III-S2 (annealed, 2% strain amplitude), showing stress and rms voltages vs. time plots.

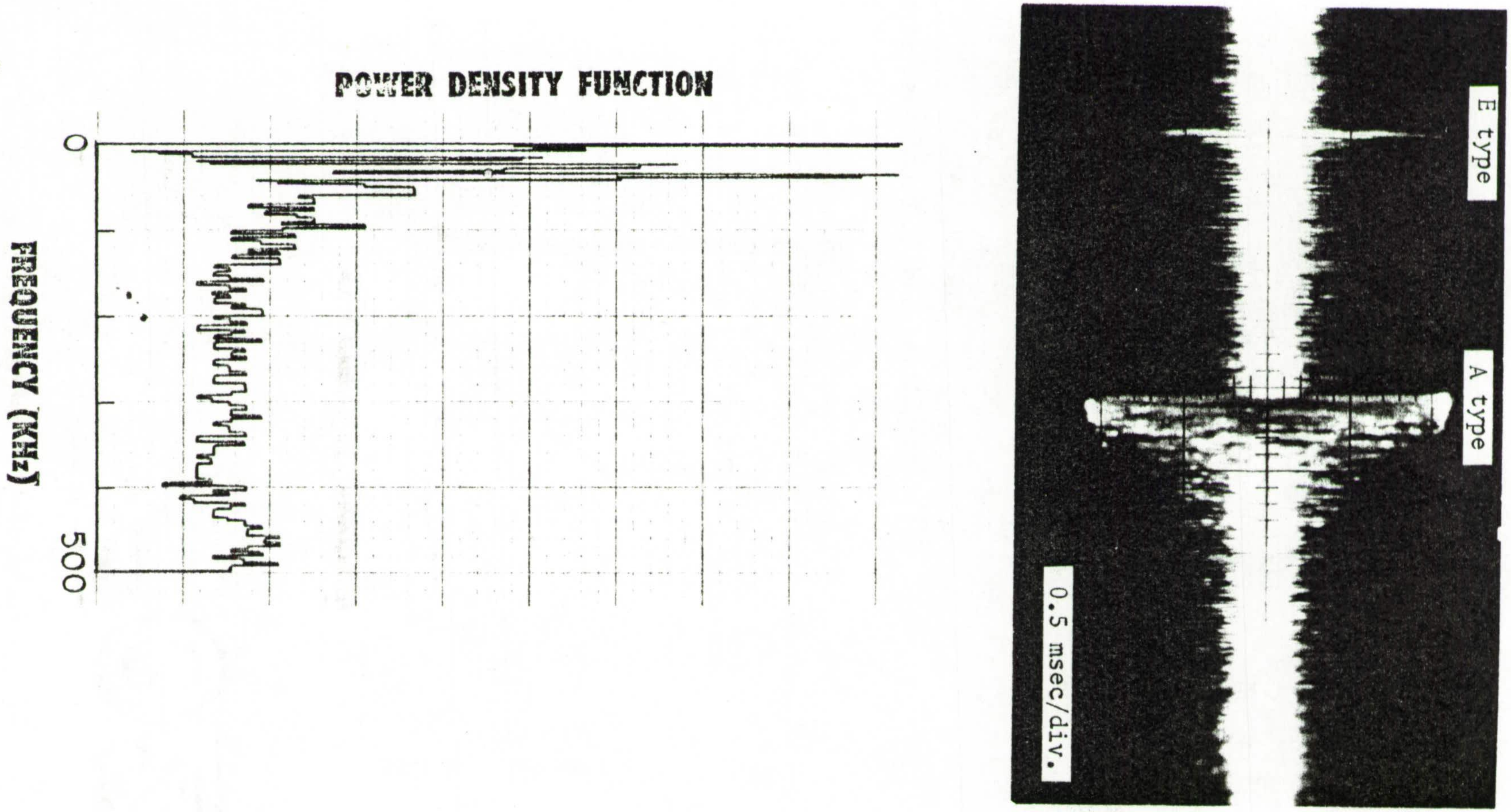

Fig. 9 Wave forms of A- and E-type burst signals and the frequency spectrum for the 5 msec segment of the AE signals, which was obtained during the plastic deformation of a tensile specimen of annealed Alloy III. The continuous signal level was approximately 50% higher than the background level (Time scale is 0.5 msec per major division).

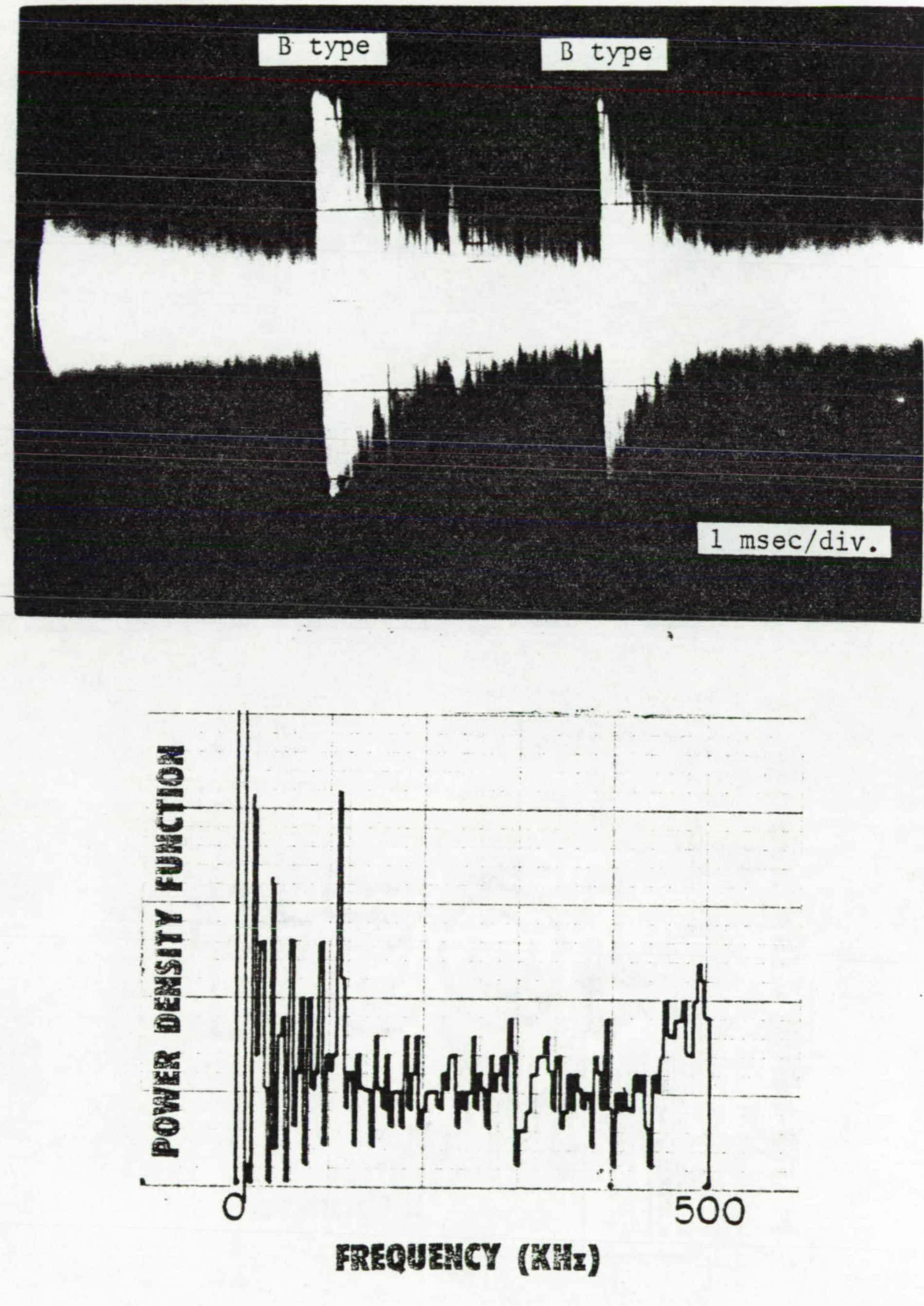

Fig. 10 Wave forms of B-type burst signals and the frequency spectrum for the 10 msec segment of the AE signals, originated during the eighth cycle of Specimen III-S2.

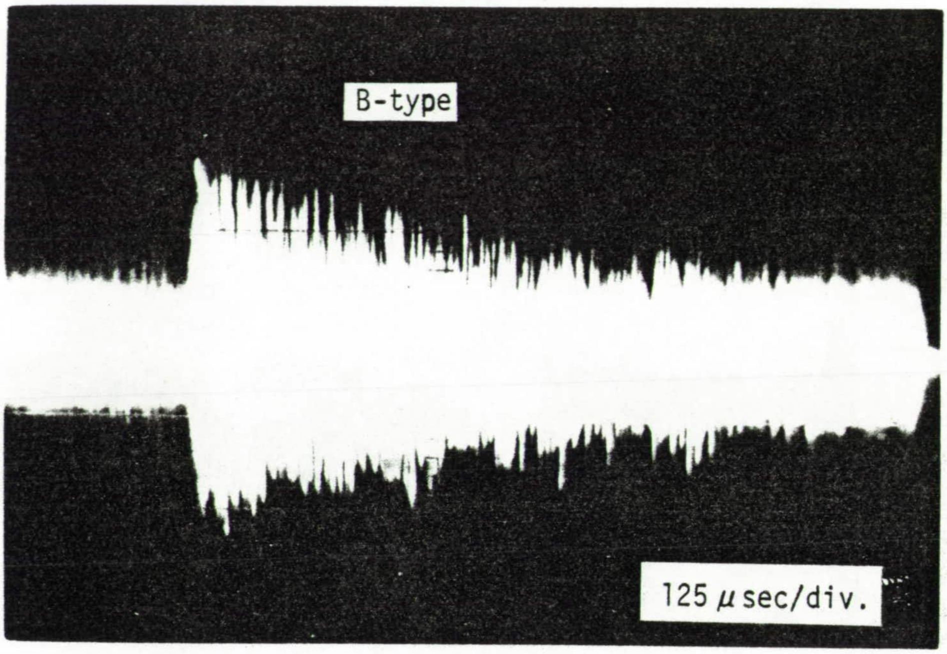

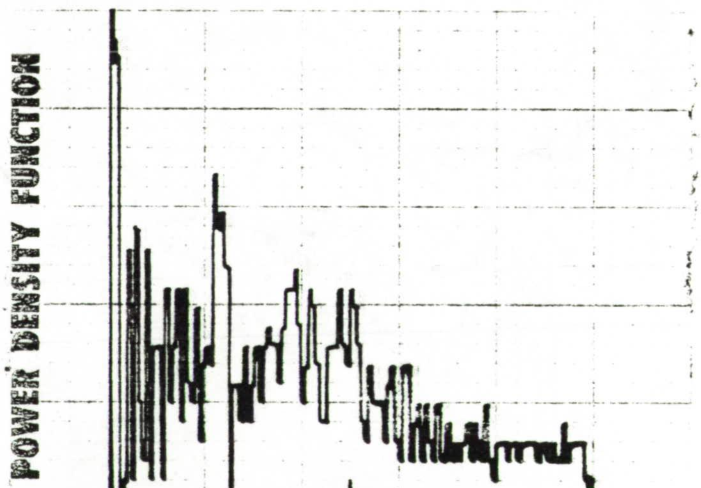

Fig. 11 Wave form and frequency spectrum of re-recorded signals, obtained at the same region as Fig. 10. Note the frequency range was extended to 2 MHz.

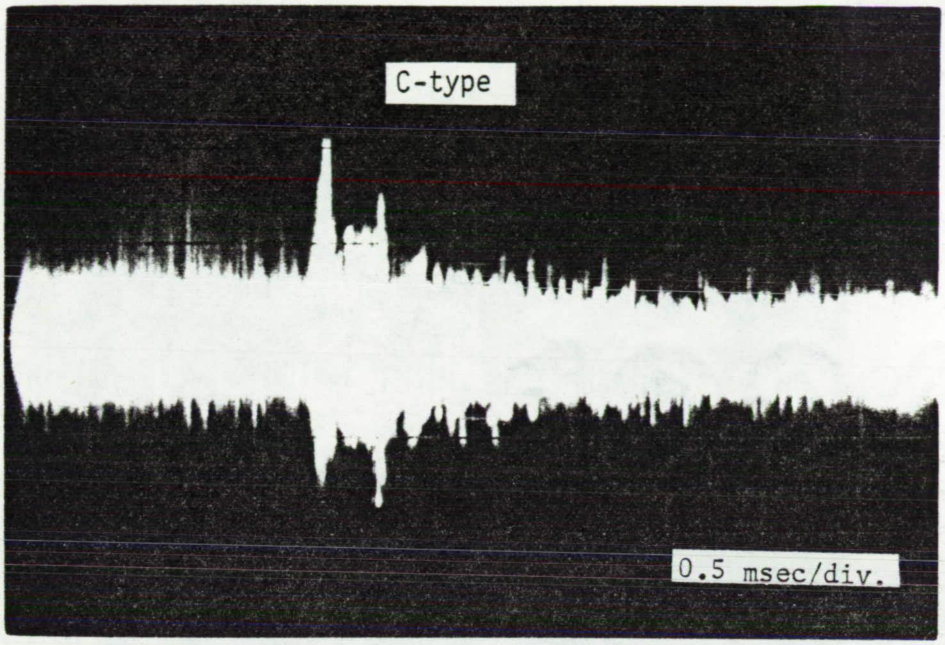

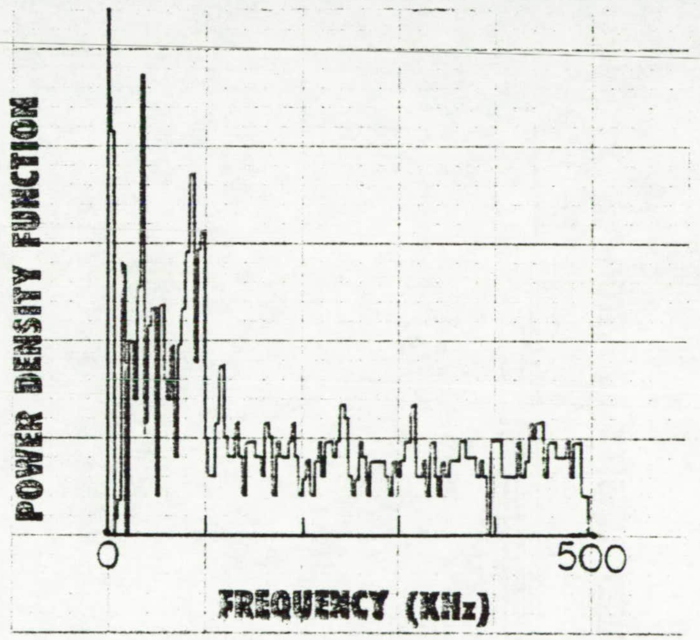

Fig. 12 Wave form of a C-type burst signal and the frequency spectrum for the 5 msec segment of the AE signals, produced during the first cycle of Specimen III-N3.

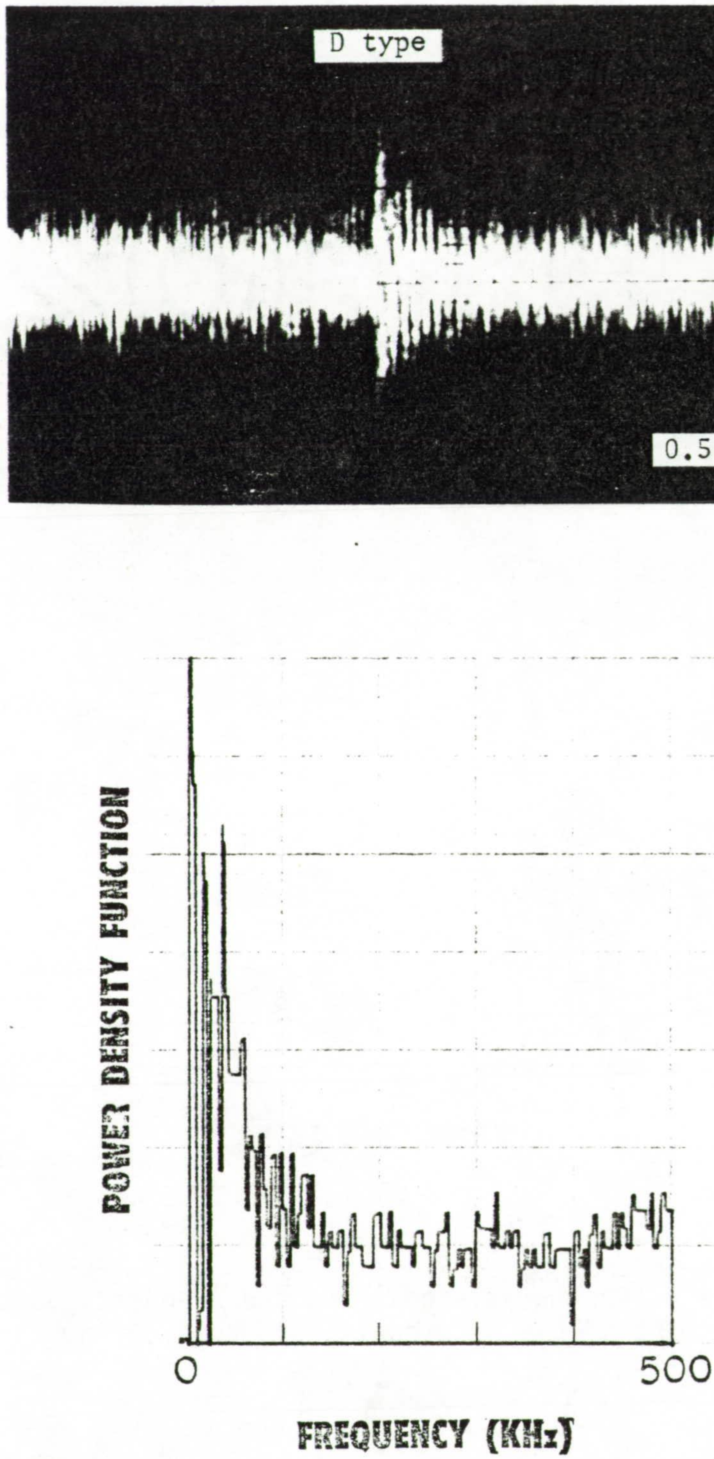

Fig. 13 Wave form of a D-type burst and the frequency spectrum for the 5 msec segment shown, taken from the first cycle of Specimen III-N3.

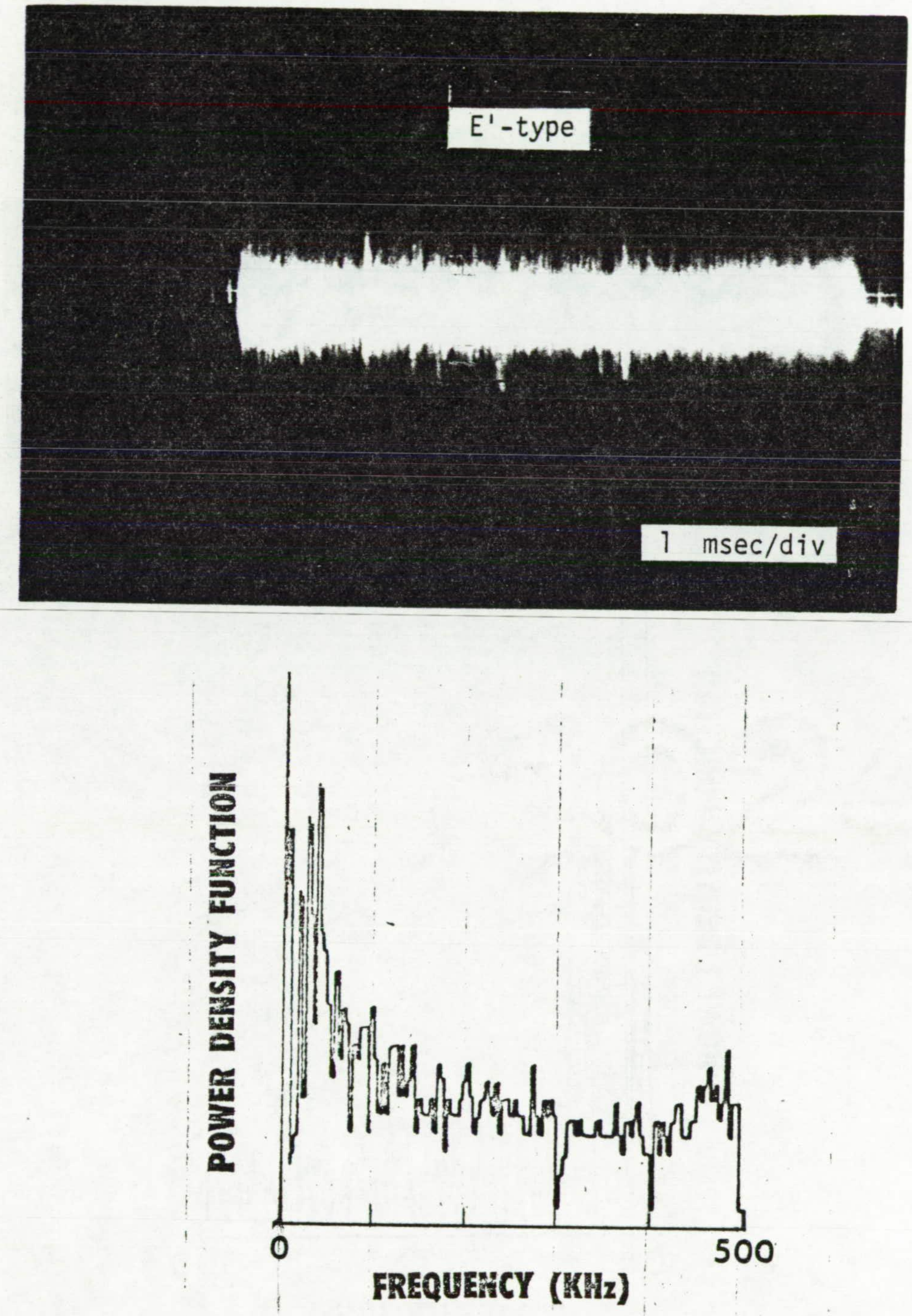

Fig. 14 Wave form of E'-type burst signals and the frequency spectrum for the 7 msec segment of the AE signals shown, produced during the fourth cycle of Specimen III-9.

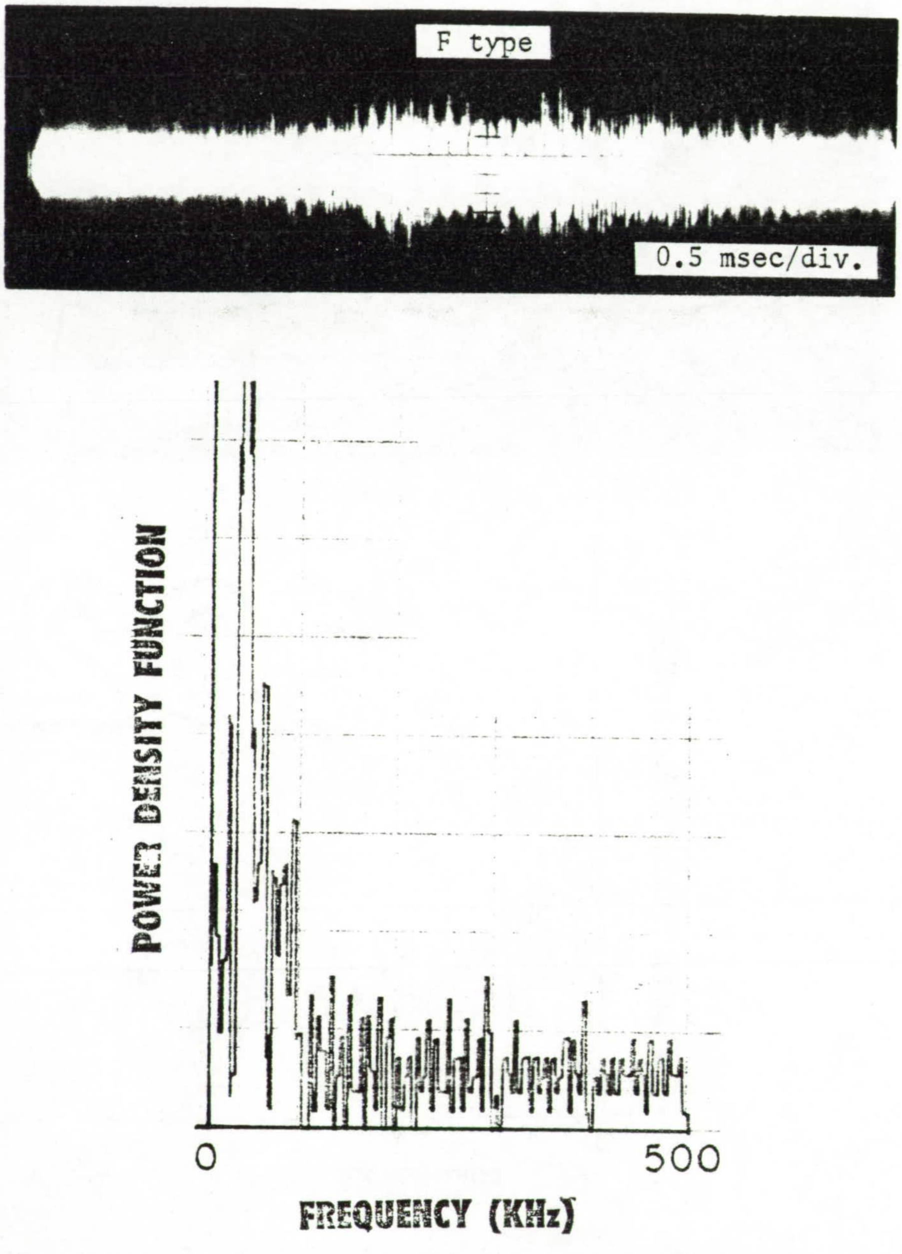

Fig. 15 Wave form of an F-type burst signal and the frequency spectrum for the 5 msec segment from the end of the third cycle of III-N3.

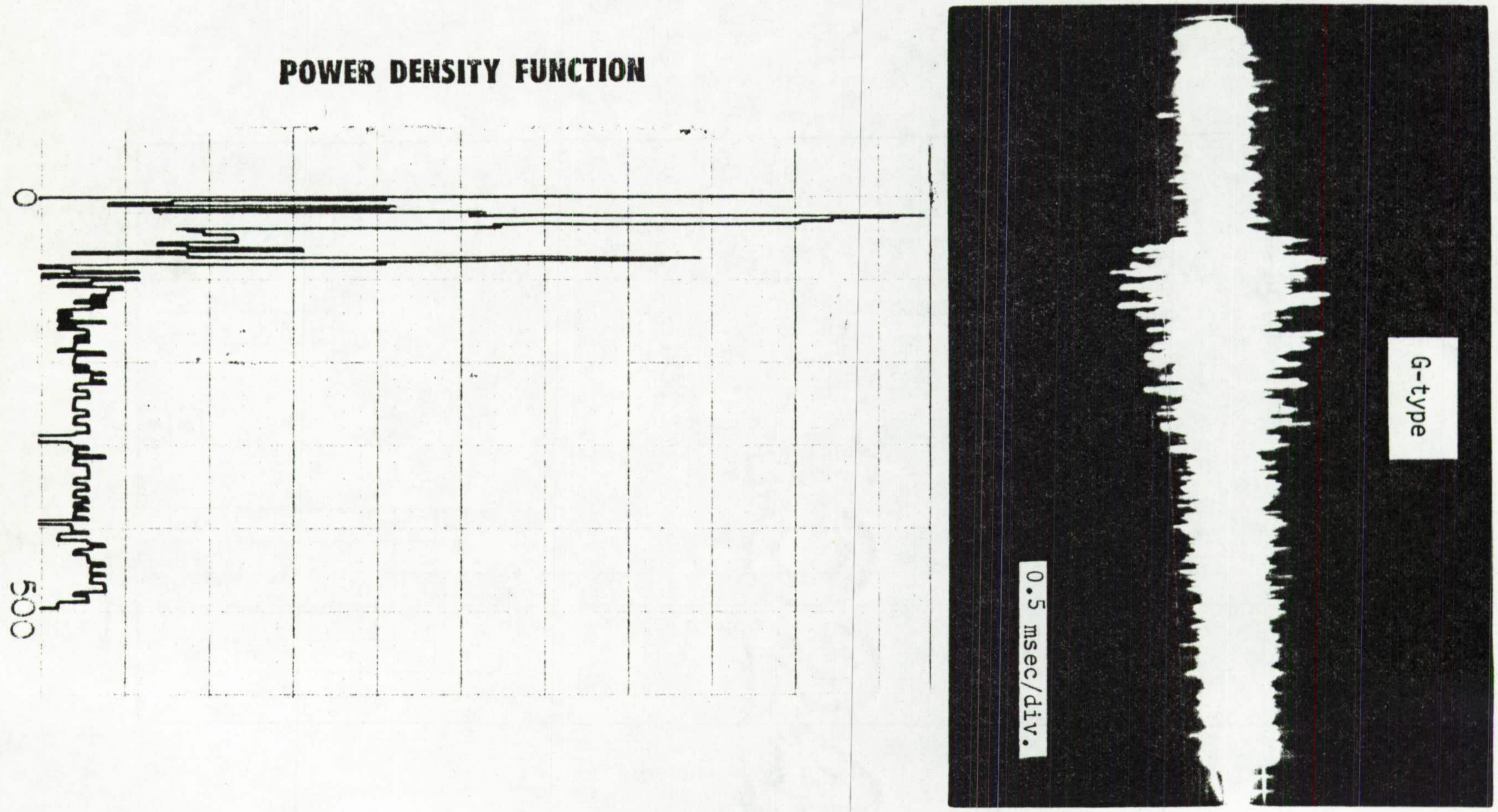

Fig. 16 Wave form of a G-type signal and the frequency spectrum of the 9.5 msec portion of the AE signals shown, taken from the yielding portion of a notched tensile test of an Alloy III sample.

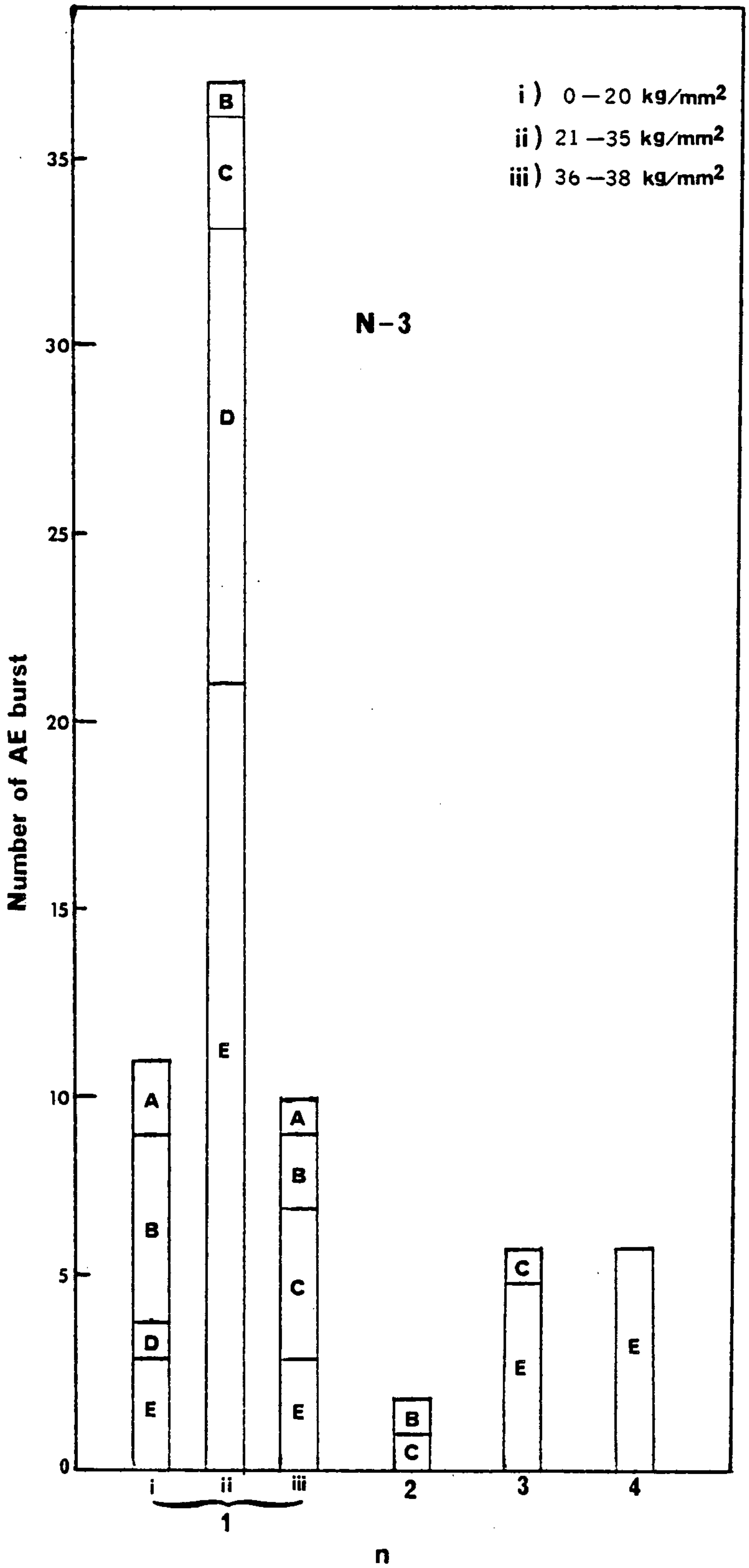

Fig. 17 The number of different burst type signals during the fatigue test of Specimen III-N3.

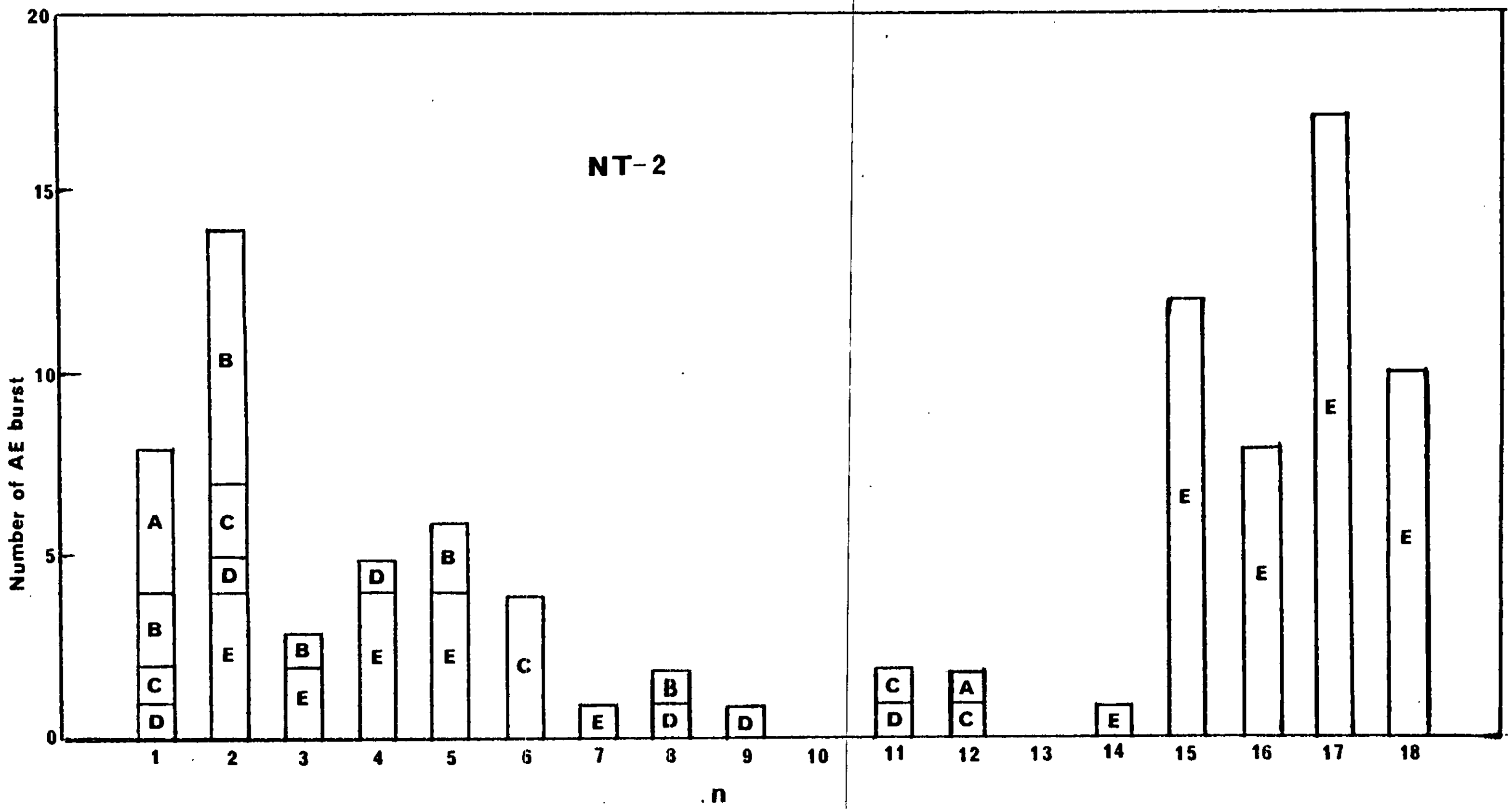

Fig. 18 The number of different burst type signals during the fatigue test of Specimen III-NT2.

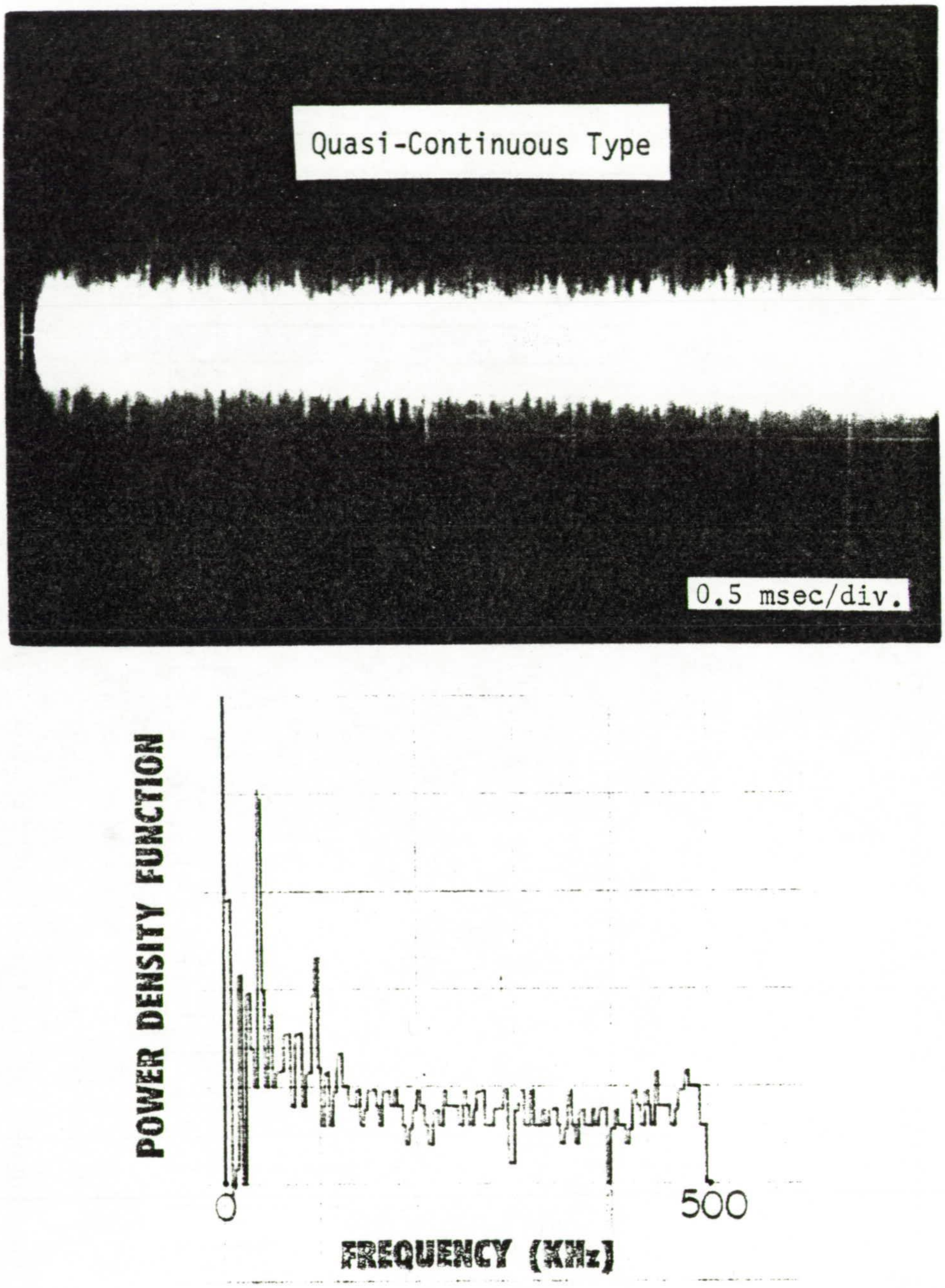

Fig. 19 Wave form and the frequency spectrum of quasi-continuous type AE signals, obtained during the first cycle of III-N3. The 5 msec segment was analyzed for the frequency spectrum.

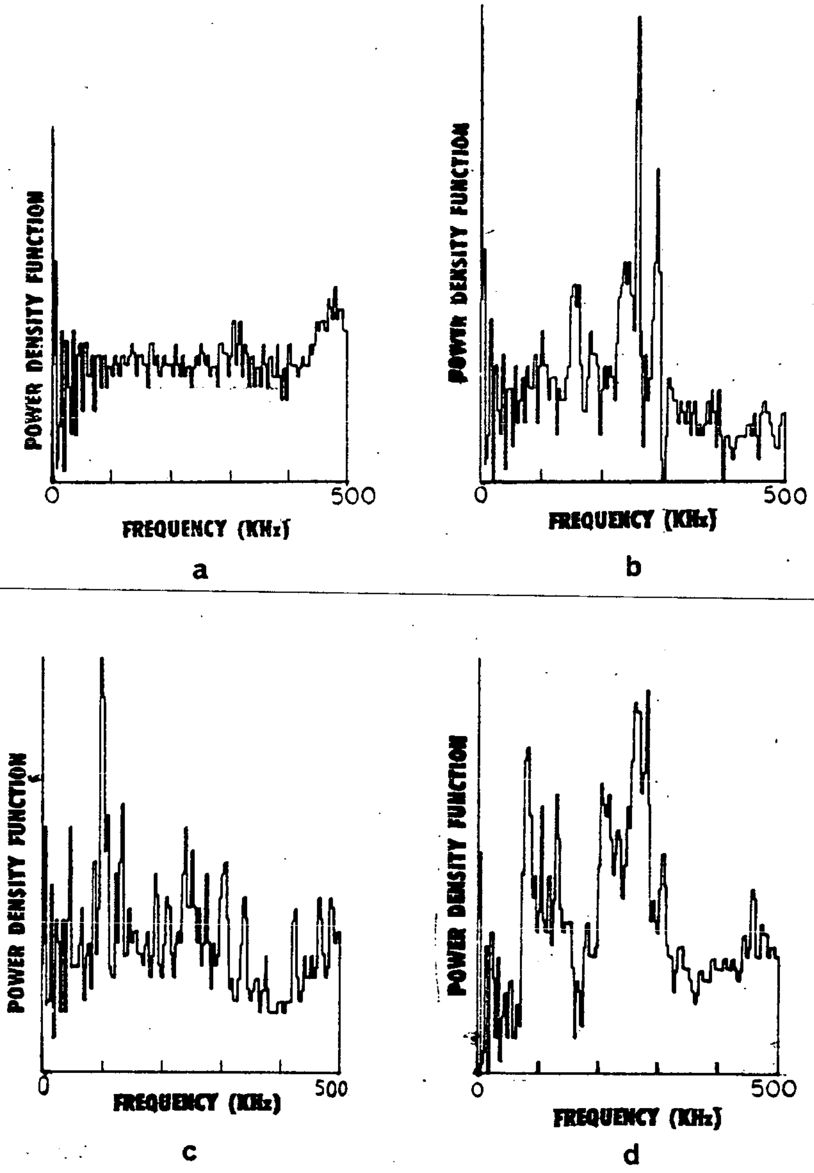

Fig. 20 Frequency spectrum resulting from random signal excitation using a wideband transducer. a) background excitation with the transducer mounted on a specimen, b) excitation by a 5 MHz transducer normal to the specimen surface, c) excitation by a 5 MHz transducer along the specimen length direction, d) shear wave excitation by a 2.25 MHz angle beam transducer.

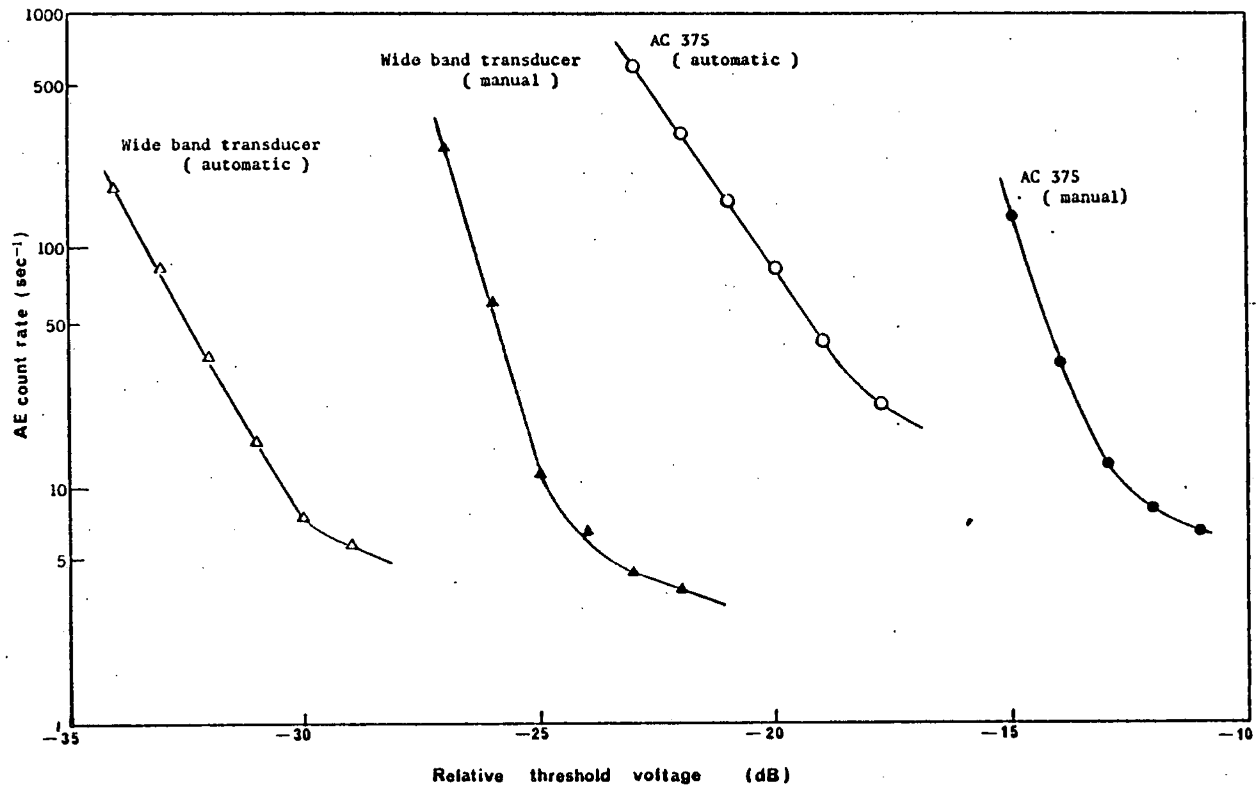

Fig. 21 AE count rate vs. relative threshold voltage for a smooth tensile sample during its initial yielding. Manual and automatic counting modes were used together with AC 375 and wideband transducers.

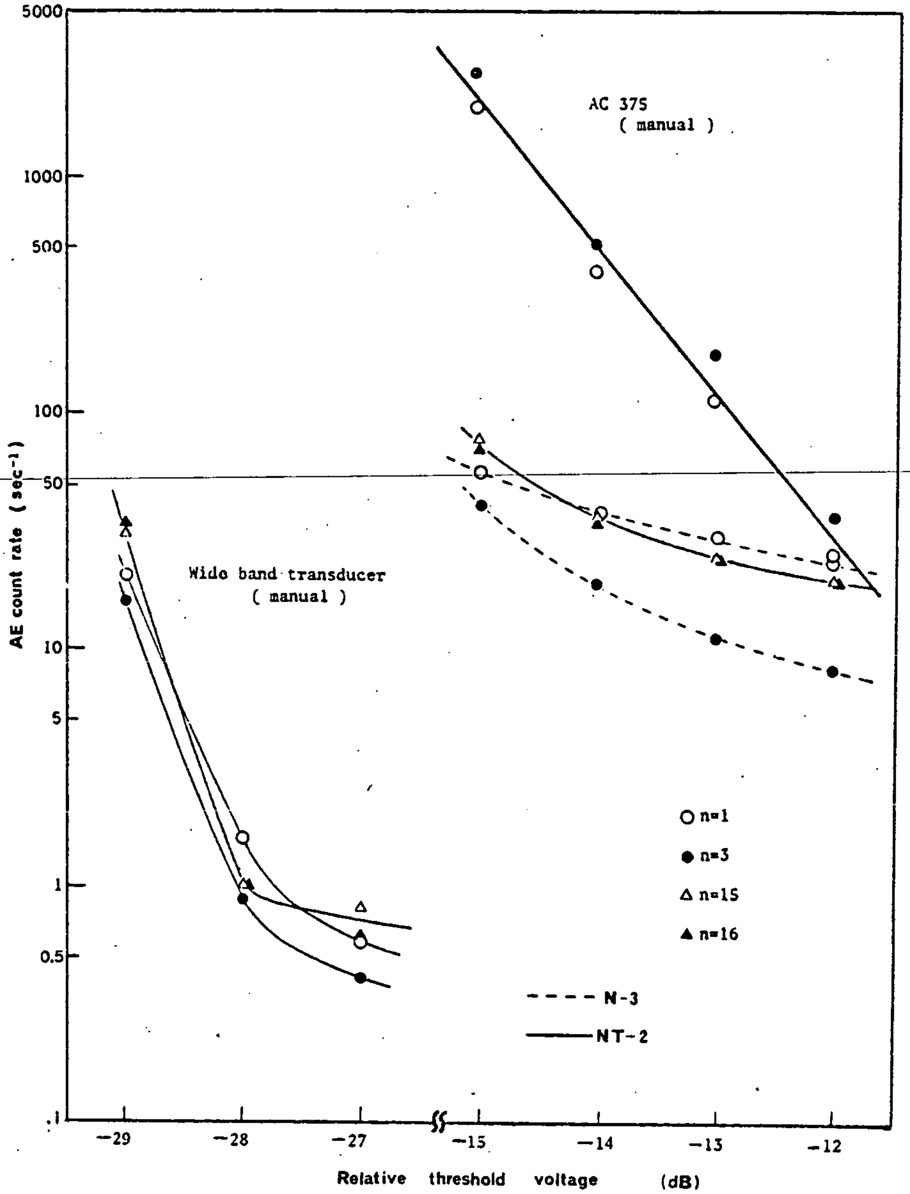

Fig. 22 AE count rate vs. relative threshold voltage for Specimens III-NT2 and III-N3.

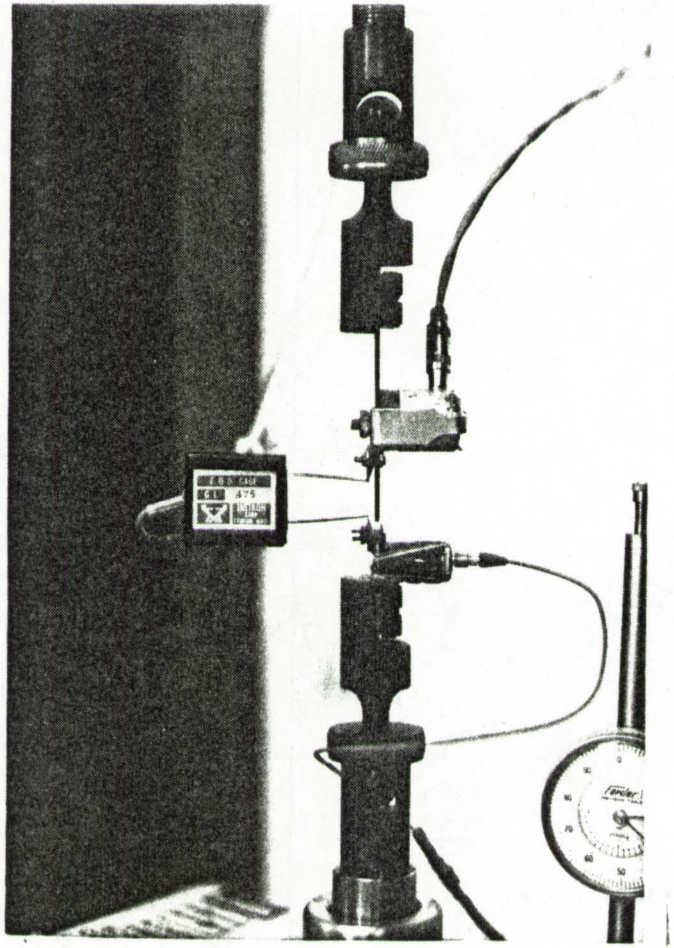

[a]

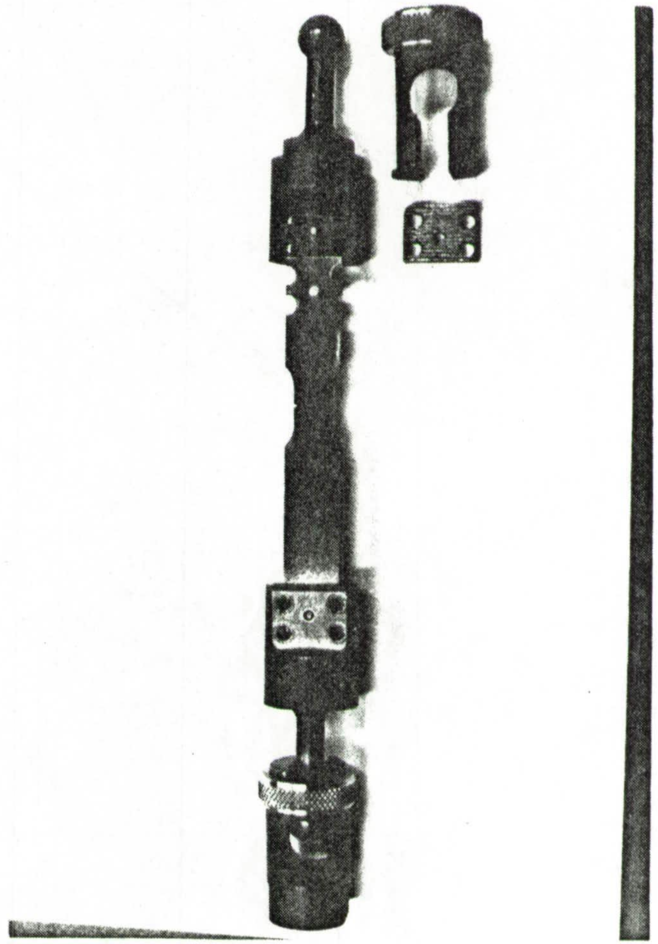

[b]

Photo 1 a) Test set-up with AE transducers and a clip gage.
b) Specimen grips and ball joints.

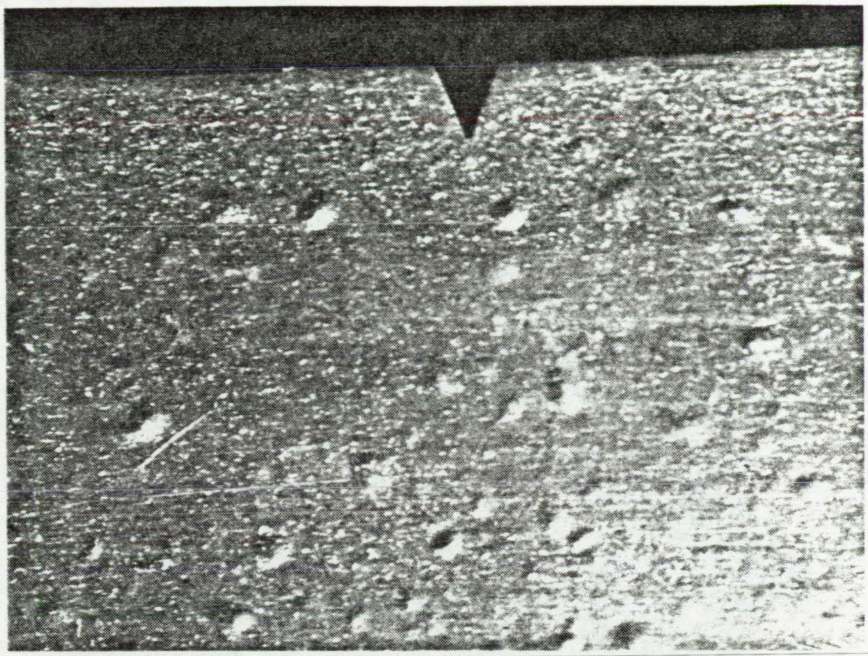

[a]

1 mm

[b]

0.1 mm

Photo 2 Blisters on the surface of annealed Alloy V specimen. a) 10X b) 100X.

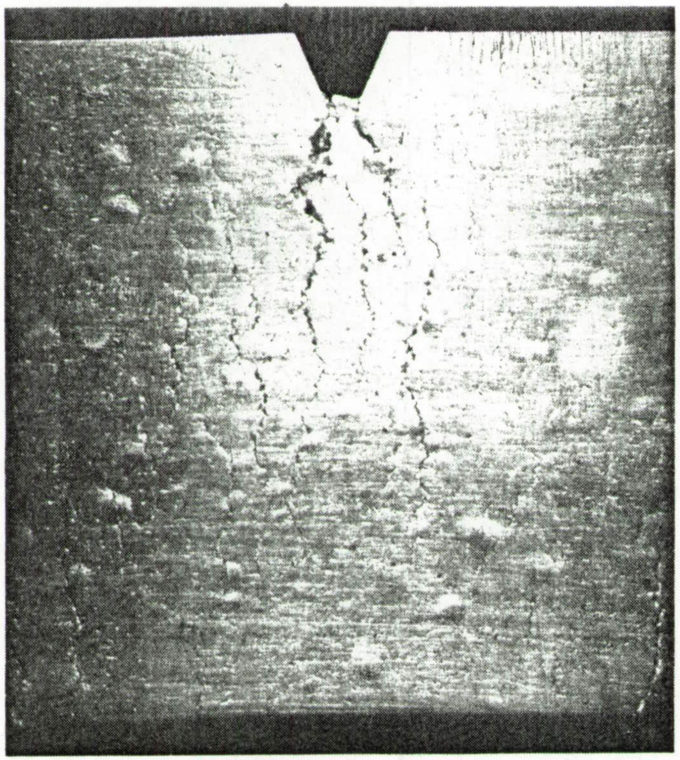

1 mm

Photo 3 Surface crack pattern of Specimen No. V-T2 after three fatigue cycles.

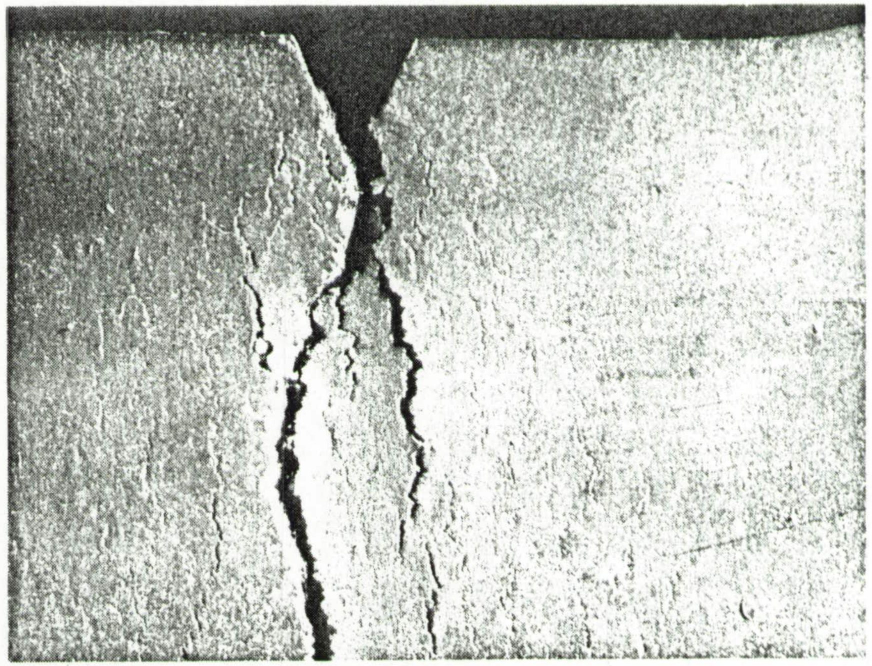

1 mm

Photo 4 Surface crack pattern of fractured Specimen No. III-T1

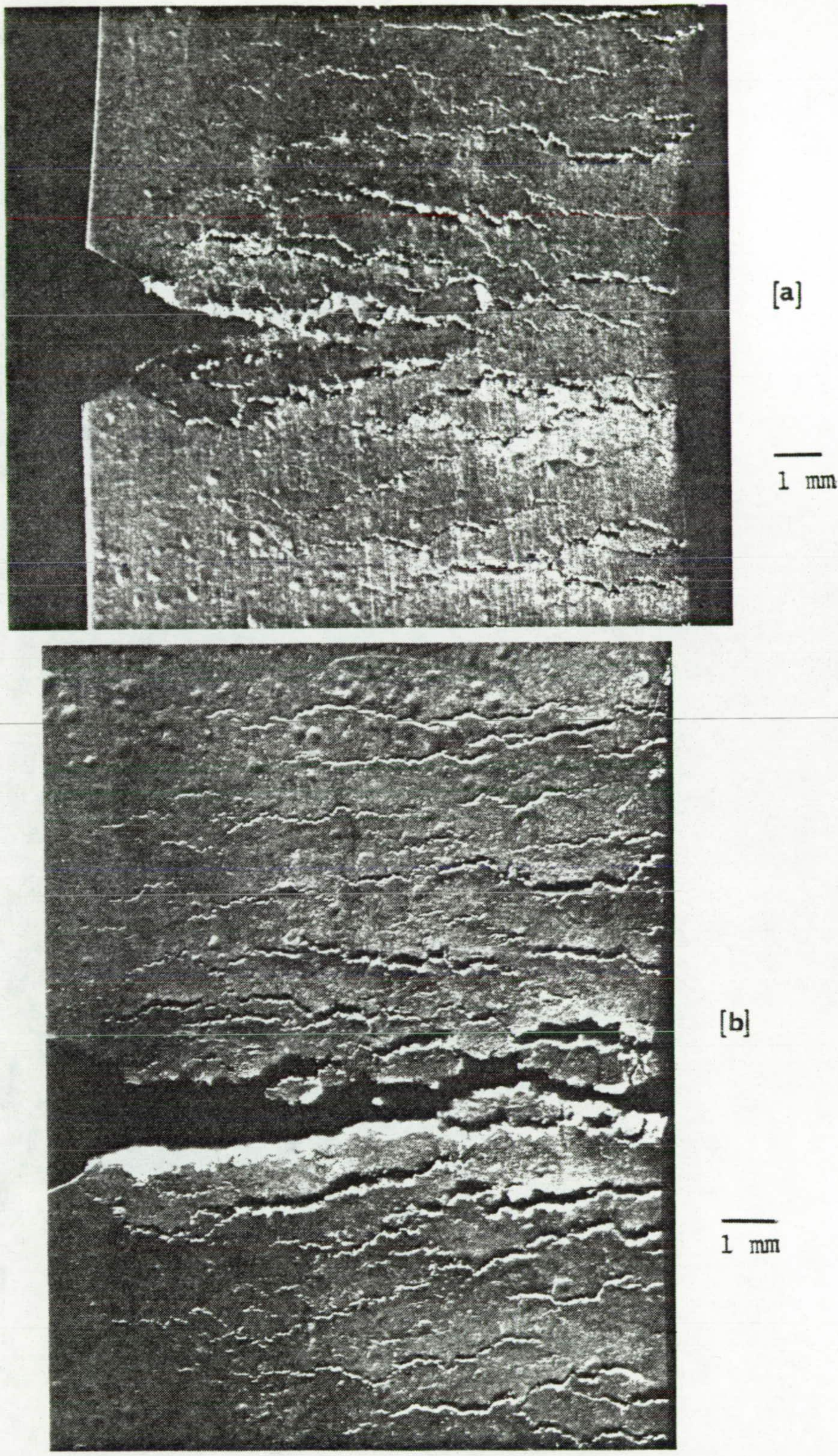

Photo 5 Surface crack pattern of Specimen No. III-T2 a) after nine cycles. b) after fracture.

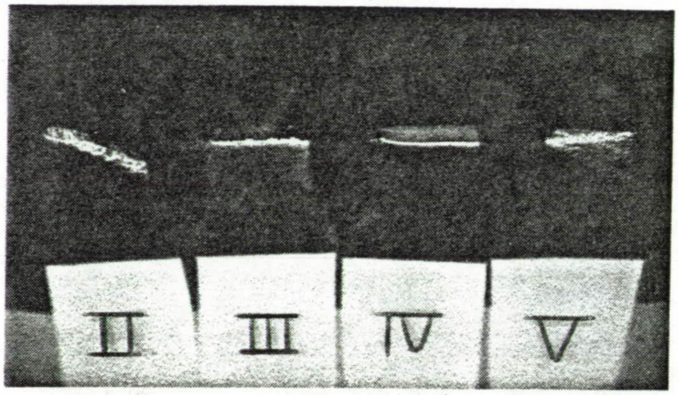

[a]

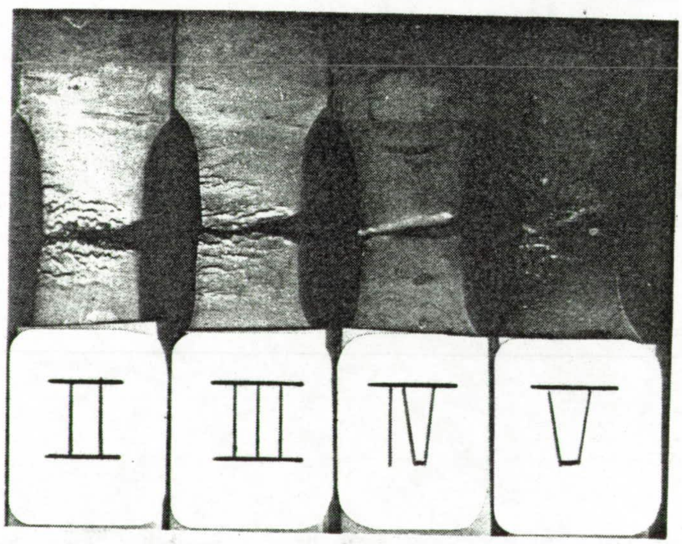

[b]

Photo 6 Macrophotographs of fractured samples a) cold worked condition. b) repeated annealed condition.

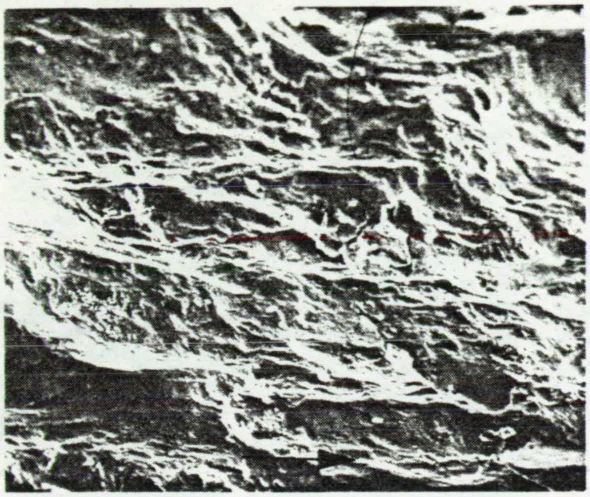

a) SPECIMEN II-5, 500X 10 μm

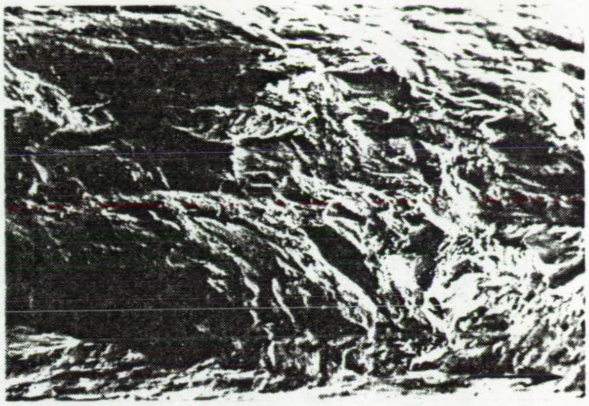

c) SPECIMEN V-2, 50X 0.1 mm

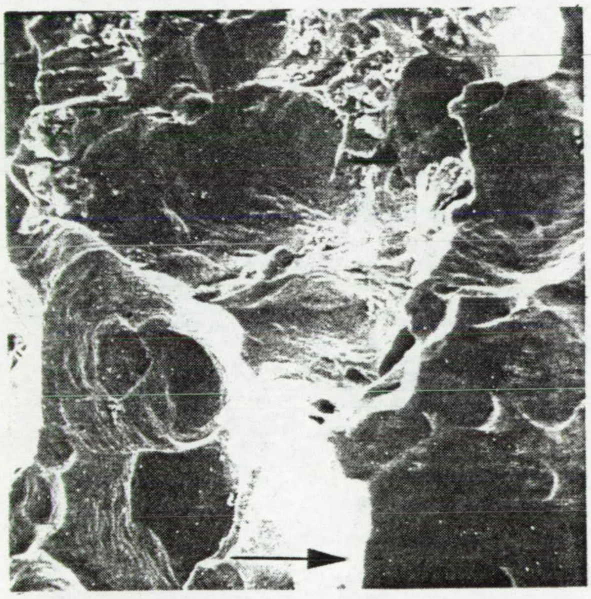

b) SPECIMEN II-3, 500X 10 μm

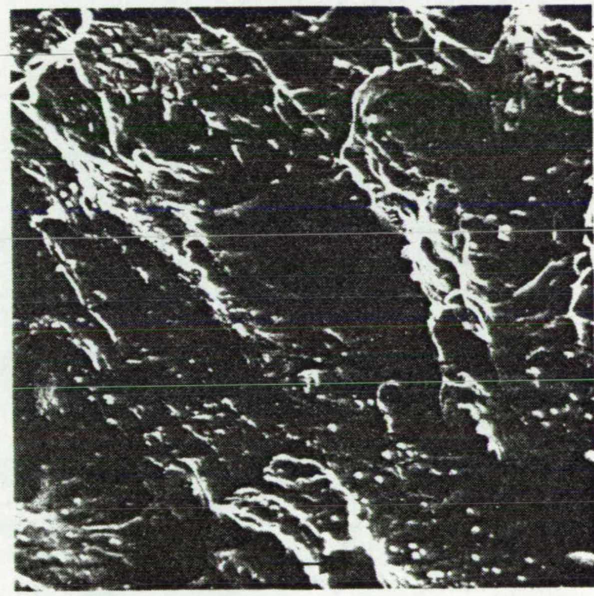

d) SPECIMEN V-2, 1000X 10 μm

Photo 7 Scanning electron micrographs of fracture surfaces of cold worked Alloys II and V. Arrows indicate the direction of macroscopic crack propagation. a) Specimen II-5, 500X. b) Specimen II-3, 500X,c) Specimen V-2, 50X, d) Specimen V-2, 1000X.

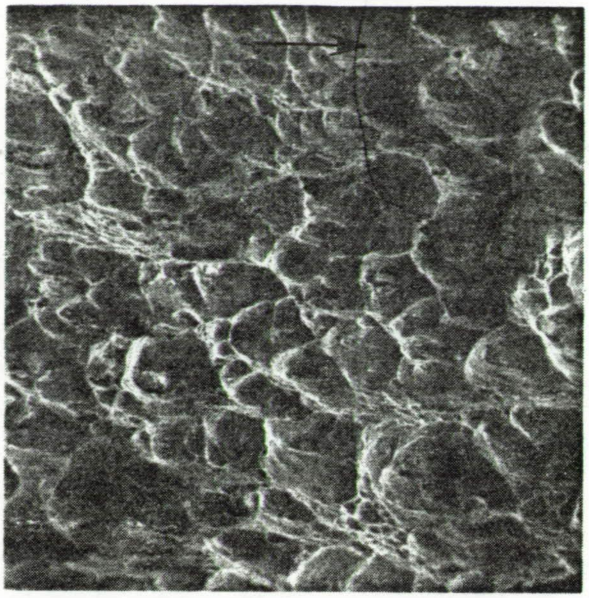

a) SPECIMEN III-4, 500X $\overline{10}\ \mu m$

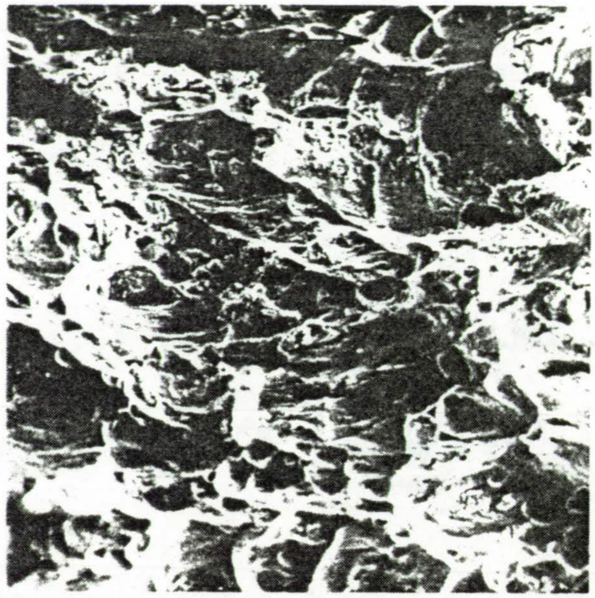

c) SPECIMEN III-N2, 500X $\overline{10}\ \mu m$

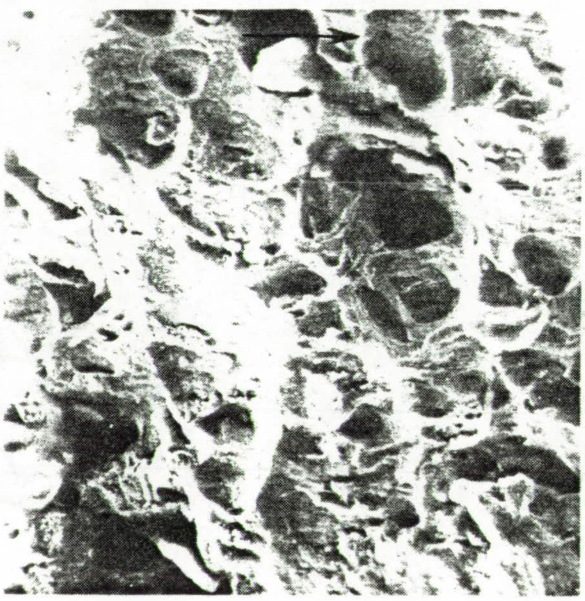

b) SPECIMEN III-8, 500X $\overline{10}\ \mu m$

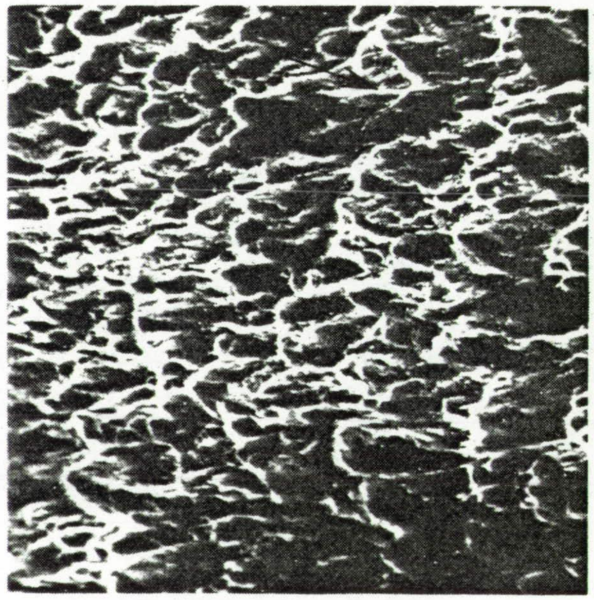

d) SPECIMEN IV-2, 2000X $\overline{5}\ \mu m$

Photo 8 Scanning electron micrographs of fracture surfaces of cold worked Alloys III and IV. Arrows indicate the direction of macroscopic crack propagation. a) Specimen III-4, 500X, b) Specimen III-8, 500X, c) Specimen III-N2, 500X, d) Specimen IV-2, 2000X.

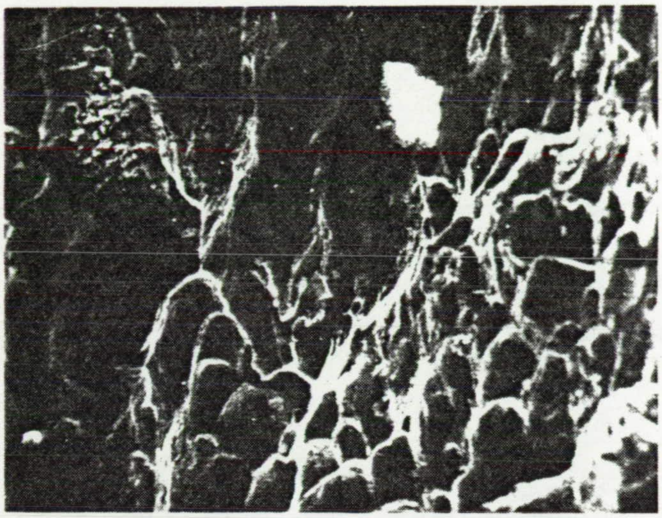

CRACK PROPAGATION

10 μm

(a) SPECIMEN III-S2, 500x

CRACK PROPAGATION

10 μm

(b) SPECIMEN III-NT2, 500x

Photo 9 Scanning electron microgeaphs of fracture surfaces of annealed Alloy III. a) Specimen III-S-2, 500X, b) Specimen III-NT2, 500X.

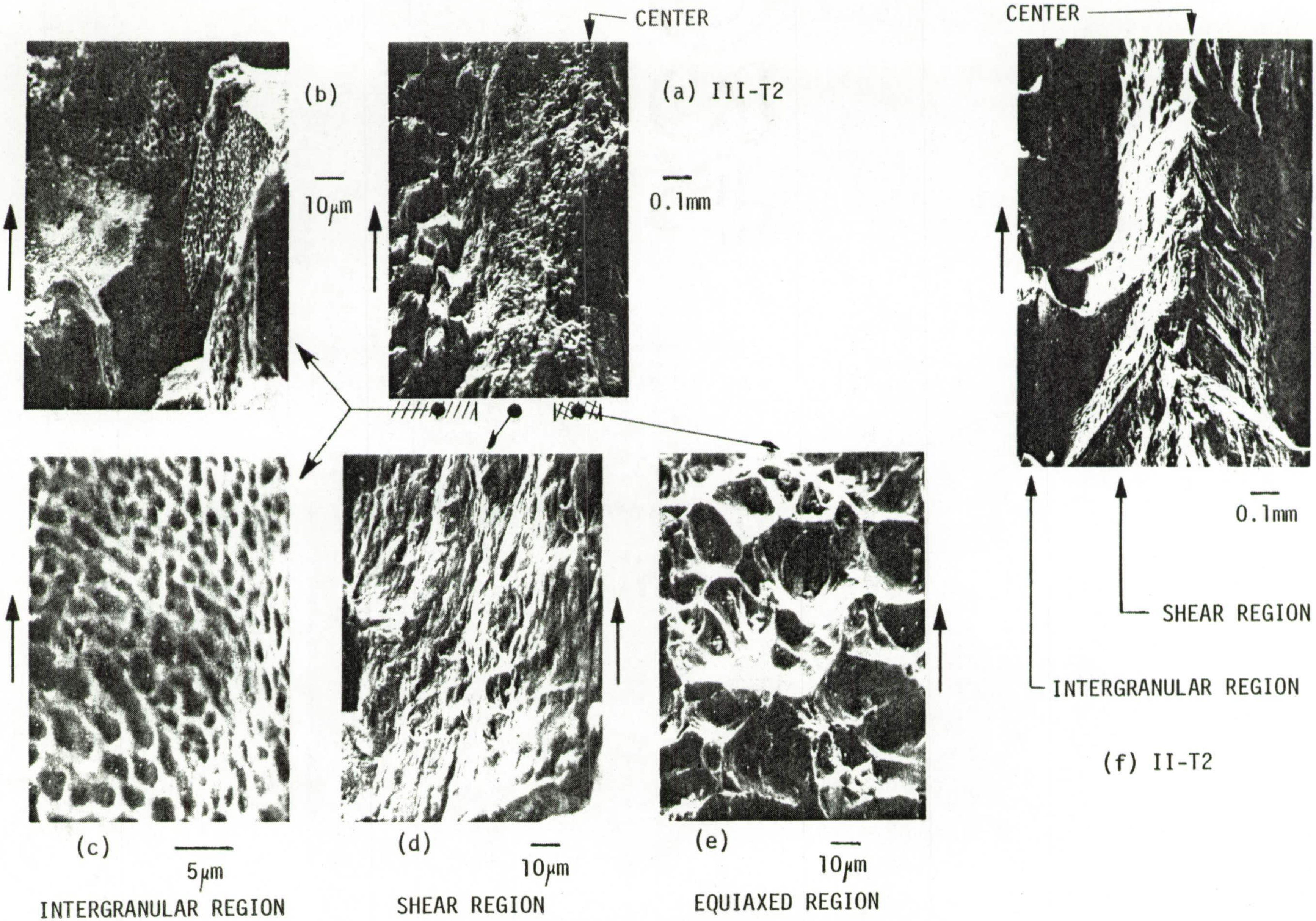

Photo 10 Scanning electron micrograph of fracture surfaces of repeatedly annealed Alloy II and III. a) Specimen III-T2, 50X, b) and c) intergranular region, 500X and 2000X, respectively, d) shear

TABLE I

Hardness of Test Materials

(Rockwell A-scale Hardness)

Material	Initial Condition	Initial Hardness	Annealed at 538°C, for 10 min.*	Vacuum-Annealed at 538°C for 2 hrs.	Annealed at 650°C for 10 min.*	After Repeated Annealing**
I (pure Cu)	as-received sheet (cold worked)	33.8	---	---	28.2 (R_E)	---
II (0.15Zr)	as-received sheet (cold worked)	40.1	39.2	36.3	35.5	33.2
III (3Ag, 0.5Zr)	as-received sheet (cold worked)	47.4	28.3	27.3	25.0	33.6
	as-received plate (annealed)	17.0	---	---	---	---
	cold-rolled from plate stock	44.2	---	---	28.8	---
IV (0.2$A\ell_2O_3$)	as-received sheet (cold worked)	48.8	---	---	41.4	40.0
V (1Ag, 0.1Zr)	as-received sheet (cold worked)	41.0	34.2	34.4	33.8	29.9

* H_2 atmosphere of 1.5cm Hg pressure

** Initially annealed at 650°C, 10 min. and repeatedly annealed at 538°C, 10 min. Measurements taken between a grip and the reduced section of a sample.

TABLE II

Tensile Test Data

a. Tensile Properties of As-received Sheet Materials

Smooth Samples*

Materials	Yield Strength	Tensile Strength	Elongation in 2.5cm
I	25.2 (kg/mm^2)	26.1 (kg/mm^2)	18%
II	33.0	34.3	9
III	42.6	44.5	7
IV	44.3	46.7	8
V	30.7	32.6	13

* Test results supplied by NASA Lewis Research Center

Notched Samples

Material	Notch Tensile Strength	Notch Sensitivity	Elongation in 1.27cm
II	31.8 (kg/mm^2)	0.93	20.0(%)
III	40.2	0.90	13.4
IV	40.2	0.86	15.6
V	31.9	0.98	28.0

b. Tensile Properties of Annealed Sheet Materials

Smooth Samples (Annealed at 650°C, 10 min.)

Materials	Yield Strength	Tensile Strength	Elongation in 2.5
II	25.2	39.4	23.0
III	16.9	39.4	31.9
IV	34.2	49.3	21.9
V**	16.4	31.7	9.2

** Failed at a pre-existing flaw

TABLE III -- Fatigue Test Data

Spec. No.	Test Condition	Cyclic Notch Strength (kg/mm^2)	Total Inelastic Strain (%)	No. of Cycles to Failure	$\Sigma \epsilon_i / \Sigma \epsilon$ (%)
<u>II (0.15Zr)</u>					
3	(i) 1f	31.8	15.0	18	84
4	(i) 1f	31.8	15.1	21	72
7	(i) 2f	33.6	27.5	16	86
9	(i) 2f	29.1	23.4	12	97
5	(i) 2s	31.6	20.0	11	91
6	(i) 2s	33.0	22.4	14	80
T2	(iii) 2s	19.7	32.0	17	94
T3	(iii) 2s	25.3	29.6	17	87
<u>III (3Ag, 0.5Zr)</u>					
3	(i) 1f	40.8	15.4	40	39
4	(i) 1f	39.3	12.5	18	70
7	(i) 2f	39.8	13.6	8	85
8	(i) 2f	39.5	14.6	9	81
10	(i) 2f	41.4	10.5	6	88
5	(i) 2s	41.3	18.6	12	78
6	(i) 2s	39.3	12.5	7	90
9	(i) 2s	40.5	12.7	7	91
T1	(ii) 2f	34.8	32.1	18	86
T3	(ii) 2f	35.6	32.3	19	85
T2	(iii) 2s	20.6	28.0	16	88

TABLE III--Cont'd Fatigue Test Data

Spec No.	Test Condition	Cyclic Notch Strength (kg/mm^2)	Total Inelastic Strain (%)	No. of Cycles to Failure	$\Sigma \epsilon_i / \Sigma \epsilon$ (%)
III (3Ag, 0.5Zr) Plate Stock					
N2	(i) 2s	35.4	14.1	9	78
N3	(i) 2f	36.7	12.1	7	86
NT2	(ii) 2f	23.6	38.9	22	88
S1	(*) 2s	23.5	41.2	25	83
S2	(*) 2s	23.5	41.3	25	83
IV (0.2 Al_2O_3)					
3	(i) 1f	40.8	12.6	51	25
4	(i) 1f	37.3	10.5	108	10
6	(i) 2f	40.8	10.1	7	72
7	(i) 2f	41.6	10.3	7	74
2	(i) 2s	40.8	11.0	6	92
5	(i) 2s	40.4	9.1	5	91
8	(i) 2s	39.6	8.1	5	81
T1	(iii) 2s	32.8	21.3	14	76

*As-received soft condition; 2.5mm thick specimen was used.

TABLE III--Cont'd Fatigue Test Data

Spec. No.	Test Condition	Cyclic Notch Strength (kg/mm^2)	Total Inelastic Strain (%)	No. of Cycles to Failure	$\Sigma \epsilon_i / \Sigma \epsilon$ (%)
V (1Ag, 0.1 Zr)					
3	(i) 1f	31.7	26.0	40	65
4	(i) 1f	32.3	33.6	58	58
6	(i) 2f	31.8	26.1	17	77
7	(i) 2f	33.6	25.1	18	70
2	(i) 2s	31.6	23.5	12	98
5	(i) 2s	31.1	21.7	15	72
8	(i) 2s	30.9	29.6	17	87
T2	(iii) 2s	19.9	34.4	18	95

Test conditions: (i) cold worked; (ii) cold worked and annealed at 650°C, 10 min; (iii) repeated annealing at 538°C, 10 min.

TABLE IV

Summary of AE Count Data on Cold Worked Condition (i)

Specimen No.	Loading Condition	Total Counts	Percentages of Elastic	Percentages of Inelastic	Unload	Total Count less 1st	Percentages of Elastic	Percentages of Inelastic	Unload	Percentages of Counts in 1st cycle
II-3	(1f)	18213	30	62	8	1403	28	29	44	92.3
4	(1f)	4814	84	13	3	214	25	35	40	95.6
7	(2f)	141680	63	31	5	36980	72	8	20	73.9
9	(2f)	17586	64	36	0	3986	88	12	0	77.3
5	(2s)	1543	24	72	4	243	50	28	22	87.3
6	(2s)	2485	46	49	5	285	54	24	22	88.5
III-3	(1f)	29331	64	34	2	8231	31	61	8	71.9
4	(1f)	9236	65	29	5	936	5	81	14	89.8
7	(2f)	34205	69	20	11	2900	53	38	9	91.3
8	(2f)	15209	63	36	1	2789	76	23	1	81.7
10	(2f)	5865	20	73	7	2647	3	96	1	54.9
N3	(2f)	2325	22	77	1	695	0	99	1	70.0
5	(2s)	9120	18	81	1	3400	4	93	3	62.7
6	(2s)	21315	9	64	27	1315	30	44	26	93.8
9	(2s)	3515	7	90	3	2040	3	95	3	42
N2	(2s)	9340	22	70	8	5890	4	93	3	57.6
IV-3	(1f)	27165	68	25	7	8915	37	49	14	67.2
4	(1f)	3928	47	39	14	2031	27	48	25	48.4
6	(2f)	11241	62	30	8	2141	22	61	17	81.0
7	(2f)	22816	76	22	2	1086	76	12	12	95.7
2	(2s)	5596	60	32	8	1116	12	65	23	95.9
5	(2s)	3701	54	40	6	151	72	13	15	80.1
8	(2s)	1553	60	35	5	397	7	81	12	74.7
V-3	(1f)	6087	19	77	4	2037	33	59	8	66.6
4	(1f)	13143	31	66	3	3543	30	59	13	73.0
6	(2f)	32615	86	12	1	4215	75	19	6	87.1
7	(2f)	17154	43	54	3	2954	49	36	13	82.8
10	(2f)	5503	54	44	1	1909	2	95	2	65.5
2	(2s)	878	35	65	0	500	0	100	0	43.1
5	(2s)	3922	15	81	4	472	18	61	21	88.0
8	(2s)	5725	11	83	6	1115	14	76	10	80.5
9	(2s)	4169	73	20	7	689	26	58	16	83.5

TABLE V

Summary of AE Count Data on Annealed Conditions

Specimen No.	Test Condition	Total Counts	Percentage of Elastic	Percentage of Inelastic	Percentage of Unload	Total Counts less 1st cycle	Percentages of Elastic	Percentages of Inelastic	Percentages of Unload
II-T2	iii-2s	91.8 x 10^4	76	23	1	89.2 x 10^4	77	22	1
T3	iii-2s	26.4	80	17	3	24.0	82	16	2
III-T2	iii-2s	60.1	78	20	2	49.4	74	23	3
IV-T1	iii-2s	54.0	61	35	4	28.5	65	31	4
V-T2	iii-2s	50.3	74	24	2	48.7	74	24	2
III-T1	ii-2f	2987	3	94	3	2647	2	95	3
T3	ii-2f	2572	4	94	2	2102	2	95	3
-NT2	ii-2f	6334	0	98	1	5404	0	98	2
-S1	*-2s	29.2 x 10^4	13	78	9	28.1 x 10^4	12	79	9
-S2	*-2s	23.1 x 10^4	0	89	10	23.0 x 10^4	0	89	10

TABLE VI

Cycle-by-Cycle Summary of AE Count Data*

Alloy II	Alloy III	
II-3	III-3	III-T1
4	4	T2
7	7	T3
9	8	NT2
5	10	S1
6	N3	S2
T2	5	
T3	6	
	9	
	N2	

Alloy IV	Alloy V
IV-3	V-3
4	4
6	6
7	7
2	10
5	2
8	5
T1	8
	9
	T2

* Individual listings follow

Specimen II-3 (i - 1f)

n	ΔN_e	ΔN_i	ΔN_u	ΔN	$\Sigma \Delta N$	f	$\Sigma\epsilon_i$(%)	ℓ(mm)
1	5000	10898	920	16810	16810	92.3	0.63	0
2	300	300	250	850	17660	97.0	1.31	0.05
3	25	65	230	320	17980	99	1.94	0.10
4	30	0	70	100	18080		2.69	0.13
5	0	5	5	10	18090		3.33	0.2
6	10	5	5	20	18110		3.83	0.3
7	2	1	12	15	18125		4.59	0.4
8	1	1	0	2	18127		5.19	0.45
9	3	2	2	7	18134		6.10	0.6
10	0	0	7	7	18141		6.90	0.8
11	5	3	4	12	18153		7.75	1.2
12	10	0	0	10	18163		8.53	2.0
13	0	3	27	30	18193		9.64	2.4
14	0	15	5	20	18213		10.48	3.0
15	0	0	0	0	18213		11.54	7.0
16	0	0	0	0	18213		12.73	
17	0	0	0	0	18213		13.73	
18	0	0	0	0	18213		14.95	
Total	5386	11290	1537		18213			
	(30)	(62)	(8)					
Total	386	400	617		1403			
less 1st	(28)	(29)	(44)					

Specimen II-4 (i - 1f)

n	ΔN_e	ΔN_i	ΔN_u	ΔN	$\Sigma\Delta N$	f	$\Sigma\epsilon_i$(%)	ℓ(mm)
1	4000	550	50	4600	4600	95.6	0.63	0.05
2	0	25	25	50	4650		1.26	0.05
3	15	15	5	35	4685		2.00	0.05
4	8	0	4	12	4697		2.67	0.1
5	5	0	5	10	4707		3.26	0.15
6	0	1	1	2	4709		3.85	0.2
7	0	5	7	12	4721		4.59	0.2
8	10	0	0	10	4731		5.22	0.5
9	2	1	5	8	4739		5.89	0.6
10	0	0	5	5	4744		6.53	0.7
11	0	2	3	5	4749	99.	7.16	0.9
12	1	0	4	5	4754		7.83	1.0
13	0	1	4	5	4759		8.36	1.2
14	2	3	3	8	4767		9.09	1.2
15	2	3	5	10	4777		9.89	1.6
16	0	0	5	5	4782		10.56	2.2
17	0	0	2	2	4784		11.36	2.6
18	2	8	0	10	4794		12.14	2.7
19	2	0	3	5	4799		12.99	2.8
20	0	5	0	5	4804		13.83	3.1
21	5	5	0	10	4814		15.05	(8.0)*

Total	4054	624	136	4814
	(84)	(13)	(3)	
Total less 1st cycle	54	74	86	214
	(25)	(35)	(40)	

* approximate value in parenthesis

Specimen II-7 (i - 2f)

n	ΔN_e	ΔN_i	ΔN_u	ΔN	$\sum \Delta N$	f	$\Sigma \epsilon_i$(%)	ℓ(mm)
1	63,000	41,300	400	104,700	104,700	73.9	1.6	0.05
2	7000	1500	950	9450	114,150	80.6	3.2	0.1
3	1900	900	280	3080	117,230	82.7	4.9	0.15
4	2750	550	650	3950	121,180		6.55	0.3
5	1750	0	450	2200	123,380	87.1	8.2	1.0
6	1000	0	450	1450	124,830		9.8	1.5
7	750	0	550	1300	126,130	88.3	11.5	2.5
8	2475	0	675	3150	129,280		13.1	3.5
9	1000	50	500	1550	130,830	92.3	14.8	4.0
10	600	0	650	1250	132,080		16.1	4.2
11	1300	0	450	1750	133,830	94.5	18.2	6.0
12	4450	0	950	5800	139,230		19.5	(7.3)
13	800	0	650	1450	140,680	94.4	21.6	(7.8)
14	450	0	150	600	141,280		23.5	(8.2)
15	400	0	0	400	141,680		25.4	(8.5)
16	0	0	0	0	141,680		27.5	(10.0)

Total	89,625	44,300	7755	141,680
	(63)	(31)	(5)	
Total less 1st cycle	26,625	3000	7355	36,980
	(72)	(8)	(20)	

Specimen II-9 (i - 2f)

n	ΔN_e	ΔN_i	ΔN_u	ΔN	$\Sigma \Delta N$	f	$\Sigma \epsilon_i$ (%)	ℓ(mm)
1	7700	5900	0	13,600	13600	77.3	1.68	0
2	900	200	5	1105	14705	83.6	3.36	0
3	500	145	2	647	15352	87.3	4.94	0.25
4	420	65	2	487	15839		6.94	0.4
5	480	10	0	490	16329	92.7	8.73	0.7
6	150	5	5	160	16489		10.52	2.4
7	97	2	1	100	16589	94.3	12.42	2.5
8	110	5	0	115	16704		14.3	3.5
9	30	10	5	45	16749		16.3	4.5
10	650	20	2	672	17421		18.52	(7.5)
11	70	3	2	75	17496		20.84	(8.0)
12	88	2	0	90	17586		23.36	
Total	11195	6367	24		17586			
	(64)	(36)	(0)					
Total less 1st cycle	3495	467	24		3986			
	(88)	(12)	(0)					

Specimen II-5 (i - 2s)

n	ΔN_e	ΔN_i	ΔN_u	ΔN	$\Sigma\Delta N$	f	$\Sigma\epsilon_i$(%)	ℓ(mm)
1	250	1050	0	1300	1300	87.3	1.62	0.05
2	55	15	10	80	1380	87.4	3.24	0.2
3	30	5	15	50	1430	92.7	4.94	0.4
4	10	5	10	25	1455	94.3	6.67	0.6
5	5	10	5	20	1475	95.5	8.42	0.8
6	5	0	7	12	1487		10.19	1.1
7	10	10	0	20	1507		12.02	2.8
8	0	0	7	7	1514		13.89	4.5
9	7	3	0	10	1524		15.79	5.0
10	0	12	0	12	1536		17.83	(8.0)
11	0	7	0	7	1543		19.95	
Total	372	1117	54		1543			
	(24)	(72)	(4)					
Total less 1st cycle	122	67	54		243			
	(50)	(28)	(22)					

Specimen II-6 (i - 2s)

n	ΔN_e	ΔN_i	ΔN_u	ΔN	$\Sigma\Delta N$	f	$\Sigma\epsilon_i$(%)	ℓ(mm)
1	1000	1150	50	2200	2200	88.5	1.36	0.1
2	80	5	15	100	2300	92.5	2.75	0.15
3	20	10	10	40	2340	94.7	4.21	0.15
4	20	5	10	35	2375	95.6	5.72	0.4
5	10	0	15	25	2400		7.26	0.8
6	10	5	10	25	2425		8.84	1.0
7	3	7	0	10	2435		10.27	2.0
8	2	6	2	10	2445		11.78	2.0
9	0	5	0	5	2450		13.40	5.0
10	2	3	0	5	2455		15.15	7.0
11	2	8	0	10	2465		16.80	(7.5)
12	1	3	1	5	2470		18.70	(8.3)
13	2	8	0	10	2480		20.40	
14	1	4	0	5	2485		22.4	
Total	1153	1219	113		2485			
	(46)	(49)	(5)					
Total less 1st cycle	153	69	63		285			
	(54)	(24)	(22)					

Specimen II-T2 (iii-2s)

n	ΔN_e	ΔN_i	ΔN_u	ΔN	$\Sigma\Delta N$	f	$\Sigma\epsilon_i(\%)$
1	12,000	13,000	1,000	26,000		2.8	1.79
2	15,5000	60,000	2,500	217,500	243,500	26.5	3.49
3	85,000	42,000	1,000	131,000	374,500	40.8	5.24
4	45,000	500	100	45,600	420,100	45.8	6.97
5	46,000	12,000	100	58,100	478,200		8.74
6	40,000	12,500	1,500	54,000	532,200	57.9	10.46
7	10,000	2,000	0	12,000	544,200		12.29
8	38,000	5,300	750	44,050	588,250	64.1	14.13
9	50,000	6,000	500	56,500	644,750		16.04
10	69,000	2,500	500	42,000	716,750	78.1	17.93
11	63,000	3,500	0	66,500	783,250		19.79
12	3,000	10,500	0	13,500	796,750	86.8	21.77
13	27,000	12,000	300	39,300	836,050		23.81
14	30,000	11,000	200	41,200	877,250	95.6	25.92
15	20,000	13,000	0	33,000	910,250		27.85
16	1,000	3,000	0	4,000	914,250		29.96
17	0	3,800	0	3,800	918,050	100.0	32.02
Total	697,000 (76)	212,600 (23)	8,450 (1)		918,050		
less 1st cycle	685,000 (77)	199,600 (22)	7,450 (1)		892,050		

Because of numerous surface cracks, ℓ could not be measured for condition iii.

Specimen II-T3 (iii-2s)

n	ΔN_e	ΔN_i	ΔN_u	ΔN	$\Sigma\Delta N$	f	$\Sigma\epsilon_i$(%)
1	15,000	8,000	1,000	24,000		9.4	1.47
2	134,000	15,000	2,000	151,000	175,000	68.5	2.94*
3	19,000	3,800	400	23,200	198,200	77.5	4.54
4	3,000	3,500	2,000	8,500	206,700		6.12
5	7,200	1,650	250	9,100	215,800		7.72
6	3,900	900	100	4,900	220,700		9.34
7	3,700	470	150	4,320	225,020		10.94
8	5,400	400	30	5,830	230,850		12.74
9	3,800	2,160	20	5,980	236,830		14.57
10	3,700	750	30	4,480	241,310		16.42
11	2,350	1,400	100	3,850	245,160		18.15
12	4,900	1,650	100	6,650	251,810		19.92
13	2,300	450	0	2,750	254,560		21.71
14	300	200	0	500	255,060		23.65
15	3,350	650	100	4,100	259,160		25.61
16	500	1,200	0	1,700	260,860		27.59
17	300	2,850	0	3,150	264,010		29.59
Total	212,300 (80)	45,430 (17)	6,280 (3)		264,010		
less 1st cycle	197,300 (82)	37,430 (16)	5,280 (2)		240,010		

*Annealed inadvertently after the first cycle at 700°C, 10 min., instead of the normal 650°C, 10 min. Other annealing was normal.

Specimen III-3 (i - 1f)

n	ΔN_e	ΔN_i	ΔN_u	ΔN	ΔN	f	$\Sigma\,\epsilon_i$(%)	ℓ(mm)
1	16000	5050	50	21100	21100	71.9	0.23	0
2	600	1700	80	2380	23480	80.0	0.33	0.05
3	300	435	55	790	24270		0.46	0.05
4	1000	600	245	1845	26115	89.	0.78	0.1
5	150	570	135	855	26970		1.07	0.1
6	320	0	5	325	27295	93.1	1.26	0.15
7	65	70	15	150	27445		1.72	0.2
8	30	108	2	140	27585	94	2.06	0.23
9	10	20	10	40	27625		2.40	0.25
10	15	40	0	55	27680	94.3	2.77	0.25
11	53	0	5	58	27738		3.09	0.3
12	18	17	5	40	27778	94.7	3.43	0.4
13	10	2	0	12	27790		3.73	0.45
14	30	35	5	70	27860	95	4.00	0.6
15	15	7	0	22	27882		4.35	0.8
16	20	0	5	25	27907	95.1	4.63	1.0
17	15	0	0	15				1.2
18	68	2	0	70	27992		5.36	1.8
19	5	5	5	15				2.8
20	20	700	5	725	28732		6.02	3.0
21	10	5	5	20				3.3
22	5	25	8	38	28790		6.42	3.6
23	8	5	3	16				3.8
24	5	0	3	8	28814		6.82	4.2
25	3	7	2	12				4.5
26	12	8	5	25	28851		7.43	5.0
27	7	15	8	30				5.3
28	3	30	7	40	28921		8.16	5.8
29	1	10	2	13				6.4
30	0	3	0	3	28937		8.84	6.6
31	0	22	1	23				7.0
32	0	35	5	40	29000		9.78	

Specimen III-3 (i - 1f) Cont'd

n	ΔN_e	ΔN_i	ΔN_u	ΔN	$\Sigma\Delta N$	f	$\Sigma\epsilon_i$(%)
33	5	20	2	27			
34	0	10	0	10	29037		10.63
35	0	12	0	12			
36	0	37	3	40	29089		12.2
37	5	45	0	50			
38	35	65	0	100	29239		13.4
39	5	35	0	40			
40	40	10	2	52	29331		15.4
Total	18888 (64)	4760 (34)	680 (2)		29331		
Total less 1st cycle	2888 (31)	4710 (61)	630 (8)		8231		

Specimen III-4 (i - 1f)

n	ΔN_e	ΔN_i	ΔN_u	ΔN	$\Sigma\ \Delta N$	f	$\Sigma\ \epsilon_i$(%)	ℓ(mm)
1	6000	1950	350	8300	8300	89.8	0.42	0.1
2	0	0	70	70	8370	90.6	0.88	0.2
3	0	45	5	50	8420	91.1	1.47	1.0
4	5	10	5	20	8440	91.4	1.89	1.3
5	15	25	8	48	8488	91.9	25.6	2.2
6	5	10	20	35	8523	92.3	2.88	3.2
7	7	83	2	92	8615		3.6	4.0
8	2	126	2	130	8745	94.7	4.1	4.5
9	1	36	1	38	8753		4.8	6.3
10	0	265	5	970	9053	98	5.7	(7.4)
11	1	2	2	5	9058		6.75	(7.9)
12	2	10	3	15	9073		7.35	(8.5)
13	1	22	2	25	9098		7.83	(9.5)
14	0	10	8	18	9110		8.65	(10.4)
15	0	44	6	50	9160		9.5	(10.4)
16	0	5	0	5	9165		10.4	(11.3)
17	0	1	0	1	9166		11.3	
18	5	65	0	70	9236		12.5	
Total	6044 (65)	2709 (29)	483 (5)		9236			
Total less 1st cycle	44 (55)	759 (81)	133 (14)	936	936			

Specimen III-7 (i - 2f)

n	ΔN_e	ΔN_i	ΔN_u	ΔN	$\Sigma\Delta N$	f	$\Sigma\ \epsilon_i(\%)$	ℓ(mm)
1	22000	5700	3600	31300	31300	91.3	1.5	0.4
2	800	400	200	1400	32700	95.6	3.05	3.0
3	500	250	30	780	33480		4.3	3.3
4	220	50	30	300	33780		5.8	5.3
5	0	0	0	0	33780		7.3	6.5
6	5	90	5	100	33880		9.1	(8.0)
7	5	85	0	70	33970		11.0	
8	0	235	0	235	34205		13.6	
Total	23530	6810	3865		34205			
	(69)	(20)	(11)					
Total less 1st cycle	1530	1110	265		2900			
	(53)	(38)	(9)					

Specimen III-8 (i - 2f)

n	ΔN_e	ΔN_i	ΔN_u	ΔN	$\Sigma\ \Delta N$	f	$\Sigma\ \epsilon_i(\%)$	ℓ(mm)
1	7500	4850	70	12420	12420	81.7	1.3	0.1
2	800	50	0	850	13270	89.8	2.65	0.5
3	1000	85	7	1092	14362		4.3	3.0
4	135	75	3	213	14575		5.75	4.3
5	55	120	4	179	14754		7.4	6.0
6	10	41	5	56	14810		9.05	(7.5)
7	70	130	2	202	15012		10.75	(8.0)
8	50	105	2	157	15109		12.68	(9.1)
9	3	37	0	40	15209		14.6	(10.5)
Total	9623	5493	93		15209			
	(63)	(36)	(1)					
Total less 1st cycle	2123	643	23		2789			
	(76)	(23)	(1)					

Specimen III-10 (i - 2f)

n	ΔN_e	ΔN_i	ΔN_u	ΔN	$\Sigma\ \Delta N$	f	$\Sigma\ \epsilon_i(\%)$	ℓ(mm)
1	1100	2020	100	3220	3220	55	1.08	1.8
2	60	300	5	365	3585	61	3.28	3.4
3	3	515	5	523	4108		5.05	4.5
4	2	390	12	404	4512	77	6.04	5.6
5	5	510	4	519	5031	86	8.63	
6	2	830	2	834	5865		10.65	
Total	1172 (20)	4565 (73)	130 (7)		5865			
Total less 1st cycle	72 (3)	2545 (96)	30 (1)		2647			

Specimen III-N-3 (i - 2f)

n	ΔN_e	ΔN_i	ΔN_u	ΔN	$\Sigma\ \Delta N$	f	$\Sigma\ \epsilon_i(\%)$	ℓ(mm)
1	520	1100	10	1630	1630	70	1.82	0.1
2	0	130	0	130	1760	76	3.81	1.0
3	0	180	0	180	1940		5.23	3.8
4	0	130	0	130	2070	89	6.71	5.5
5	0	110	0	110	2180		8.63	7.0
6	0	100	5	105	2285	98	10.52	
7	0	40	0	40	2325		17.63	
Total	520 (22)	1740 (77)	15 (1)		2325			
Total less 1st cycle	0 (0)	690 (99)	5 (1)		695			

Specimen III-5 (i-2s)

n	ΔN_e	ΔN_i	ΔN_u	ΔN	$\Sigma\ \Delta N$	f	$\Sigma\ \varepsilon_i$(%)	ℓ (mm)
1	1500	4200	20	5720	5720	62.7	1.3	0.1
2	20	555	15	590	6310	69.2	2.6	0.3
3	30	520	10	560	6870	75.3	4.0	1.6
4	10	320	15	345	7215		5.5	3.0
5	10	400	15	425	7640	83.8	6.9	3.9
6	10	380	10	400	8040		8.3	5.3
7	30	330	10	370	8410	92.2	9.7	6.0
8	10	140	5	155	8565		11.3	7.0
9	10	110	10	130	8695	95.3	12.9	(8.0)
10	10	140	10	160	8855		14.6	(8.6)
11	0	150	5	155	9010	98.8	16.5	(10.0)
12	0	110	0	110	9120	100.0	18.6	(10.5)
Total	1640	7355	125		9120			
	(18)	(81)	(1)					
Total less 1st cycle	140	3155	105		3400			
	(4)	(93)	(3)					

Specimen III-6 (i-2s)

n	ΔN_e	ΔN_i	ΔN_u	ΔN	$\Sigma\ \Delta N$	f	$\Sigma\ \varepsilon_i$(%)	ℓ (mm)
1	1500	13100	5400	2000	2000	93.8	1.5	0.1
2	200	50	300	550	20550	96.4	3.0	0.5
3	110	50	10	170	20720	97.2	5.15	3.5
4	60	275	15	350	21070	98.6	6.8	6.0
5	10	30	13	53	21123		8.4	(8.0)
6	10	100	5	115	21238		10.2	(10.0)
7	0	77	0	77	21315	100.0	12.5	(10.7)
Total	1890	13682	5743		21315			
	(9)	(64)	(27)					
total less 1st cycle	390	582	343		1315			
	(30)	(44)	(26)					

Specimen III-9 (i-2s)

n	ΔN_e	ΔN_i	ΔN_u	ΔN	$\Sigma \Delta N$	f	$\Sigma \varepsilon_i$ (%)	ℓ (mm)
1	200	1240	35	1475	1475	42.	1.49	0.1
2	10	415	10	435	1910	54.3	3.05	1.8
3	30	590	18	638	2548	72.5	5.05	3.4
4	5	310	7	322	2870	81.6	6.8	4.4
5	3	105	6	114	2984	84.9	8.8	6.8
6	2	318	5	325	3309	94.1	10.7	
7	1	200	5	206	3515		12.7	
Total	251	3178	86		3515			
	(7)	(90)	(3)					
Total less 1st cycle	51	1938	51		2040			
	(3)	(95)	(3)					

Specimen III-N2 (i-2s)

n	ΔN_e	ΔN_i	ΔN_u	ΔN	$\Sigma \Delta N$	f	$\Sigma \varepsilon_i$ (%)	ℓ (mm)
1	1850	1100	500	3450	3400	31.4	1.26	0
2	0	300	0	300	3750		2.74	0.5
3	0	150	0	150	3900	40.8	4.21	3.0
4	0	100	0	100	4000		5.68	5.5
5	100	1600	30	1730	5730	61.4	7.24	7.0
6	100	700	30	830	6560		8.80	
7	0	900	50	950	7510	80.5	10.90	
8	0	600	30	630	8140		12.21	
9	50	1130	20	1200	9340		14.13	
Total	2100	6580	660		9340			
	(22)	(70)	(8)					
Total less 1st cycle	250	5480	110		5890			
	(4)	(93)	(3)					

Specimen III-T1 (ii-2f)

n	ΔN_e	ΔN_i	ΔN_u	ΔN	$\Sigma \Delta N$	f	$\Sigma \epsilon_i$ (%)	ℓ (mm)
1	50	270	20	340	340	10	2.0	
2	0	135	0	135	475		3.7	
3	10	125	0	135	610	18	5.79	
4	0	50	15	65	675		7.68	
5	2	185	10	197	872		9.43	0.2
6	2	280	5	287	1159		11.26	0.2
7	3	310	10	323	1482		12.95	0.2
8	32	550	5	557	2039	61	14.63	0.4
9	3	125	2	130	2169		16.25	0.5
10	2	90	8	100	2269		17.93	0.8
11	4	85	3	92	2361		19.52	2.0
12	3	105	4	112	2473	74	21.2	3.2
13	6	70	3	79	2552		22.89	3.4
14	3	60	0	63	2615		24.54	4.8
15	2	82	5	89	2704		26.26	5.5
16	8	50	2	60	2764		28.11	7.0
17	0	115	0	115	2879		30.08	
18	0	108	0	108	2987		32.08	
Total	100	2795	92		2987			
	(3)	(94)	(3)					
Total less 1st cycle	50	2525	72		2647			
	(2)	(95)	(3)					

Specimen III-T2 (iii-2s)

n	ΔN_e	ΔN_i	ΔN_u	ΔN	$\Sigma \Delta N$	f	$\Sigma \epsilon_i$ (%)
1	10000	4000	3000	17000	17000	2.8	1.68
2	25000	1800	3200	30000	47000	7.8	3.36
3	67000	5000	4200	76200	123200	20.5	5.12
4	53000	34000	1700	88700	211900	35.2	6.88
5	28000	11700	1000	40700	252600	42.0	8.62
6	51000	6500	500	58000	310600	51.6	10.3
7	61800	7200	100	69100	379700		11.98
8	46000	6000	1000	53000	432700	72.	13.66
9	12000	5000	1-1500	17000	449700		15.37
10	19000	11000	300	28300	478000	79.5	17.05
11	30500	11500	500	42500	520500		18.79
12	24000	5600	200	29800	550300	91.5	20.6
13	27000	6700	100	33800	584100	97.1	22.43
14	11000	3100	0	14100	598200	99.5	24.32
15	0	50	20	70	598270		26.13
16	1000	2100	20	3120	601390		28.02
Total	466300 (78)	118250 (20)	16840 (2)	601390	601390		
Total less 1st cycle	366300 (74)	114250 (23)	13840 (3)		494390		

Specimen III-T3 (ii-2f)

n	ΔN_e	ΔN_i	ΔN_u	ΔN	$\Sigma \Delta N$	f	$\Sigma \epsilon_i$ (%)	ℓ (mm)
1	50	410	10	470	470	18	1.68	
2	2	98	0	100	570		3.39	
3	5	77	2	84	654		5.10	
4	2	240	3	245	899	35	6.74	
5	2	425	2	429	1328		8.42	
6	3	100	3	106	1434	56	10.00	
7	3	80	10	93	1527		11.68	0.2
8	2	60	4	66	1593		13.40	0.25
9	6	35	2	43	1636		15.09	0.3
10	2	50	2	54	1690	61	16.77	0.5
11	3	32	2	37	1727		18.48	0.8
12	2	60	1	63	1790		20.10	2.2
13	2	100	3	105	1893		21.74	3.6
14	2	175	2	179	2074	81	23.38	4.5
15	2	85	2	89	2163		25.05	6.0
16	3	50	2	55	2218		26.79	7.0
17	2	60	4	66	2284		28.52	
18	2	145	2	149	2433		31.41	
19	1	137	1	139	2572		32.31	
Total	96 (4)	2419 (94)	57 (2)		2572			
Total less 1st cycle	46 (2)	2009 (95)	47 (3)		2102			

Specimen III-NT2 (ii-2f)

n	ΔN_e	ΔN_i	ΔN_u	ΔN	$\Sigma \Delta N$	f	$\Sigma \epsilon_i$ (%)	ℓ (mm)
1	10	920	0	930	930	15	1.85	0
2	0	500	0	500	1430		3.68	0
3	10	740	0	750	2180	34	5.47	0
4	5	130	5	140	2320		7.20	0
5	0	550	5	555	2875		8.96	0
6	0	50	10	60	2935	46	10.74	0
7	10	10	5	25	2960		12.48	0
8	0	40	5	45	3005		14.25	0
9	3	40	0	43	3048		15.90	0
10	4	80	0	84	3132	49	17.62	0
11	0	110	10	120	3252		19.3	0
12	0	930	20	250	3502		21.4	0
~~13~~	~~0~~	~~120~~	~~5~~	~~125~~	~~3627~~		~~23.2~~	~~0.1~~
14	4	180	0	184	3811	60	24.8	0.25
15	0	250	0	250	4061		26.4	1.5
16	0	180	0	180	4241		28.2	2.5
17	3	250	10	263	4504		29.7	3.3
18	0	420	0	420	4924		31.5	4.8
19	0	300	0	300	5224	82	33.2	5.4
20	0	510	10	520	5744		34.4	
21	0	320	0	320	6064	96	36.2	
22	0	270	0	270	6334		38.4	
Total	49	6200	85		6334			
	(0)	(98)	(1)					
Total less 1st cycle	39	5280	85		5404			
	(0)	(98)	(2)					

Specimen III-S1 (as-received, annealed - 2s)

n	ΔN_e	ΔN_i	ΔN_u	ΔN	$\Sigma \Delta N$	f	$\Sigma \epsilon_i$ (%)	ℓ (mm)
1	3000	7000	800	10800	10800	3.6	1.8	0
2	4000	4500	500	9000	19800	6.7	3.57	0
3	1200	12900	1000	15100	34900		5.34	0
4	100	13400	1800	30400	50200	17.	7.05	0
5	2000	16100	1200	49700	69500		8.76	0
6	1000	12900	1100	15000	84500		10.44	0
7	5600	11100	2000	18700	103200		12.12	0
8	500	16500	2300	19300	122500	42.	13.76	0
9	1500	15100	2400	19000	141500		15.4	0
10	2000	16500	800	19300	160800		16.94	0
11	2000	19300	2900	29200	18500		18.94	0
12	1000	33900	2000	36900	221900		19.94	0
13	1500	25500	2200	29400	251100		21.48	0
14	3000	11000	3700	17700	268800		23.06	.5
15	3500	1500	700	5700	274500		24.56	1.5
16	1000	1500	600	3100	277600		26.06	2.2
17	500	1100	200	1800	279400	96.	27.56	3.5
18	300	950	100	1350	280750		28.82	3.9
19	500	1050	200	1750	282500		30.25	5.4
20	500	700	100	1300	283800		31.6	6.1
21	200	1250	20	1470	285270		33.07	7.1
22	700	1000	10	1710	286980		34.56	
23	100	1200	10	1310	288290		36.14	
24	500	1700	50	2250	290540		37.87	
25	50	800	10	860	291400		39.34	
26	0	800	0	800	292200		41.23	
Total	36250 (13)	228750 (78)	27200 (9)		292200			
Total less 1st cycle	33250 (12)	221750 (79)	26400 (9)		281400			

Specimen III-S2 (as-received, annealed - 2s)

n	ΔN_e	ΔN_i	ΔN_u	ΔN	$\Sigma\Delta N$	f	$\Sigma\epsilon_i$ (%)	ℓ (mm)
1	0	1300	30	1330	1330		1.89	0
2	0	1950	100	2050	3380		3.79	0
3	0	2000	20	2020	5400		5.37	0
4	0	1950	10	1960	7360		7.05	0
5	0	1700	60	1760	9120		8.74	0
6	0	6150	20	6170	15290	7.1	10.42	0
7	0	93000	15600	108600	123890	54.	12.00	0
8	0	56000	3700	59700	183590	79	13.68	0
9	150	20000	2650	22800	206390		15.26	0
10	0	3900	250	4150	210540	91	16.84	0
11	150	5600	550	6300	216840		18.42	0
12	50	4100	250	4400	221240		20.53	0
13	0	1250	150	1400	222640		22.00	0.3
14	200	800	10	1010	223650		23.65	0.8
15	10	1100	20	1130	224780		25.16	1.3
16	20	680	10	710	225490		26.7	2.0
19	0	500	70	570	226060		28.32	2.8
18	0	700	0	700	226760		29.79	3.5
19	0	600	0	600	227360		31.41	4.0
20	0	700	10	710	228070		32.95	5.6
21	0	500	10	510	228580		34.48	6.8
22	0	490	10	500	229080		36.06	
23	0	580	10	590	229670		37.53	
24	0	980	0	980	230650		39.32	
25	0	300	0	300	230950		41.32	
Total	580	206830	23540	230950				
	(0)	(89)	(10)					
Total less 1st cycle	580	205530	23510		229620			
	(0)	(89)	(10)					

Specimen IV-3 (i-1f)

n	ΔN_e	ΔN_i	ΔN_u	ΔN	$\Sigma \Delta N$	f	$\Sigma \epsilon_i$ (%)	ℓ (mm)
1	15000	2508	750	18250	18250	67.2	0.21	0
2	2000	4000	300	6300	24550	90.4	0.32	0
3	750	5	95	850	25400	93.5	0.52	0.05
4	40	4	21	65	25465	93.7	0.52	0.1
5	140	5	85	230	25695	94.6	0.52	0.15
6	30	5	50	85	25780		0.63	0.20
7	10	4	141	155	25935		0.78	0.20
8	10	125	165	300	26235		0.78	0.25
9								
|	(192	0	221	413)	26648	98.0		
29							1.03	0.25
30	5	100	10	115	26763		1.26	0.4
31	10	0	10	20	26783		1.47	0.5
32	5	5	40	50	26833	98.8	1.62	0.7
33	6	0	2	8	26841		1.62	0.9
34	65	0	15	80	26921	99.1	1.68	0.9
35	25	95	5	125	27046		2.10	1.1
36	10	0	5	15	27061		3.37	2.8
37	5	0	5	10	27071		3.83	3.2
38	2	0	8	10	27081		4.15	3.5
39	6	0	4	10	27091		4.53	4.4
40	2	0	10	12	27103		4.95	5.2
41	0	0	10	10	27113		5.47	5.5
42							6.04	6.0
43							6.53	6.3
44							7.05	6.6
45							7.68	6.6
46	12	0	40	52			8.11	6.6
47							9.31	
48							10.00	
49							10.74	
50							11.50	
51					27165		12.60	
Total	18325	6848	1992		27165			
	(68)	(25)	(7)					
Total less 1st cycle	3325	4848	1242		8915			
	(37)	(49)	(14)					

Specimen IV-4 (i-1f)

n	ΔN_e	ΔN_i	ΔN_u	ΔN	$\Sigma \Delta N$	f	$\Sigma \epsilon_i$ (%)	ℓ(mm)
1	1300	550	50	1900	1900	48.4	0.21	
2	0	300	100	400	2300	58.6	0.32	
3	0	0	0	0	2300	58.6	0.32	
4	0	11	2	13	2313	58.9	0.32	
5	2	6	4	12	2325		0.42	
6	2	3	13	18	2343		0.42	
7	0	0	0	0	2343		0.48	
8	0	160	5	165	2508	63.8	0.53	
9	0	370	5	375	2883	73.8	0.57	
10	50	0	5	55	2938		0.63	
11	50	0	35	85	3023	77.0	0.63	
12	0	30	20	50	3073		0.67	
13	0	0	30	30	3103	79.0	0.72	
14	0	85	5	90	9193	81.8	0.76	
15								0.05
⋮	397	0	258					
85				655	3848	98.	1.47	0.05
86							1.54	0.3
87							1.58	0.35
88							1.64	0.45
	19	6	10	35				
89							1.73	0.50
90					3883		2.50	2.50
91							2.91	3.8
92							3.12	4.8
93							3.24	5.0
94							3.58	6.0
	25	10	18	45				
95							3.79	6.5
95							4.42	(7.5)
⋮								
108					3928		10.52	
Total	1845 (47)	1531 (39)	552 (14)		3928			
Total less 1st cycle	548 (27)	981 (48)	502 (25)		2031			

Specimen IV-6 (i-2f)

n	ΔN_e	ΔN_i	ΔN_u	ΔN	$\Sigma \Delta N$	f	$\Sigma \epsilon_i$ (%)	ℓ(mm)
1	6500	2100	500	9100	9100	81.0	1.05	0.05
2	200	1250	280	1730	10830	96.3	2.31	1.5
3	150	0	50	200	11030	98.1	3.68	4.5
4	115	60	18	193	11223		4.84	7.0
5	1	2	10	13	11236		6.32	
6	3	2	0	5	11241		8.11	
7	0	0	0	0	11241	100.0	10.11	
Total	6969	3414	858		11241			
	(62)	(30)	(8)					
Total less 1st cycle	469	1314	358		2141			
	(22)	(61)	(17)					

Specimen IV-7 (i-2f)

n	ΔN_e	ΔN_i	ΔN_u	ΔN	$\Sigma \Delta N$	f	$\Sigma \epsilon_i$ (%)	ℓ (mm)
1	16500	4800	430	21730	21730	95.7	1.4	1.0
2	500	50	70	620	22350	98.0	2.53	3.0
3	80	85	5	170	22520		3.7	5.0
4	15	0	25	40	22560		5.05	6.5
5	228	0	28	256	22816		6.6	(7.8)
6	0	0	0	0	22816		8.3	(9.2)
7	0	0	0	0	22816		10.32	(10.5)
Total	17323	4935	558		22816			
	(76)	(22)	(2)					
Total less 1st cycle	823	135	128		1086			
	(76)	(12)	(12)					

Specimen IV-2 (i-2s)

n	ΔN_e	ΔN_i	ΔN_u	ΔN	$\Sigma\Delta N$	f	$\Sigma\epsilon_i$ (%)	ℓ (mm)
1	3200	1080	200	4480	4480	80.1	1.4	0.05
2	90	450	130	670	5150		3.4	2.0
3	20	250	110	380	5530		5.05	4.5
4	7	10	8	25	5555		6.52	7.0
5	8	10	8	26	5581		8.42	
6	5	5	5	15	5596		10.63	
Total	3330 (60)	1805 (32)	461 (8)		5596			
Total less 1st cycle	130 (12)	725 (65)	261 (23)		1116			

Specimen IV-5 (i-2s)

n	ΔN_e	ΔN_i	ΔN_u	ΔN	$\Sigma\Delta N$	f	$\Sigma\epsilon_i$ (%)	ℓ(mm)
1	1900	1450	200	3550	3550	95.9	1.68	1.0
2	85	15	10	110	3660		3.26	4.5
3	12	1	7	20	3680		4.99	(7.3)
4	7	3	3	13	3693		6.97	(9.5)
5	5	1	2	8	3701		9.05	(10.6)
Total	2009 (54)	1470 (40)	222 (6)		3701			
Total less 1st cycle	109 (72)	20 (13)	22 (15)		151			

Specimen IV-8 (i-2s)

n	ΔN_e	ΔN_i	ΔN_u	ΔN	$\Sigma\Delta N$	f	$\Sigma\epsilon_i$(%)	ℓ(mm)
1	900	230	30	1160	1160	74.7	1.68	1.5
2	2	5	20	27	1187		3.07	4.0
3	15	10	12	37	1224	78.8	4.50	5.8
4	7	300	8	315	1539	99.	6.14	(8.0)
5	6	5	3	14	1553		8.10	
Total	930 (59.9)	550 (35.4)	73 (4.7)		1553			
Total less 1st cycle	30 (7)	320 (81)	47 (12)		397			

Specimen IV-T1 (iii-2s)

n	ΔN_e	ΔN_i	ΔN_u	ΔN	$\Sigma \Delta N$	f	$\Sigma \epsilon_i$ (%)	ℓ (mm)
1	144000	102000	9000	255000		47.2	1.47	0.5
2	53000	60000	8800	121800	376800	69.7	2.86	1.5
3	12000	10500	3000	25500	402300		4.29	2.3
4	2000	500	0	2500	404800		5.74	3.5
5	46000	6200	100	52300	457100	85.0	7.21	4.0
6	32000	3000	0	35000	492100		8.73	4.5
7	0	75	45	120	492220		10.2	5.0
8	5000	1700	0	6700	498920	92.3	11.69	5.7
9	850	700	0	1550	500470		13.25	6.2
10	12000	2000	0	14000	514470		14.72	6.6
11	15300	2500	0	17800	532270	98.5	16.19	(7.5)
12	2000	100	300	2400	534670		17.81	
13	900	200	30	1130	535800		19.49	
14	3200	1400	50	4650	540450	100.0	21.28	
Total	328250	190875	21325	540450				
	(61)	(35)	(4)					
Total less 1st cycle	184250	88875	12325		285450			
	(65)	(31)	(4)					

Specimen V-3 (i-1f)

n	ΔN_e	ΔN_i	ΔN_u	ΔN	$\Sigma\Delta N$	f	$\Sigma\epsilon_i$(%)	ℓ(mm)
1	500	3500	50	4050	4050	66.6	0.52	0
2	0	650	0	650	4700	79.3	0.95	0.05
3	2	1	7	10	4710	79.5	1.41	0.1
4	10	255	5	270	4980	81.9	1.89	0.1
5	20	1	5	26	5006	82.4	2.42	0.15
6								0.15
7								0.2
8								0.2
9								0.3
10								0.7
11								1.1
12	[55]	[9]	[48]	[112]				1.3
13								1.4
14								1.4
15								1.7
16								2.0
17								2.0
18								2.1
19								2.1
20								2.2
21								2.3
22					5118	84.2	11.47	3.0
23	20	240	28	288	5406	88.9	12.04	3.4
24	10	40	8	58	5464	89.7	12.54	4.2
25	318	0	5	323	5787	95.2	13.1	4.6
26	8	1	1	10	5797			5.6
27	16	1	3	20	5817		14.48	5.8
28	10	0	1	11	5828			6.0
29	2	4	10	16	5844		15.79	
30	22	0	2	24	5868			
31–40	(170)	(6)	(43)	(219)	6087		26.0	
Total	1163 (19)	4708 (77)	216 (4)		6087			
Total less 1st cycle	663 (33)	1208 (59)	166 (8)		2037			

Specimen V-4 (i-1f)

n	ΔN_e	ΔN_i	ΔN_u	ΔN	$\Sigma \Delta N$	f	$\Sigma \epsilon_i$ (%)	ℓ(mm)
1	3000	6600	0	9600	9600	73.0	0.42	0
2	500	1360	120	1980	11580	88.1	0.77	0
3	300	250	0	550	12130	92.3	1.05	0
4	100	142	5	247	12377	94.1	1.47	0.05
5	0	10	10	20	12397		1.83	0.1
6	0	140	5	145	12542	95.4	2.21	0.1
7	0	0	0	0	12542		2.52	0.15
8	0	0	0	0	12542		2.94	0.15
9	0	0	5	5	12547		3.26	0.15
10	25	83	5	113	12660		3.74	0.25
11	2	1	4	7	12667		4.2	0.25
12	0	0	120	120	12787		4.67	0.3
13							5.05	0.3
14							5.36	0.3
15							5.86	0.4
16							6.31	0.5
17	43	6	51	100	12887		6.73	0.6
18							7.15	0.7
19							7.62	0.75
20							8.04	0.8
21							8.46	1.3
22							8.94	1.5
23							9.47	1.7
24							9.93	1.75
25							10.98	2.2
26							11.57	2.3
27	29	20	42	91	12978		12.04	2.5
28							12.50	2.5
29								2.5
30							13.51	2.6
31								2.7
32							14.52	2.8
33								3.0
34							15.6	3.4
35								3.8
36							16.77	4.2
37	15	20	10	45	13023			4.5
38							18.04	4.8
39								5.0
40								5.3
41							19.85	5.5
42								5.7
43								6.1
44								6.2
45							22.5	6.4
46	40	50	30	120	13143			6.7
47								7.0
48								
⋮								
58							33.57	
Total	4054 (31)	8682 (66)	407 (3)		13143			
Total less 1st cycle	1054 (30)	2082 (59)	407 (13)		3543			

Specimen V-6 (i-2f)

n	ΔN_e	ΔN_i	ΔN_u	ΔN	$\Sigma\Delta N$	f	$\Sigma\epsilon_i$ (%)	ℓ (mm)
1	25000	3200	200	28400	28400	87.1	1.35	0.1
2	950	60	180	1190	29590	90.5	2.88	0.15
3	450	165	5	620	30210	92.4	4.4	0.5
4	203	8	2	213	30423		6.1	0.8
5	118	3	0	121	30544		7.6	1.3
6	67	5	23	95	30639		9.1	1.6
7	165	135	5	205	30844	94.6	10.4	1.8
8	130	1	5	136	30980		11.9	2.4
9	350	425	5	780	31760		13.3	3.1
10	165	5	1	171	31931		14.7	3.4
11	319	0	6	325	32256		16.40	3.7
12	40	30	2	72	32328		17.8	4.1
13	150	3	3	156	32484	99.6	19.3	5.2
14	25	4	2	31	32515		20.8	5.4
15	5	2	0	7	32522		22.4	5.6
16	6	1	2	9	32531		24.0	5.6
17	31	53	0	84	32615	100.0	26.1	
Total	28174 (86)	4000 (12)	441 (1)		32615			
Total less 1st cycle	3174 (75)	800 (19)	241 (6)		4215			

Specimen V-7 (i-2f)

n	N_e	ΔN_i	ΔN_u	ΔN	$\Sigma\Delta N$	f	$\Sigma\epsilon_i$(%)	ℓ(mm)
1	6000	8200	50	14200	14200	82.8	1.2	0
2	800	350	250	1400	15600	90.9	2.3	0.1
3	350	150	100	600	16200	94.4	3.5	0.15
4	50	60	0	110	16310	95.1	4.7	0.2
5	0	20	0	20	16330		5.9	1.0
6	150	5	5	160	16490		7.3	2.0
7	0	180	0	180	16670		8.5	2.2
8	2	3	5	10	16680		9.85	2.8
9	8	130	2	140	16820		11.1	4.0
10	5	25	0	30	16850		12.4	4.4
11	2	10	2	14	16864		13.6	4.6
12	55	2	7	64	16928		14.95	5.6
13	0	15	2	17	16945		16.35	6.0
14	25	0	10	35	16980		17.8	(7.5)
15	0	162	8	170	17150		19.3	(9.0)
16	0	1	1	2	17152		21.16	
17	0	1	1	2	17154		22.95	
18	0	0	0	0	17154		21.1	
Total	7447 (43)	9264 (54)	443 (3)		17154			
Total less 1st cycle	1447 (49)	1064 (36)	393 (13)		2954			

Specimen V-10 (i-2f)

n	ΔN_e	ΔN_i	ΔN_u	ΔN	$\Sigma \Delta N$	f	$\Sigma \epsilon_i$ (%)	ℓ (mm)
1	2955	620	19	3594	3594	65	1.49	0
2	17	14	1	32	3626		3.09	0.1
3	10	63	3	76	3702	67	4.78	0.2
4	3	27	2	32	3734		6.38	0.6
5	1	70	2	73	3807		8.04	1.1
6	1	3	0	4	3811	69	9.68	3.5
7	3	411	6	420	4231		11.37	3.6
8	0	360	3	363	4594		12.99	4.0
9	2	20	8	30	4624	84	14.67	5.2
10	2	190	3	195	4819		16.42	6.2
11	1	2	2	5	4824		18.21	6.9
12	2	86	4	92	4916		20.00	
13	0	1	3	4	4920		21.81	
14	1	235	3	239	5159		23.79	
15	0	330	2	332	5491		25.89	
16	0	10	2	12	5503		28.42	
Total	2998	2442	63		5503			
	(54)	(44)	(1)					
Total less 1st cycle	43	1822	44		1909			
	(2)	(95)	(2)					

Specimen V-2 (i-2s)

	n	ΔN_e	ΔN_i	ΔN_u	ΔN	$\Sigma\Delta N$	f	$\Sigma\epsilon_i$ (%)	ℓ (mm)
	1	305	73	0	378	378	43.1	1.76	0.05
	2	0	0	0	0	378		3.78	0.1
	3	0	0	0	0	378		5.64	0.6
	4	0	0	0	0	378		7.53	2.0
	5	0	500	0	500	878	100.0	9.47	2.3
	6	0	0	0	0	878		11.30	3.0
	7	0	0	0	0	878		13.26	5.3
	8	0	0	0	0	878		15.15	6.3
	9	0	0	0	0				7.0
	10	0	0	0	0				
	11	0	0	0	0				
	12	0	0	0	0			23.51	
Total		305 (35)	573 (65)	0 (0)		878			
Total less 1st cycle		0 (0)	500 (100)	0 (0)					

Specimen V-5 (i-2s)

	n	ΔN_e	ΔN_i	ΔN_u	ΔN	$\Sigma\Delta N$	f	$\Sigma\epsilon_i$(%)	ℓ(mm)
	1	500	2900	50	3450	3450	88.0	1.43	0.1
	2	10	10	30	50	3500		2.75	0.1
	3	10	10	2	22	3522	89.8	4.21	0.2
	4	10	45	15	70	3592		5.62	0.6
	5	10	2	8	20	3612		6.8	1.0
	6	10	0	10	20	3632	92.6	8.25	1.4
	7	5	1	1	7	3639		9.72	1.7
	8	5	2	1	8	3647		11.05	2.8
	7	5	2	8	15	3662		12.42	3.2
	10	2	2	4	8	3670	93.7	13.78	4.3
	11	2	2	3	7	3677		15.2	4.3
	12	0	80	5	85	3762	96.0	16.67	4.8
	13	5	120	5	130	3892		18.3	5.0
	14	2	2	1	5	3897		19.83	5.8
	15	10	10	5	25	3922		21.72	7.0
Total		586 (15)	3188 (81)	148 (4)		3922			
Total less 1st cycle		86 (18)	288 (61)	98 (21)		472			

Specimen V-8 (i-2s)

n	ΔN_e	ΔN_i	ΔN_u	ΔN	$\Sigma \Delta N$	f	$\Sigma \epsilon_i$ (%)	ℓ(mm)
1	500	3900	210	4610	4610	80.5	1.66	0
2	75	15	15	105	4715		3.32	0.1
3	5	3	15	23	4738	82.7	5.05	0.2
4	3	8	6	17	4755		6.70	0.4
5	15	5	20	40	4795		8.31	1.0
6	4	4	10	18	4813	84.	10.0	1.8
7	3	4	5	12	4825		11.64	2.5
8	4	3	3	10	4835		13.22	3.5
9	15	2	10	27	4862		14.8	4.3
10	14	180	8	202	5064	88.5	16.6	4.5
11	5	40	8	53	5117		18.3	5.3
12	5	140	5	150	5267	92.	20.0	6.8
13	5	240	4	249	5516	96.3	21.89	
14	5	80	9	94	5610	98.	23.75	
15	1	2	1	4	5614		25.6	
16	0	110	1	111	5725		27.47	
17	0	0	0	0	5725		29.58	
Total	659	4736	330		5725			
	(11)	(83)	(6)					
Total less 1st cycle	159	836	110		1115			
	(14)	(76)	(10)					

Specimen V-9 (i-2s)

n	ΔN_e	ΔN_i	ΔN_u	ΔN	$\Sigma\Delta N$	f	$\Sigma\epsilon_i$ (%)	ℓ (mm)
1	2860	435	185	3480	3480	83	1.70	0.1
2	90	150	26	266	3746		3.49	0.2
3	14	23	12	49	3795	91	5.20	0.35
4	10	15	15	40	3835		6.90	1.20
5	14	86	10	110	3945		8.63	1.9
6	10	60	13	83	4028		10.42	4.2
7	0	48	4	52	4080	98	12.15	4.7
8	12	2	8	22	4102		13.96	5.0
9	11	2	6	19	4121		15.83	5.6
10	3	1	8	12	4133		17.71	6.7
11	8	0	1	9	4142		19.58	7.0
12	2	3	5	10	4152		21.54	
13	2	2	2	6	4158		23.56	
14	0	8	3	11	4169		25.83	
Total	3036	835	298		4169			
	(43)	(20)	(7)					
Total less 1st cycle	176	400	113		689			
	(26)	(58)	(16)					

Specimen V-T2 (iii-2s)

n	ΔN_e	ΔN_i	ΔN_u	ΔN	$\Sigma\Delta N$	f	$\Sigma\epsilon_i$ (%)
1	9300	5700	1000	16000		3.2	1.78
2	300000	51500	6000	357500	373500	74.3	3.56
3	21000	25000	700	46700	420200	83.8	5.45
4	1500	3500	200	5200	425400		7.25
5	750	16500	600	17850	443250		9.23
6	650	500	150	1300	444550	88.7	11.12
7	24100	4900	250	29250	473800		13.1
8	6200	1450	100	7750	481550		15.00
9	4400	200	100	4700	486250		16.89
10	1650	2600	0	4250	490500	97.7	18.78
11	1000	2550	200	3750	494250		20.61
12	100	600	0	700	494950		22.61
13	300	650	10	960	495910		24.57
14	0	270	0	270	496180		26.53
15	0	1300	80	1380	497560		28.42
16	0	1050	0	1050	498610		30.38
17	0	1700	0	1700	500310		32.36
18	0	2650	0	2650	502960		34.4
Total	370950 (74)	122620 (24)	9390 (2)		502960		
Total less 1st cycle	361650 (74)	116920 (24)	8390 (2)		486960		

TABLE VII--Amplitude Distribution Analysis of Alloy III Samples

Specimen	Transducer	Counting Mode	Observed c values (cycles tested)		
Smooth		Manual	13, 1.5	The initial yielding	
	AC 375	Auto	5.5		
Tensile		Manual	15, 1.5		
Sample	Wideband	Auto	7	$\epsilon = 0 \sim 3\%$	
N-2	AC 375	Manual	2~3 (n=1);	10,3 (n=2,3);	18, 6 (n=4,5)
N-3	AC 375	Manual	2.2 (n=1)	3~6 (n=2,6)	
	AC 375	Manual	13	14	13, 2
T-3		Auto	6 (n=1,2)	6 (n=8,9)	6, 1.6 (n=12, 13)
		Manual	14	14	14
	Wideband	Auto	8	8	8
NT-2	AC 375	Manual	13 (n=1~4)	2.7, 4 (n=15~17)	
	Wideband	Auto	20, 3 (n=1~4)	26, 2 (n=15~17)	
S-2	AC 375	Manual	3~5 (n=3,4)	1.0 (n=7,8)	3~7 (n=13, 15, 18)
	Wideband	Manual	5 (n=3,4)	1.8 (n=7,8)	4~5 (n=13, 15, 18)

DISTRIBUTION LIST FOR FINAL REPORT
NAS3-18904 AETC CR134766

National Aeronautics & Space Administration
Lewis Research Center
21000 Brookpark Road
Cleveland, Ohio 44135

1	Attn:	Contracting Officer, MS 500-313
5		E. A. Bourke, MS 500-205
1		Technical Utilization Office, MS 3-16
1		Technical Report Control Office, MS 5-5
2		AFSC Liaison Office, MS 501-3
2		Library, MS 60-3
1		Office of Reliability & Quality Assurance, MS 500-211
14		R. A. Duscha , Project Manager, MS 500-313

National Aeronautics & Space Administration
Headquarters
Washington, D.C. 20546

	Attn:	Office of Aeronautics & Space Technology
1		Director, Manned Space Technology/RS
1		Director, Space Propulsion & Power/RP
1		Director, Materials & Structures/RW
1		F. W. Stephenson/RPI
	Attn:	Office of Manned Space Flight
1		Director, Advanced Manned Mission/MT
	Attn:	Office of Space Science
1		Director, Physics & Astronomy Programs/SG
1		Director, Planetary Programs/SL
1		Director, Launch Vehicles & Propulsion/SV
	Attn:	Office of Technology Utilization Division
1		Director, Technology Utilization/KT

1 National Aeronautics & Space Administration
Ames Research Center
Moffett Field, Calidfornia 94035
Attn: Library

1 National Aeronautics & Space Administration
Flight Research Center
P. O. Box 273
Edwards, California 93523

3 National Aeronautics & Space Administration
George C. Marshall Space Flight Center
Huntsville, Alabama 35912

Attn: Library J. Thomson Dr. Ray Gause

1 National Aeronautics & Space Administration
Goddard Space Flight Center
Greenbelt, Maryland 20771
Attn: Library

1. National Aeronautics & Space Administration
John F. Kennedy Space Center
Cocoa Beach, Florida 32931

Attn: Library

4 National Aeronautics & Space Administration
Lyndon B. Johnson Space Center
Houston, Texas 77001

Attn: Library J. G. Thibadaux
C. W. Yodzis W. L. Castner

3 National Aeronautics & Space Administration
Langley Research Center
Langley Station
Hampton, Virginia 23365

Attn: Library
Lewis Thurston
E. Hoffman

10 NASA Scientific & Technical Information Facility
P. O. Box 33
College Park, Maryland 20740
Attn: NASA Representative

1 Office of the Director of Defense
Research & Engineering
Washington, D. C. 20301
Attn: Office of Ass't Director(Chemical Technology)

1 Jet Propulsion Laboratory
4800 Oak Grove Drive
Pasadena, California 91103

Attn: Library

1 Defense Documentation Center
Cameron Station
Building 5
5010 Duke Street
Alexandria, Virginia 22314
Attn: TISIA

1 Advanced Research Projects Agency
Washington, D. C. 20525
Attn: Library

1 Aeronautical Systems Division
Air Force Systems Command
Wright-Patterson Air Force Base
Dayton, Ohio
Attn: Library

1 Air Force Missile Test Center
Patrick Air Force Base
Florida
Attn: Library

1 Air Force Systems Command
Andrews Air Force Base
Washington, D. C. 20332
Attn: Library

4 Air Force Rocket Propulsion Laboratory(RPR)
Edwards, California 93523

Attn: Library
R. L. Wiswell, LKDS
W. W. Wells, LKDS
D. A. Hart

1 Air Force Rocket Propulsion Laboratory(RPM)
Edwards, California 93523
Attn: Library

1 Air Force FTC (FTAT-2)
Edwards Air Force Base
California 93523
Attn: Library

1 Air Force Office of Scientific Research
Washington, D. C. 20333

Attn: Library

1 U. S. Air Force
Washington, D. C.
Attn: Library

2 Air Force Aero Propulsion Laboratory
Research & Technology Division
Air Force Systems Command
U. S. Air Force
Wright-Patterson AFB, Ohio 45433
Attn: Library (APRP)
Tom Cooper

1 Arnold Engineering Development Center
Air Force Systems Command
Tullahoma, Tennessee
Attn: Library

1 Space & Missile Systems Organization
Air Force Unit Post Office
Los Angeles, California 90045

Attn: Library(Technical Data Center)

1 Office of Research Analyses(OAR)
Holloman Air Force Base
New Mexico 88330
Attn: Library (RRRD)

1 RTD (RTNP)
Bolling Air Force Base
Washington, D. C. 20332

1 Bureau of Naval Weapons
Department of the Navy
Washington, D. C.
Attn: Library

1 Naval Research Branch Office
1030 E. Green Street
Pasadena, California 91101
Attn: Library

1 Picatinny Arsenal
Dover, New Jersey 07801
Attn: Library

1 U.S. Naval Research Laboratory
Washington, D. C. 20390
Attn: Library

1 U. S. Army Research Office(Durham)
Box CM, Duke Station
Durham, North Carolina 27706
Attn: Library

1 U. S. Army Missile Command
Redstone Scientific Information Center
Redstone Arsenal, Alabama 35808
Attn: Document Section

1 U. S. Naval Missile Center
Point Mugu, California 93041
Attn: Technical Library

1 U. S. Naval Weapons Center
China Lake, California 93557
Attn: Library

1 Aerojet-General Corporation
Space Division
9200 East Flair Drive
El Monte, California 91734
Attn: Library

3 Aerojet Liquid Rocket Company
P. O. Box 15847
Sacramento, California 95813
Attn: Technical Library 2484-2015A
R. J. LaBotz
B. Blubaugh

1 Aerospace Corporation
2400 E. El Segundo Blvd
Los Angeles, California 90045
Attn: Library

1 Garrett Corporation
Airesearch Mfg. Division
9851 Sepulveda Blvd
Los Angeles, California
Attn: Library

1 Garrett Corporation
Airesearch Mfg. Division
402 South 36th Street
Phoenix, Arizona 85034
Attn: Library

1 Aro Incorporated
Arnold Engineering Development Center
Arnold AF Station, Tennessee 37389
Attn; Library

2 Battelle Memorial Institute
505 King Avenue
Columbus, Ohio 43201
Attn: Library
R. P. Meister

4 Bell Aerosystems Inc
Box 1
Buffalo, New York 14240

Attn: Library
R. Wood
J. Flanagan
G. Malone

1 Boeing Company
Space Division
P. O. Box 868
Seatle, Washington 98124

Attn: Library

1 Boeing Company
P. O. Box 1680
Huntsville, Alabama 35801

1 Chemical Propulsion Information Agency
Applied Physics Laboratory
8621 Georgia Avenue
Silver Spring, Maryland 20910

1 Chrysler Corporation
~~Missile Division~~
P. O. Box 2628
Detroit, Michigan
Attn: Library

1 Chrysler Corporation
Space Division
P.O. Box 29200
New Orleans, Louisiana 70129
Attn: Library

1 Curtiss-Wright Corporation
Wright Aeronautical Division
Woodridge, New Jersey
Attn: Library

1 Dunegan/Endevco
Rancho Viejo Road
San Juan Capistrano, Ca 92675
Attn: Dr. David Harris

1 Fairchild Hiller Corporation
Research Center
Germantown, Maryland
Attn: Library

2 General Dynamics/Convair
P. O. Box 748
Fort Worth, Texas 76101
Attn: Library
B. O. McCauley

1 General Electric Company
Missiles & Space Systems Center
Valley Forge Space Technology Center
P. O. Box 8555
Philadelphia, Pennsylvania 19101
Attn: Library

1 General Electric Company
Apollo Support Department
P. O. Box 2500
Daytona Beach, Florida 32015
Attn: C. Bay

1 Grumman Aircraft Engineering Corporation
Bethpage, L. I. N.Y.
Attn: Library

1 Honeywell Inc.
Aerospace Division
2600 Ridgeway Road
Minneapolis, Minnesota
Attn: Library

1 IIT Research Institute
Technology Center
Chicago, Illinois 60616
Attn: Library

1 International Nickel Company
One New York Plaza
New York, N. Y. 10004
Attn: C. B. Sanborn

1 Lawrence Livermore Laboratory
P. O. Box 808
Livermore, Ca 94550
Attn: Dr. C. A. Tatro

1 Ling-Temco-Vought Corporation
P. O. Box 5907
Dallas, Texas 75222
Attn: Library

1 Lockheed Missiles & Space Company
P. O. Box 504
Sunnyvale, California 94087
Attn: Library

1 Lockheed Propulsion Company
P. O. Box 111
Redlands, California 92374
Attn: Library

1 Marquardt Corporation
16555 Saticoy Street
Box 2013 South Annex
Van Nuys, California 91409

Attn: Library

1 Martin-Marietta Corporation
P. O. Box 179
Denver, Colorado 80201

Attn: Library

1 McDonnell Douglas Astronautics
5301 Bosa Avenue
Huntington Beach, California 92647

Attn: Library

1 McDonnell Douglas Aircraft Corporation
P. O. Box 516
Lambert Field, Missouri 63166

Attn: Library

1 Northrop Space Laboratories
3401 West Broadway
Hawthorne, California
Attn: Library

3 Rocketdyne
A Division of Rockwell International
6633 Canoga Avenue
Canoga Park, California 91304

Attn: Library
Donald Fulton
Fred Schuler

---

1 Rocket Research Corporation
Willow Road At 116th Street
Redmond, Washington 98052
Attn: Library

1 Stanford Research Institute
333 Ravenswood Avenue
Menlo Park, California 94025
Attn: Library

1 Sandia Laboratory
P. O. Box 969
Livermore, Ca 94550
Attn: J. W. Dini

1 Thiokol Chemical Corporation
Redstone Division
Huntsville, Alabama
Attn: Library

2 TRW Systems Inc.
1 Space Park
Redondo Beach, California 90278

Attn: Library

H. Burge

2 TRW
TAPCO Division
23555 Euclid Avenue
Cleveland, Ohio 44117
Attn: Library
Frank Stattler

1 United Aircraft Corporation
Corporation Library
400 Main Street
East Hartford, Connecticut 06108

1 United Aircraft Corporation
United Technology Center
P. O. Box 358
Sunnyvale, California 94038
Attn: Library

2 United Aircraft Corporation
Pratt & Whitney Division
Florida Research & Development Center
P. O. Box 2691
West Palm Beach, Florida 33402

Attn: Library
R. M. Wallace

1 University of Michigan
Dept. of Mechanical Engineering
2046 East Engineering Bldg
Ann Arbor, Michigan 48105
Attn: Dr. J. R. Frederick

1 Cornell University
Lab of Atomic & Solid State Physics
Clark Hall
Ithica, N. Y. 14850
Attn: Dr. B. W. Maxfield

C. R. Whitsett 324/33/23874

25 MAR 82

ACOUSTIC EMISSION TECHNOLOGY CORPORATION
1828A Tribute Road, Sacramento, Calif. 95815
Phone (916) 927-3861

SPECIALIZING IN THE
PRACTICAL APPLICATIONS
of
ACOUSTIC EMISSION

SACRAMENTO CALIF.
JUL 22'75
U.S. POSTAGE
0.19
PB METER
1134745

McDonnell Douglas Aircraft Corp.
P.O. Box 516
Lambert Field, Missouri 63166
Attention: Library

SPECIAL
4th CL. RATE